002 1392 02

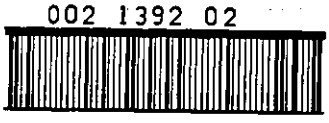

THE AERODYNAMICS OF ELECTRIC ARCS IN AXIAL FLOW

by

D.R. TOPHAM

SUPERVISORS

MR. D.W. KEW,
Department of
Transport Technology.

MR. L.A.H. KING,
Head of the Circuit
Interruption Laboratory,
G.E.C. - E.E. Co. Ltd.,
Stafford.

Submitted for the Degree of Doctor of Philosophy

of Loughborough University of Technology.

JUNE 1970

ACKNOWLEDGEMENTS

The author wishes to express his sincere thanks to Mr. D.W. Kew of Loughborough University and Mr. L.A.H. King of the G.E.C. - E.E. Co., Ltd., under whose supervision the work was carried out. In particular the latter, whose long experience in the field of arc physics contributed much to the author's understanding of electric arc phenomena.

The author also wishes to thank the G.E.C. - E.E. Co., Ltd., for permission to submit this thesis and who supported the work in the Circuit Interruption Laboratory, Stafford.

CONTENTS

Page No.

SUMMARY

This thesis investigates the behaviour of a d.c. electric arc under the influence of a number of different axial gas flow conditions. The work is directed towards obtaining a greater understanding of the electric arcs produced within gas blast circuit breakers. In order to eliminate as many variables as possible, detailed experiments have been carried out in constant pressure, subsonic nitrogen flow provided by a low Mach number shock tube. This facility enables the flow velocity and pressure to be varied independently, thus allowing their effect on arc behaviour to be studied separately. A simplified theoretical model of the arc in this flow field has been developed which gives excellent agreement with the shock tube experiments. The solution of the theoretical model is obtained in non-dimensional terms as a universal characteristic for the constant pressure axial flow arc. The theoretical model has been extended to the case of an axial flow arc with a strong negative pressure gradient, the situation encountered in a circuit breaker nozzle. Solutions have been obtained for two special cases, the high power arc with an arbitrary pressure distribution, and the linear pressure gradient arc whose solution can be extended over the whole power range. The solution of the latter is compared with published experimental measurements on arcs approximating to these flow conditions. Within the range of validity of the basic assumptions, the agreement with the theory is excellent, showing that the high heat losses of arcs in nozzle flow can be satisfactorily explained on the basis of laminar flow.

Nitrogen was selected as the working gas for detailed study as the arc characteristics were known to be similar to those of air, the gas commonly used in circuit breakers. In addition, the physical

properties are reasonably well established up to 20,000°K, and are known to give good agreement with measurements on simplified arcs dominated by radial thermal conduction.

The method adopted for the solution of the theoretical model is approximate in nature, but permits real gas properties to be used throughout. The solution makes use of a number of universal arc functions which can be calculated for a particular gas, and then applied to the axial flow arc with particular pressure distributions. The errors introduced by the approximate method of solution are of the same order as those introduced by uncertainties in the gas properties and the limitations imposed by the basic assumption of thermal equilibrium. The solutions presented provide considerable insight into the effects of the gas properties and flow conditions on arc voltage-current characteristics. The non-dimensional presentation of the results is similar to the Nusselt number - Reynolds number plots used for solid body heat transfer data. In the case of the electric arc, the Reynolds number is combined with an additional parameter which takes account of the arc current. Thus for a particular flow geometry and gas, the arc voltage gradient can be calculated for any desired combination of arc current, flow velocity, and pressure.

NOTATION

a	Constant of proportionality in linear pressure gradient distribution.
a_2	Constant in power law approximation to experimental voltage distributions.
b	Constant in power law, equation 7.5.
d	Distance to achieve equilibrium in thermal gradients.
e	Charge on the electron.
h	Enthalpy.
h_1	Non-dimensional enthalpy.
k	Thermal conductivity.
l	Representative length.
m	Power law index, equation 7.5.
m_e	Mass of electron.
m_s	Mass of heavy gas particle.
n	Index in power law outer profile distribution.
n_2	Index in power law approximation to experimental voltage distribution.
p	Static pressure.
r	Radial co-ordinate.
r_δ	Radial co-ordinate of outer layer.
u	Axial component of velocity.
v	Radial component of velocity.
x	Axial co-ordinate.

B	Constant in linear $\sigma \sim S$ relationship.	
C	Convection constant, Appendix III.	
C_p	Specific heat at constant pressure.	
E	Arc voltage gradient.	
I	Total arc current.	
J_o	Zero order Bessel function.	
K	Boltzmann's constant.	
M_s	Shock Mach number.	
N	Dependent Nusselt number.	$\frac{EI}{2\pi (h/\rho)_o (h_o - h_\infty)}$
N_u	Independent Nusselt number.	$\frac{I^2}{(h/\rho)_o (h_o - h_\infty) \sigma_o x^2}$
P	Radiation density.	
P_r	Prandtl number.	$\frac{\rho_o \mu_o}{k_o}$
R	Gas constant.	
R_e	Reynolds number.	$\frac{\rho_o u_o x}{\mu_o}$
S	Heat flux potential.	$\int_o^T k\, dT$
T	Equilibrium temperature.	
T_e	Electron temperature.	
T_g	Gas temperature.	
V	Arc column voltage.	
V_{tot}	Total arc voltage.	
X	Radial similarity co-ordinate $E\eta$.	
Z	Gas compressibility factor.	

β See equation 7.6.

δ Outer thermal layer thickness.

γ Ratio of specific heats.

η Non-dimensional radial co-ordinate.

λ Mean free path of electrons.

μ Viscosity.

ρ Gas density.

σ Electrical conductivity.

σ_o Reference value of electrical conductivity, 100 mhos/cm.

$g_{(N)}$ Combined functions of N, equation 6.8.

$f_{(x)}$ Distribution of pressure gradient along arc axis.

$g_{(x)}$ Velocity distribution factor.

Subscripts

∞ Freestream conditions

c Arc axis conditions

o Arc boundary conditions, taken as 4,000°K (except in the case of σ_o)

1 Non-dimensional quantities, normalised with respect to conditions at 4,000°K

TABLES

FIGURES

1. INTRODUCTION

The term 'electric arc' has been used to describe gas discharges under a wide range of conditions, varying from low pressure glow discharges to lightning strokes. In practice, the various discharge regimes merge into each other to give a continuous spectrum of operating conditions. The discharges considered in this thesis are high pressure electric arcs, in which the thermodynamic and transport processes are considered to be in thermal equilibrium. Maximum temperatures varying between 6,000°K and 50,000°K have been measured within such arcs, depending upon the operating conditions of the particular arc in question.

The stimulus for the present work was provided by the need for a greater understanding of the energy transfer processes involved in the electric arcs produced within modern gas blast circuit breakers. These devices are used for the control and protection of high power electricity supply systems. The majority of these circuit breakers operate on the axial flow principle, in which a high pressure gas, usually air, is exhausted through a nozzle. The electric arc is drawn between a pair of electrodes spaced on either side of the nozzle; the arc is thus held stationary and the gas is forced to flow through the high temperature region created by the arc. Such an arc, whose axis coincides with the flow direction and is held stationary against the gas flow will henceforth be referred to as an axial flow arc. A schematic drawing of such an arc in a circuit breaker is shown in figure 1.

It is known that the voltage-current characteristics of the arc and its diameter are important factors affecting circuit breaker performance, and from the designer's point of view, it is important to know the relationship between these parameters and the aerodynamic

flow field of the circuit breaker. Although electric arcs have been studied for many years, it is only recently that serious attention has been given to the problem of the interaction between electric arcs and aerodynamic flow fields. In particular, the arc which is constrained wholly by an axial gas flow has received comparatively little attention. This situation arises in an axial flow circuit breaker when the current is low, and the arc diameter is small compared with that of the nozzle. In the case of an alternating current arc, this occurs as the current approaches zero, a period of time which is known to be critical for the successful interruption of current. Furthermore, the a.c. arc in a circuit breaker is known to follow closely the d.c. voltage-current characteristic of the arc.

Practical experience suggests that the flow in an actual circuit breaker is of a complex and often unpredictable nature, and in order to obtain reliable experimental results an arc in a simplified flow situation has been chosen for detailed study. This is the steady state axial flow arc in a uniform velocity, constant pressure flow field. The flow field is assumed to be large compared with the arc diameter, so that the main flow is undisturbed by the arc. This situation is the equivalent of the constant pressure boundary layer problem in aerodynamics.

2. REVIEW OF PREVIOUS WORK ON AXIAL FLOW ARCS

A vast body of literature exists on electric arcs and this review will be confined to those having a substantial element of axial flow. An excellent summary of general electric arc work and plasma physics up to 1956 is given by Finkelnburg and Maecker [1].

The first electric arc to be discovered burnt freely between electrodes under atmospheric conditions. This 'free burning' arc as it is known was studied extensively by early workers, such as Ayrton [2], who derived voltage-current relationships for arcs of different lengths and with different electrode materials. These investigations identified three components of arc voltage, the cathode drop, the anode drop, and the arc column, the latter having an approximately linear voltage distribution. The low current arc column was found to have a negative voltage-current characteristic, the voltage required to sustain the discharge falling as the current was increased. Above 100 amps current the voltage of the free burning arc in air remains almost independent of current. These characteristics are similar in form for many types of arc, except where the arc is physically restrained in a tube, in which case at high currents, the arc voltage rises linearly with current.

The characteristics of the vertical free burning arc are determined by self generated flows, and it represents one of the most complex types of axial flow arc. At low currents free convection dominates the flow field, and this regime has been investigated by Suits [3] up to 10 amps current in nitrogen, helium, hydrogen, and argon, under pressures between 1 and 10 atmospheres. Several authors have correlated these results using different hypotheses. Suits and Poritsky [4] base their method on the free convection heat loss from vertical rods and plates, McAdams [5], using the electrical diameter of

the arc as a length dimension. Elenbaas [6] makes the assumption that the temperature gradient at the edge of the arc is independent of the diameter. This effectively defines the edge of the outer thermal envelope rather than the electrical diameter. The resulting heat transfer law differs considerably from that of Suits and Poritsky, due to the different definitions of diameter employed, the outer thermal diameter being almost ten times the electrical diameter. More recently, Rowe [7] has correlated Suits's results using experimental evidence that the voltage gradient is independent of axial length. The axial length is used as a characteristic dimension and the resulting heat transfer law is similar tc that of Elenbaas.

At high currents the flow field is largely determined by magnetic pinch forces, as demonstrated by Maecker [1]. The arc assumes a conical shape near the cathode, and since the magnetic pinch force of the current increases with current density, an internal pressure is created which is high at the cathode and decreases along the arc axis. The resulting pressure gradient accelerates the flow along the arc axis, and velocities up to 2×10^4 cm/sec have been measured close to the cathode of a 200 amp free burning arc, Wienecke [8]. The voltage gradient-current characteristics of the free burning arc in air and nitrogen at 1 atmosphere pressure have been investigated in detail by King [9] over the current range 10^{-4} to 10^4 amps. Under these conditions the arc is considered to be in thermal equilibrium down to about 0.1 amp current.

In recent years the employment of electric arcs as high enthalpy sources in space re-entry simulation facilities has greatly stimulated research into the interaction between electric arcs and aerodynamic flow fields. The main lines of development can be broadly divided into those employing the crossflow arc, in which magnetic forces are

used to move an arc in a transverse direction through the gas, and those with co-axial arc and gas flow systems. The arc usually operates in a chamber, from which the arc heated gas is expanded through a nozzle into the test section.

The magnetically driven crossflow arc has been investigated experimentally by several authors and a correlation of many of their results is given by Adams et al [10]. Lord [11] has studied the problem theoretically and has obtained a solution valid for low Reynolds numbers. The high Reynolds number solution of this arc represents a difficult mathematical problem and attention has been concentrated on developing general correlation parameters for such arcs, Lord [12] and Yas'ko [13].

In the axial flow heater the arc is confined in a tube with a superimposed axial gas flow, the growth in arc diameter being ultimately limited by the tube walls. The heat addition to the gas takes place during the growth region of the arc, and after the wall limited condition has been reached, further power input to the arc must be absorbed into the wall material. In these axial flow arc heaters the arc and flow passages are of comparable size, and there is strong coupling between the arc and the imposed gas flow. This interaction between the arc and the gas flow presents considerable difficulties in the theoretical solution of such problems, and usually an iterative procedure is employed.

Several authors have proposed theoretical models for this growth region, mainly with the object of predicting the length required to attain fully developed exit conditions. Stine and Watson [14] obtain an analytical solution for a circular cylindrical arc having an increasing central temperature along the axis. This takes account of the axial

convection and radial heat conduction terms in the energy equation. The solution relies on the assumption of a constant massflow per unit area and linearisation of the gas properties. This model is physically unrealistic, since in practice it is found that the arc is initially small in diameter with a high central temperature. With increasing arc length the diameter increases, and the central temperature falls until the wall limited condition is reached. Chen [15] and Weber [16] present analyses for arcs of this type based on a simplified column model containing radial heat conduction as the only form of heat loss. Chen accounts for the heat transfer to the cold flow by applying solid body heat transfer laws to the column surface; Weber also uses the simple radial heat conduction column model, but assumes that all the energy is absorbed within the growing electrically conducting region. Skifstad [17] bases his analysis on similarity solutions of the energy and momentum equations, and uses a Pohlhausen integral technique to solve for particular entry conditions. All these solutions require iteration procedures, and as shown by Watson and Pegot [18], the computation required by these models is as great as that required for a full numerical solution of the problem.

Russian workers have also investigated a series of axial flow arc devices, designated 'Plasmatrons'. In these, conditions are such that the arc does not fill the tube at the exit, and the arc length is limited by an arc root whose position along the wall is determined by the gas flow conditions, for example Dautov and Zhukov [19], Dautov et al [20], Dautov and Sazonov [21]. Considerable effort has been made by the Russian workers to develop correlation parameters for a large number of arcs, including the free burning arc, the wall controlled arc, the crossflow arc, and the axial flow arc. These are summarised by Yas'ko [13] who demonstrates their success in correlating experimental results.

The arc which is constrained wholly by an axial gas flow has received comparatively little attention. Several experimental investigations have been published, but little attention appears to have been paid to the theoretical solution of such problems. In discussing axial flow arcs it is important to distinguish between flows which are purely axial, and those having a component of rotational flow. By means of the latter it is possible to obtain stable arcs of great length. These were investigated by Grotian [22] who obtained arcs greater than 1 metre in length. More detailed experiments were later carried out by Aartz [23] who investigated arcs in flows with varying degrees of rotational flow. It is difficult to interpret such results, as the flow field of the arc is dependent on the design of the apparatus, and the flow with the arc present may differ from the cold flow.

Kirschstein and Koppelmann [24,25], studied an arc in constant pressure pure axial air flow, photographing arc behaviour and measuring voltage distributions. In a later paper [26] they made a detailed study of arc behaviour in the divided flow between a pair of opposing nozzles. King [27] has further investigated the voltage gradient-current characteristics of arcs in air and nitrogen under various flow conditions. These results are shown in figure 2, together with the free burning arc characteristic. Rowe [28] has recently completed a study of an arc in a shock tube, giving voltage gradient-current characteristics for arcs in nitrogen at atmospheric pressure with different flow velocities. He correlates his results on a semi-emperical basis, which, although collapsing the results to a single curve, gives little insight into the fundamental factors affecting arc behaviour.

Swanson [29] has studied the dynamic arc in SF_6 theoretically, using boundary layer techniques. His solution takes the values of certain

integrals across the flow profiles to be constant over the current cycle. From the solution of the dynamic energy equation he calculates the diameter of the plasma remaining at current zero. This solution does not accurately represent the steady state arc, as the variation of some of the quantities which are regarded as fixed at the maximum current value are responsible for the basic d.c. arc characteristic.

Frind [30] has carried out measurements on argon arcs of 70 cm length confined in tubes of 0.3, 0.5, 0.7 and 1.0 cm diameter at between 1 and 10 atmospheres pressure for currents up to 80 amps. At the higher flow rates photographs showed the flow to be turbulent in character, with higher arc voltage gradients than for the laminar arcs obtained at lower flow rates. For the 1 cm diameter tubes the arc was small compared with the tube and wall heat transfer measurements showed that the flow was not fully developed at the exit. Measurements from photographs of the turbulent arc fluctuations showed that the hot arc plasma was travelling much faster than the mean cold flow velocity.

3. GAS PROPERTIES AND THEIR INFLUENCE ON ARC BEHAVIOUR

It is found that the voltage-current characteristics of arcs in different gases differ considerably. These differences arise from the molecular structure of the gas, and some of the important features will now be described and the gas properties of nitrogen presented in detail.

3.1. The formation of dissociation cores:

A striking feature of many arcs is the appearance of high temperature regions within the main discharge at certain critical currents. These were first noted in the case of the free burning arc, and their existance was at first attributed to magnetic pinch effects, since they were accompanied by high speed plasma flows.

King [31] showed that these high temperature cores arose from maxima in the variation of thermal conductivity with temperature. A study of free burning arcs revealed that the formation of the core occurred at different currents, according to the dissociation potential of the gas. King's observed values of transition current for arcs in various gases are compared with their respective dissociation potentials in Table I.

The effect of dissociation is to cause a maximum in the variation of thermal conductivity with temperature. This increase is caused by the inter-diffusion of molecules and atoms, which transports large quantities of dissociation energy along the temperature gradients. The negative rates of change of thermal conductivity with temperature are reflected as increases in temperature gradient within the arc. The change in gas composition

gives rise to a characteristic change in colour within the high temperature core. By observing the transition current in a free burning nitrogen arc, King was able to confirm that the dissociation potential of nitrogen was 9.762 e.v. rather than the previously accepted figure of 7.38 e.v.

3.2. The material properties of nitrogen:

Nitrogen was selected as the working gas for the present experiments, and the material properties used as a basis for the theoretical calculations will now be discussed. Wells [32] has recently made a comparison between published values of the thermal conductivity, electrical conductivity and radiation density of nitrogen at one atmosphere pressure. He concludes that King's [31] calculations of electrical and thermal conductivity best represent the observed arc characteristics, and these values are used as a basis for the present theoretical calculations. However, since Wells's survey, some criticism has been made of the method previously used to obtain values of thermal conductivity from measured arc temperature profiles. In addition, recently published measurements extend the operating range of the apparatus used for such work from arc central temperatures of 15,000°K to 26,000°K. In the light of this recent work the essential differences between the various published values will be briefly reviewed.

The principal differences between the published values of thermal conductivity are shown in figure 3 which compares the calculations of King with those of Yos [33]. There is good agreement up to about 8,000°K, above which there is

considerable difference between the two calculations. The large maximum in thermal conductivity at 15,000°K in King's calculations arises from the first ionisation level of nitrogen atoms, the inter-diffusion of electrons, ions and atoms increasing the thermal conductivity. The magnitude of this increase depends on the value taken for the collision cross section of the nitrogen atom - ion interaction. This is not known with any certainty and the different values used accounts for the difference between the calculations of King and Yos. Maecker's [34] published values of experimentally derived thermal conductivity up to 15,000°K confirm King's calculated values.

Yos [35] contends that Maecker's derived values of thermal conductivity in this temperature range do not take into account internally absorbed ultra-violet radiation, and when allowance is made for this, the derived thermal conductivity is reduced to the level of his calculations. These corrections rely on theoretically calculated absorbtion of ultra-violet radiation whose accuracy is difficult to assess. Hermann [36] claims to have developed a method of analysing Maecker's measured arc temperature profiles which takes account of internally absorbed radiation. He thus reduces the derived values of thermal conductivity close to the calculations of Yos. Schade [37] has recently published measurements on a wall cooled arc with central temperatures up to 26,000°K. As will be shown in the next chapter, his measured variation of arc central temperature with power input clearly reflects a maximum in effective thermal conductivity, closely following calculations based on King's values. Although the exact contributions to

the maximum at 15,000°K are still open to doubt, it appears that for practical purposes it can be regarded as an effective total thermal conductivity. There is little data on the thermal conductivity of nitrogen at pressures greater than one atmosphere. In general, dissociation and ionisation temperatures increase slowly with increasing pressure, causing the maxima to occur at higher temperatures, but to decrease slightly in magnitude.

The published calculations of electrical conductivity are in close agreement up to 26,000°K and are confirmed by recent experimental measurements by Schade [37]. The theories of King [31] and Yos [33] together with the experimental measurements of Schade are shown in figure 4. Above 26,000°K there is no direct experimental information available. Yos's calculations extend up to 100,000°K and above 30,000°K are based on Spitzer's [38] theory for a fully ionised plasma. Also shown on figure 4 are some unpublished calculations by King extending up to 70,000°K. These calculations are somewhat higher in value than his published figures and were performed to investigate the general trend at high temperatures and show the electrical conductivity to be almost constant above 30,000°K. These calculations take into account the change in collision cross sections at each ionisation level, which prevents the electrical conductivity from rising in accordance with the fully ionised theory. Again there is little data on the effect of pressure on electrical conductivity, Yos extends his calculations up to 30 atmospheres pressure and above 20,000°K, these suggest that it varies approximately as the one fifth power of pressure. An examination of published data on high pressure arcs in Chapter 4 suggests that in this temperature range electrical conductivity can be regarded as almost independent of pressure.

The radiation density of nitrogen derived by Wells [32] and Yos [33] are shown in figure 5, Yos's calculations differ considerably from the values presented by Wells's critical survey of the available experimental data. Yos's calculations however, illustrate the rapid increase of radiation with pressure.

The theoretical solution of the overall energy balance of the arc also requires the density, enthalpy and specific heat of nitrogen. There is close agreement between the various published values, and those of Burhorn and Wienecke [39] have been used and are shown in figures 6, 7 and 8. An important parameter from the point of view of the convection heat transfer is the specific enthalpy difference $\rho(h - h_\infty)$, where h_∞ is the free stream enthalpy. This parameter is shown in non-dimensional form in figure 9 where,

$$\rho_1 h_1 = \frac{\rho(h - h_\infty)}{\rho_0(h_0 - h_\infty)}$$

and ρ_0 and h_0 are reference values at 4,000°K and the freestream temperature is 288°K. Burhorn and Wienecke's calculations extend up to 30 atmospheres pressure, however as the electrical and thermal conductivity data was not available to these pressures, the parameter $\rho_1 h_1$ was based on the 1 atmosphere values. In all the following calculations $\rho_1 h_1$ has been taken to be directly proportional to the local static pressure of the gas.

4. SURVEY OF ARC COLUMN THEORIES

In the past, a number of theoretical models have been developed to represent the electrically conducting arc column with various forms of radial heat loss. In general, boundary conditions are chosen which reduce the arc to the form of a circular cylinder. Of these, the cases of arcs with radial heat conduction only, with conduction and transparent radiation, and with conduction and radial convection represent the principal modes of heat loss. By comparing these solutions an important similarity can be deduced concerning the radii of arcs with different types of heat loss.

4.1. The simple conduction arc:

This was the first arc model to be solved in detail and only considers radial conduction losses. In spite of its simplicity this model has contributed more to the understanding of arc behaviour than any other. In this form the energy equation can be written:

$$\frac{1}{r}\frac{d}{dr}\left(r\lambda\frac{dT}{dr}\right)+\sigma E^2=0\,. \tag{4.1}$$

where σ and λ, the electrical and thermal conductivity are non-linear functions of temperature. In this form the equation is popularly known as the Elenbaas-Heller equation.

This can be simplified by a transformation due to Brinkman [40],

$$Er=X\,. \tag{4.2}$$

Equation (4.1) then becomes

$$\frac{1}{X}\frac{d}{dX}\left(X\lambda\frac{dT}{dX}\right)+\sigma=0\,. \tag{4.3}$$

If the variation of σ and λ with temperature is known, equation

(4.3) can be solved numerically to give T as a function of X. If this is carried out for a number of arc central temperatures, the transformation (4.2) can be used to generate families of temperature profiles, each with a fixed central temperature but different voltage gradients and diameters.

Integration of the electrical conductivity across the temperature profiles of equation (4.3) gives the total power input per unit length of arc as follows:-

$$2\pi \int_0^{X_0} \sigma \, X \, dX = 2\pi E^2 \int_0^{r_0} \sigma \, r \, dr. \qquad (4.4)$$

where the subscript o denotes the effective limit of electrical conductivity. Applying Ohm's law to equation (4.4):

$$2\pi E^2 \int_0^{r_0} \sigma \, r \, dr = E I,$$

where I is the total current flowing in the cross section. From equation (4.4) it follows that the arc similarity radius X_0 and the power gradient EI are unique functions of arc central temperature. The realisation of the significance of the power gradient rather than current alone in determining arc temperatures has proved of great importance in understanding arc behaviour under widely differing operating conditions. This emphasises the importance of the arc voltage gradient in determining arc behaviour.

Schmitz [41] has further simplified equation (4.2), replacing temperature by the heat flux potential S, where,

$$S = \int_0^T k \, dT.$$

Equation (4.2) then becomes

$$\frac{1}{X} \frac{d}{dX} \left(X \frac{dS}{dX} \right) + \sigma = 0. \qquad (4.5)$$

For most gases the relationship between σ and S is relatively smooth and is approximately linear up to about 10,000°K. For this linear relationship, equation (4.5) can be solved analytically.

Assuming a linear variation of σ with S of the form:

$$\sigma = B(S - S_o) \qquad S_o < S < S_c$$

equation (4.5) has the solution:

$$\frac{S - S_o}{S_c - S_o} = J_o(X\sqrt{B}).$$

J_o is the zero order Bessel function and subscripts c and o denote conditions at the arc centre and boundary.

Goldenberg [42] has extended this method by approximating the gas properties by a number of linear segments. If a computer is available, it is generally easier to solve the original equation by numerical methods.

This has been done using the programme of Yos [33], (Appendix I) and the nitrogen properties of King, figures 3 and 4. The resulting temperature profiles are shown in figure 10 in terms of the similarity variable X, and clearly show the formation of the high temperature cores. The calculations are terminated at 4,000°K, this being taken as the lower limit of electrical conductivity.

The relationship between arc central temperature and power gradient is shown in figure 12, where it is compared with a number of experimentally measured arc temperatures. The agreement between the calculated and measures values is excellent, Schade's [37] measurements reflecting the irregularities due to the formation of the ionisation core at 15,000°K. King's approximation:

$$T_c = 1.5 \times 10^3 (EI)^{\frac{2}{7}}$$

is also shown, and is a good fit as a mean over the whole power range.

The radius characteristic for a 4,000°K boundary is shown in figure 13 as a function of power gradient. For temperatures above 20,000°K the electrical conductivity is taken to be substantially independent of temperature. In this region the arc can be represented by a simple application of Ohm's law,

$$EI = \sigma \pi X_*^2 \quad , \text{ where } \quad \sigma = 120 \text{ mhos/cm}$$

irrespective of the energy loss mechanism. In this region the electrical conductivity of air, nitrogen, oxygen and argon are similar.

A number of measurements of arc diameter have been published in this power range, and are shown on figure 13. For the water turbine arc of Burhorn, Maecker and Peters [45], the radius at 4,000°K was obtained from the measured temperature profiles at atmospheric pressure. The agreement with the calculated nitrogen radii is excellent.

Marston et al [46], have made measurements on an air arc confined in a narrow tube at pressures between 35 and 130 atmospheres. These diameters were measured photographically and probably over-estimate the electrical diameter. It is to be noted these results do not exhibit any marked pressure dependence.

Kirschstein and Koppelmann [26] measured arc diameter for arcs in nozzle flow at pressures between 2 and 11 atmospheres and currents between 200 and 1,500 amps. These results all collapse to a single curve, again showing no dependence of electrical conductivity on pressure. The diameters were

measured from photographs of the arc in a small region between an opposing pair of nozzles, this arrangement keeping the arc free of metal vapour. The voltage gradients were taken as mean values over a much longer length of arc, it is probable that this under-estimates the gradients appropriate to the measured diameter, accounting for the low values in comparison with the other measurements.

Allen and Craggs [47] measured rapidly expanding spark channels at currents of 188 kA yielding powers of 10^8 Watts/cm. These are in general agreement with the constant electrical conductivity model although the scatter is rather large.

At the low power end of the scale comparison with experiment becomes difficult, as the calculated radius depends more strongly on the assumed boundary temperature. Another difficulty arises from the sensitivity of the electrical conductivity to metal vapour at these temperatures, King [48]. This is illustrated by comparing the results of Foitzik [49] on a rotating nitrogen arc with metal electrodes, with those of Suits [3] using carbon electrodes. The arc diameters with metal electrodes are considerably smaller than those with carbon, in spite of the fact that metal vapour increases the luminosity greatly in the outer regions, exaggerating the visible diameter.

4.2. Conduction arc with radiation:

The general problem of the radiating plasma column is extremely complex and solution is only possible at present with certain simplifications. The usual assumptions to be made are that the column is cylindrical, and the plasma is optically thin, all the radiated energy being transmitted. The energy equation

can then be written:-

$$\frac{1}{r}\frac{d}{dr}\left(r k \frac{dT}{dr}\right) + \sigma E^2 - P = 0$$

where P is the radiated energy per unit volume of plasma, a unique function of temperature.

For this arc the central temperature is no longer a unique function of power gradient and depends on the individual values of E and I. The radiation loss depends on the volume of the arc and is approximately proportional to $\frac{1}{E^2}$.

Lord has derived the following similarity groups for the arc with transparent radiation, all of which are unique functions of central temperature.

$$EI - P, \qquad \frac{I}{E r_0^2}, \qquad \frac{P}{r_0^2}.$$

Wells [32] has carried out detailed numerical calculations on the cylindrical arc column with transparent radiation loss, and shows that the above parameters collapse the results to unique functions of central temperature. The effect of radiation on the individual temperature profiles is shown in figure 11 for arcs with a fixed power input of 10 Kw/cm, at different voltage gradients. The arcs with a low voltage gradient have a lower central temperature, and a flatter profile in the centre than the corresponding radiation free arc.

Although the simple power input-central temperature relationship of the conduction dominated arc no longer holds, it is found that the radial similarity-power input relation (figure 13) still holds closely when radiation is included.

This is shown in Table II where the figures from Wells's calculations are compared for different voltage gradients.

It can be seen that the radial similarity $E r$, still holds closely even with 30% radiation loss. It can also be seen that the proportion of radiation decreases very rapidly as the voltage gradient is increased. Above 20,000°K the radiation density of nitrogen becomes almost independent of temperature, as shown in figure 5.

In the case of forced convection arcs, the high voltage gradients result in small diameters which in turn decrease the proportion of radiation loss. This is shown by the measurements of Kirschstein and Koppelmann [26] for arcs of 2,000 amps in nozzle flow at a pressure of 10 atmospheres. The radiation loss in this case amounted to about 3% of the total power input.

For arcs where the optical depth is small compared to the arc diameter, the radiation heat transfer can be regarded in the same way as thermal conductivity. This is the case at very high pressure, as in the work of Borovik [50] et al approaching 1,000 atmospheres pressure.

4.3. The transpiration cooled arc:

An arc having a uniform radial inflow of gas along its length is known as a transpiration cooled arc. To satisfy the flow equations this boundary condition also requires that the pressure gradient increases linearly along the axis. With the simplifying assumptions that the gas properties within the arc are independent of pressure, and that the kinetic energy is small

compared with the thermal energy, the solution yields a cylindrical arc column whose voltage gradient is independent of length, Cowley [51].

A study of this problem for a 12,000°K nitrogen arc has been published by Schmitz and Druxes and Patt [52]. A more detailed numerical solution is given by Eckert and Anderson [53] who compare the characteristics of the transpiration cooled arc with those of the wall cooled arc with hydrogen as a working gas. The comparison showed that about 15% more power was required to reach a given central temperature than for the wall cooled case, depending on the chosen value of wall temperature.

Some of the results of this study are shown in Table III, where it can be seen that the radius characteristic $E\eta_0$ of the two cases is similar. In practice, a small amount of inflow resulted in high voltage gradients, and the temperature profiles remained close to the wall cooled case, except in the outer regions. The radius characteristic of the transpiration cooled arc containing radial inflow is thus close to that of the simple conduction arc.

In Appendix III a mathematical model of the electrically conducting column of the arc in constant pressure axial flow is developed. The column increases in diameter along the axis and takes account of radial and axial convection terms in the energy equation. The local slope of the edge of the electrically conducting column is regarded as part of an overall convection constant. The model is thus similar in form to the transpiration cooled arc, the slope of the boundary being equivalent to a radial

inflow. The resulting temperature profiles indicate that the radius characteristic E_{η_0} can still be used to represent the radius of the arc.

4.4. A universal arc radius characteristic:

As shown in section 4.3, the arc radius characteristic calculated from the simple Elenbaas-Heller equation which contains radial conduction losses only, can be applied as a close approximation to arcs with other modes of heat loss. This includes those with a large proportion of radiation loss, and the transpiration cooled arc with a radial convection term. Thus for nitrogen arcs dominated by radial heat losses, there appears to be an almost unique relationship between $E\,I$ and E_{η_0}.

This leads to great simplification of the solution of axial flow arc problems, as arc radius can be expressed simply in terms of E and I without considering in detail the energy exchange mechanisms within the electrically conducting column.

For arc power inputs greater than 10^5 Watts/cm, examination of measured arc diameters suggests that the arc in air or nitrogen is well represented by a constant electrical conductivity of about 120 mhos/cm. On the evidence of the measured arc diameters this value is substantially independent of pressure up to 130 atmospheres, although photographic measurements of arc diameters are difficult to interpret accurately.

5. THE GENERAL PROBLEM OF THE ELECTRIC ARC IN AXIAL FLOW

In the preceeding chapter discussion was confined to the electrically conducting region of the arc column. Attention will now be turned to the main subject of this thesis, the overall energy balance of an electric arc column in axial flow. In order to formulate the problem in mathematical terms the following assumptions have been made.

(1) The problem can be described by the continuum equations of fluid dynamics and equilibrium thermodynamics.

(2) Radiation can be neglected.

(3) The kinetic energy of the gas can be neglected in comparison with the thermal energy.

(4) Self magnetic pinch pressures can be neglected.

(5) Electrode wake effects can be neglected.

(6) The arc diameter is small compared with the main flow field which remains unchanged by the presence of the arc.

(7) The arc is axisymmetric and in a steady state, with laminar flow throughout.

(8) The boundary layer approximations are valid.

(9) Where flows with pressure gradients are considered, viscous forces can be neglected in comparison with the pressure forces.

The conditions for local thermal equilibrium are discussed at length by Finkelnberg and Maecker [1]. Thermal and electrical conduction are essentially non-equilibrium phenomena, but if the departures from equilibrium are small, they can be treated by equilibrium methods. This is the concept of local thermal equilibrium, in which the transport and thermodynamic properties of the gas are considered to be unique functions of temperature and pressure. For the discharges considered here departures from equilibrium can arise between the electrons and the heavier gas particles. In the presence of electric fields and thermal gradients the effective temperature of the electrons can be raised above that of the heavier gas particles. The criteria for local thermal equilibrium in the presence of electric fields and thermal gradients for nitrogen at one atmosphere pressure have been calculated by Yos [35].

In the case of electric fields the temperature difference between the electrons and heavy gas particles is given by the relation,

$$\frac{T_e - T_g}{T_e} = \frac{m_e (\lambda_e E)^2}{4 m_g \left(\frac{3}{2} K T_e\right)^2}$$

For conditions in a wall cooled arc of 40 amps and 22v/cm Yos calculates $\frac{T_e - T_g}{T_e} \simeq 0.1$.

The nozzle flow arc at one atmosphere pressure on figure 2 has a voltage gradient of 100v/cm at 40 amps current, giving a figure of $\frac{T_e - T_g}{T_e} \simeq 1$, a large departure from equilibrium.

For radial thermal gradients, a distance d is defined, beyond which the gas is considered to be in equilibrium. Yos has calculated this distance as a function of temperature for nitrogen at one atmosphere pressure. Using the universal radius characteristic

of figure 13, the diameter of the atmospheric pressure nozzle flow arc has been compared with the distance d with the following results.

I	20 amps	10 amps
T_c	14,000°K	13,000°K
r_o	0.04 cms	0,027 cms
d	0.01 cms	0.015 cms

The equilibrating distance is of the same order as the arc diameter and considerable departure from equilibrium is to be expected under these conditions. The criteria are based on simplified theories and Yos suggests that the figures may be in error by an order of magnitude and give pessimistic results. These estimations, however, suggest that departure from equilibrium is to be expected for low current arcs with high voltage gradients, such as the arc in nozzle flow.

Inspection of the known characteristics of arcs in flowing gases suggests that radiation can be neglected for most axial flow arcs. At sonic velocity and one atmosphere pressure, figure 2 shows the constant pressure flow arc to have a voltage gradient of 30 volts/cm for currents greater than 100 amps. Wells's calculations in Table III shows approximately 4% radiation loss for a 300 amp arc of this voltage gradient. The maximum current obtained in the shock tube experiments on this type of arc was 48 amps, and for this current radiation is negligible.

Kirschstein and Koppelmann [26] measured about 3% radiation loss from a 2,000 amp arc in nozzle flow at 10 atmospheres pressure. From these figures it can be seen that radiation can also be neglected in the high power nozzle arc.

If the analysis is restricted to conditions where the kinetic energy is small compared with the thermal energy, the pressure work and frictional heating terms in the energy equation can be neglected. Under sonic flow conditions at 10,000°K, the kinetic energy amounts to about 7% of the thermal energy.

Magnetic pinch forces give rise to internally generated jets due to pressure gradients in a conically shaped arc column. For the case of the constant pressure axial flow arc, these are expected to play some part at high currents. The magnitude of such effects can be estimated by referring to the 200 amp free burning arc of Wienecke [8], where velocities of the order of 10^4 cm/sec were measured close to the cathode. The same momentum change required to accelerate the gas from rest to 10^4 cm/sec, can be obtained by accelerating from a free stream velocity of 10^4 cm/sec to 1.6×10^4 cm/sec. This represents much less of a jet effect than in the case of the free burning arc. In the case of the 48 amp arc in the shock tube experiments, plasma jets were not expected to play much part. For flows with large pressure gradients, the self generated gradients are negligible compared to those in the main flow.

The effect of the wake from the upstream electrode is expected to be of importance in the constant pressure flow arc, causing a local reduction in flow velocity close to the electrode. Ideally the electrode should be small in diameter compared with the arc. This proved difficult to achieve in practice, and considerable trouble was taken in the shock tube experiments to minimise the wake and to assess its effect on the results.

The flow equations of the axial flow arc can be further simplified by the introduction of the Prandtl boundary layer

approximations, which form the starting point for the solution of many viscous flow and heat transfer problems. These can be applied to flow situations where radial derivatives are large compared to the axial derivatives, changes being assumed to take place within a transverse distance which is small compared to a typical axial length. In the case of the electric arcs studied here typical length to diameters are of the order of 10:1 and the flow deflections are small. The derivation of the boundary layer equation is given in standard texts on the subject, Goldstein [54], Schlichting [55].

For axisymmetric flow the boundary layer approximations reduce the flow equations to the following form:-

GAS LAW

$$\frac{p}{\rho} = Z R T$$

AXIAL MOMENTUM EQUATION

$$\rho u \frac{\partial u}{\partial x} + \rho v \frac{\partial u}{\partial r} = \frac{1}{r} \frac{\partial}{\partial r}\left(\mu r \frac{\partial u}{\partial r}\right) - \frac{dp}{dx} \qquad (5.1)$$

RADIAL MOMENTUM EQUATION

$$\frac{\partial p}{\partial r} = 0 \qquad (5.2)$$

MASS CONTINUITY EQUATION

$$\frac{\partial(\rho u r)}{\partial x} + \frac{\partial(\rho v r)}{\partial r} = 0. \qquad (5.3)$$

ENERGY EQUATION

$$\rho u \frac{\partial h}{\partial x} + \rho v \frac{\partial h}{\partial r} = \frac{1}{r} \frac{\partial}{\partial r}\left(r \frac{k}{c_p} \frac{\partial h}{\partial r}\right) + \sigma E^2 + u \frac{dp}{dx} + \mu\left(\frac{\partial u}{\partial r}\right)^2 - P.$$

With assumptions 2 and 3, this reduces to the form:

$$\rho u \frac{\partial h}{\partial x} + \rho v \frac{\partial h}{\partial r} = \frac{1}{r} \frac{\partial}{\partial r}\left(r \frac{k}{c_p} \frac{\partial h}{\partial r}\right) + \sigma E^2. \qquad (5.4)$$

From the solution of the radial momentum equation, the pressure remains constant across planes normal to the axis. The arc can then be regarded as a heat addition process, introducing density changes into the flow, whilst the pressure is impressed by the external flow.

In solving these equations it is convenient to divide the flow into two regions, the electrically conducting arc column and an outer thermal layer. In order to clarify the boundary conditions at the junction between these two regions, the energy equation will next be examined to determine the relative orders of magnitude of the terms within the electrically conducting region.

5.1. Order of magnitude estimation of convection within the electrically conducting regions:

The energy equation of the electrically conducting region of the arc will now be examined to determine the importance of convection. Taking the simplified form of the energy equation:

$$\rho u \frac{\partial h}{\partial x} + \rho v \frac{\partial h}{\partial r} = \frac{1}{r} \frac{\partial}{\partial r}\left(r \frac{k}{c_p} \frac{\partial h}{\partial r} \right) + \sigma E^2$$

Dividing by reference values of ρ, u, h, k, c_p and a representative length l, the energy equation is obtained in the form:

$$\rho^* u^* \frac{\partial h^*}{\partial x^*} + \rho^* v^* \frac{\partial h^*}{\partial r^*} = \frac{k}{\rho u c_p l}\left[\frac{1}{r^*} \frac{\partial}{\partial r^*}\left(r^* \frac{k^*}{c_p^*} \frac{\partial h^*}{\partial r^*} \right) \right] + \frac{\sigma E^2 l}{\rho u h} \qquad (5.5)$$

The starred quantities are the non-dimensional variables and the group $\frac{\rho u c_p l}{k}$ is known as the Péclét number. This can be written in the more familiar form $R_e . P_r$, where

$$R_e = \frac{\rho u l}{\mu} \qquad \text{Reynolds number}$$

$$P_r = \frac{c_p \mu}{k} \qquad \text{Prandtl number}$$

The group $\frac{\sigma E^2 l}{\rho u h}$ represents the ratio of the electrical heating terms to the convection terms.

If the non-dimensional quantities h^*, ρ^*, u^*, k^*, c_p^* and x^* are regarded as $o(1)$, the order of magnitude of the terms in equation (6.6) can be estimated as follows:

$$\rho^* u^* \frac{\partial h^*}{\partial x^*} + \rho^* v^* \frac{\partial h^*}{\partial r^*} = \frac{1}{R_e P_r}\left[\frac{1}{r^*} \frac{\partial}{\partial r^*}\left(r^* \frac{k^*}{c_p^*} \frac{\partial h^*}{\partial r^*} \right) \right] + \frac{\sigma E^2 l}{\rho u h}$$

$$o(1) \qquad o(1) \qquad \frac{1}{R_e P_r} o\left(\frac{l}{r}\right)^2 \qquad \frac{\sigma E^2 l}{\rho u h}$$

The group $R_a . P_r \left(\frac{r}{l}\right)^2$ represents the ratio $\frac{\text{convection}}{\text{conduction}}$ of the rate of change of which will now be expressed in terms of non-dimensional numbers appropriate to the axial flow arc.

The ratio $\left(\frac{r}{l}\right)$ can be written in the form:

$$\frac{r}{l} = \frac{r_o}{l} \times \frac{r}{r_o}$$

where r_o is the radius of the electrically conducting region, taken here to be the 4,000°K isothermal.

Using Ohm's law in the form:

$$\frac{I}{E} = 2\pi\sigma_o r_o^2 \int_o^{'} \sigma, r, dr, \qquad (5.6)$$

the radius r_o can be expressed in terms of electrical parameters. The reference value of electrical conductivity, σ_o, is taken as 100 mhos/cm, this being representative of the value above 20,000°K, where it becomes almost independent of temperature. This reference value is of no significance in itself, serving only to render the integral in equation (5.6) non-dimensional. The ratio $\left(\frac{r_o}{l}\right)$ can now be written:

$$\left(\frac{r_o}{l}\right)^2 = \frac{I}{2\pi\sigma_o E l^2 \int_o^{'} \sigma, r, dr,}$$

and the ratio $\frac{\text{convection}}{\text{conduction}}$ becomes

$$\frac{\rho u C_p l}{k} \cdot \frac{I}{2\pi\sigma_o E l^2} \cdot \frac{1}{\int_o^{'} \sigma, r, dr,} .$$

At this point it is convenient to define a Nusselt number for the arc N, where,

$$N = \frac{EI}{2\pi \left(\frac{h}{C_p}\right)_o (h_o - h_\infty)}$$

This will be called the Dependent Nusselt Number, and is the non-dimensional power gradient of the arc.

The ratio convection / conduction can now be written as:

$$\frac{N_u R_e P_r}{4\pi^2 N} \cdot \frac{1}{\int_0^{r_1} \sigma_1 r_1 dr_1} \cdot \left(\frac{r}{r_0}\right)^2 \left(\frac{\rho u}{\rho_0 u_0}\right) \left(\frac{h_0}{h}\right) \left(\frac{C_p}{C_{p_0}}\right)$$

where $R_e = \frac{\rho_0 u_0 l}{\mu_0}$ Reynolds Number

$P_r = \frac{C_{p_0} \mu_0}{k_0}$ Prandtl Number

$N_u = \frac{I^2}{\left(\frac{k}{C_p}\right)_0 (h_0 - h_a) \sigma_0 l^2}$ Independent Nusselt Number

The gas properties are evaluated at 4,000°K.

The integral $\int_0^{r_1} \sigma_1 r_1 dr_1$ has been calculated from the universal radius characteristic of figure 13, and is shown in figure 14 as a function of N. These non-dimensional groups are those which occur later in the solution of the energy equation, and give a satisfactory correlation of experimental measurements. Making use of the data shown in figure 21, the ratio of the convection to the conduction terms has been calculated for the differential equation of the electrically conducting region.

Conditions at the 4,000°K boundary are shown in figure 15 for the cases of the constant pressure flow arc and the nozzle flow arc. It can be seen that the convection terms are less important within the electrically conducting region of the nozzle flow arc than for the constant pressure flow arc. This is because the decrease in arc diameter due to the higher voltage gradient of the nozzle flow arc outweighs the effect of the increased flow velocity within the column. The distribution of the convection terms across a particular temperature profile for the constant pressure flow arc is shown in figure 16. The temperature profile has been calculated from the simple conduction arc, and the actual profile will differ from this in the outer regions.

It can be seen that the convection terms are of some importance well within the electrically conducting region. The simple Elenbaas-Heller equation cannot be applied directly to axial flow arcs without further justification.

The model of the electrically conducting column of the constant pressure flow arc presented in Appendix III includes the effects of radial and axial convection. Temperature profiles are presented for various convection conditions and the distribution of total convected energy across a particular profile shown. It is found that the radius characteristic is close to that of the simple conduction arc, even with a considerable proportion of convection loss at the 4,000°K boundary.

5.2. The integral method of solution:

The method of solution adopted is based on Pohlhausen's method for solving boundary layer problems [54,55]. Using the mass continuity equation, the momentum and energy equations are expressed in terms of integrals of the axial flow parameters over the flow cross section. These integral equations are then solved by choosing approximate temperature and velocity profiles which satisfy certain of the boundary conditions. When applied to skin friction problems the method gives excellent results and the solutions are relatively insensitive to the actual shapes of the profiles used.

The derivation of the integral form of the momentum and energy equations is given in standard texts [54,55]. The case of the energy equation is given in Appendix II, as the electrical

heating terms are not normally included. The equations then take the following form:-

Momentum equation

$$\frac{d}{dx}\int_0^\infty \rho u(u-u_\infty)\, r\, dr = -\frac{dU_\infty}{dx}\int_0^\infty (\rho - \rho_\infty)\, r\, dr \quad (5.8)$$

Energy equation

$$2\pi \frac{d}{dx}\int_0^\infty \rho u(h-h_\infty)\, r\, dr = I\,\frac{dV}{dx}.$$

This can be integrated directly to give:

$$2\pi\int_0^\infty \rho u(h-h_\infty)\, r\, dr = IV. \quad (5.9)$$

where V is the arc column voltage measured from the origin.

This equation forms the basis of the solution of the axial flow arc, and the problem is to express the integral in terms of suitable electrical parameters. The following special cases have been chosen for solution:-

(1) The arc in constant pressure, uniform velocity axial flow.

(2) The high power arc with an arbitrary pressure distribution.

(3) The arc with a linearly increasing pressure gradient.

For the last two cases the flow is of a stagnation point type, in which the velocity is zero at the origin and the flow accelerates along the axis.

6. SOLUTION FOR THE ARC IN CONSTANT PRESSURE AXIAL FLOW

Considering the special case of an arc in constant pressure, uniform velocity axial flow, the momentum equation (5.8) becomes,

$$\frac{d}{dx}\int_0^\infty \rho u(u-u_\infty) r\, dr = 0 .$$

Neglecting self generated plasma flows and electrode wake effects (assumptions 4 & 5), this is satisfied by the solution,

$$u = u_\infty$$

This is confirmed by figure 17 which shows the passage of metal vapour along a 40 amp arc on successive frames of an image converter camera photograph. The luminous front of the disturbance remains undistorted across the arc diameter and travels at the cold flow velocity.

The arc thus acts as a constant pressure heat addition process, expansion of the heated gas introducing radial velocities into the flow, leaving the axial component unchanged. With this solution of the momentum equation, the energy equation (5.9) becomes:

$$u_\infty 2\pi \int_0^\infty \rho (h-h_\infty) r\, dr = IV .$$

Dividing the flow into an electrically conducting column and an outer thermal layer, this can be written,

$$\int_0^{r_0} \rho (h-h_\infty) r\, dr + \int_{r_0}^\infty \rho (h-h_\infty) r\, dr = \frac{IV}{2\pi u_\infty} .$$

The arc is assumed to grow from zero thickness at the origin and increase in diameter along the axis. The general features of the arc model are shown in figure 18.

It was shown in Chapter 4 that the radii of many arcs, including those with a large proportion of radiation and convection, can be represented by a universal radius characteristic in which ξr_0 is almost a unique function of power gradient, E.I. Thus the arc

radius r_0 can be expressed in terms of current and voltage gradient alone, without considering in detail the energy exchange mechanisms within the core.

It is difficult to define a precise radius for the arc, since there is no definite point at which the electrical conductivity is zero. In the computation of the simple Elenbaas-Heller profiles in Section 4.1, a value of 4,000°K was selected as the boundary. The dissociation energy is then included in the integral over the electrically conducting core. Below 4,000°K the nitrogen gas properties change smoothly with temperature and a simple profile can be used to represent the outer layers. The outer layer profile is chosen so that the conduction heat flow is matched at the 4,000°K boundary. This assumes that there is no convection at this boundary, which as has been shown earlier, is not in general justified. It is found however, that the solution is dominated by the growth of the inner region, and the outer layer only plays a significant part at low powers where the assumption is more justified. This error tends to under-estimate the contributions of the outer layers.

In an attempt to overcome this difficulty a method was tried based on an arc diameter containing 98% of the electrical input. At this radius the proportion of convection is much reduced, but at the higher powers the dissociation energy is included in the outer layers. This, and the rapid variation of thermal conductivity with temperature make it difficult to represent the outer profile satisfactorily. The integral method

of solution is such that the errors introduced by using the fixed 4,000°K boundary model are minimised, only changing the effective shape of the temperature profile, not the overall energy balance.

It is convenient at this stage to express the energy equation in non-dimensional form by dividing through by reference values of the gas properties. The equation then becomes:

$$\int_0^{1} \rho_1 h_1 r_1 \, dr_1 + \int_1^{\infty} \rho_1 h_1 r_1 \, dr_1 = \frac{IV}{2\pi r_0^2 \rho_0 u_0 (h_0 - h_\infty)} \qquad (6.1)$$

where $\rho_1 = \frac{\rho}{\rho_0}$, $h_1 = \frac{h - h_\infty}{h_0 - h_\infty}$, $r_1 = \frac{r}{r_0}$, the subscript 0 denoting conditions at 4,000°K. By choosing the reference temperature at the edge of the conducting boundary, the non-dimensional core integral becomes almost independent of the freestream temperature. As it is the core integral which dominates the solution over a large power range, the final non-dimensional solution is also almost independent of the free-stream temperature.

The product $\rho_1 h_1$ is shown in figure 9 as a function of temperature. It is almost constant above 7,000°K and for temperatures above this the enthalpy integrals are independent of the temperature profiles. The integral $\int_0^{1} \rho_1 h_1 r_1 \, dr_1$ has been calculated from the Elenbaas-Heller profiles of figure 10, and is shown in figure 19 as a function of the dependent Nusselt number N. As expected, the integral is constant a high powers where the major portion of the profile is above 7,000°K. For central temperatures below this, the Elenbaas-Heller profile becomes a better approximation to the central core profile.

The outer layer integral is evaluated by assuming a simple profile for the product $\rho_1 h_1$ and matching the temperature gradient at the boundary r_0. A finite outer layer of thickness δ is defined such that,

$$\int_{r_0}^{\infty} \rho(h-h_\infty) r\, dr = \int_{r_0}^{r_0+\delta} \rho(h-h_\infty) r\, dr.$$

Changing the radial co-ordinate to r_δ where:-

$$r_\delta = r - r_0$$

and defining a non-dimensional co-ordinate η where:-

$$\eta = \frac{r_\delta}{\delta},$$

the non-dimensional outer integral becomes:

$$\int_1^{\infty} \rho_1 h_1 r_1\, dr_1 = \left(\frac{\delta}{r_0}\right)^2 \int_0^1 \left(\frac{r_0}{\delta}+\eta\right) \rho_1 h_1\, d\eta . \qquad (6.2)$$

The distribution of the product $\rho_1 h_1$ across the outer layer is represented by the simple power law relation:

$$\rho_1 h_1 = (1-\eta)^n , \qquad (6.3)$$

which satisfies the boundary conditions

$$\rho_1 h_1 = 0 \qquad \eta = 1$$
$$\rho_1 h_1 = 1 \qquad \eta = 0$$

The conduction balance across the boundary r_0 gives:

$$EI = -2\pi r_0 \left(\frac{k}{c_p}\right)_0 \frac{dh}{dr}$$

which can be written in non-dimensional terms as:

$$N = -\frac{r_0}{\delta}\left(\frac{dh_1}{d\eta}\right)_{\eta=0} . \qquad (6.4)$$

The non-dimensional enthalpy gradient can be expressed in terms of $\rho_1 h_1$, as follows:

$$\frac{dh_1}{d\eta} = \frac{d(\rho_1 h_1)}{d\eta} \cdot \frac{dh_1}{d(\rho_1 h_1)}$$

Differentiating equation (6.3), this becomes:

$$\left(\frac{dh_1}{d\eta}\right)_{\eta=0} = -n\left[\frac{dh_1}{d(\rho_1 h_1)}\right]_{h_1=1}$$

for nitrogen,

$$\left[\frac{dh_1}{d(\rho_1 h_1)}\right]_{h_1=1} \approx 3$$

and hence

$$\left(\frac{dh_1}{d\eta}\right)_{h_1=1} = -3n$$

Equation (6.4) therefore becomes:

$$\frac{\delta}{r_0} = \frac{3n}{N} \tag{6.5}$$

With the flow distribution of equation (6.3), the outer layer integral can be written in the form:

$$\left(\frac{\delta}{r_0}\right)^2\int_0^1\left(\frac{r_0}{\delta}+\eta\right)\rho_1 h_1\, d\eta = \left(\frac{\delta}{r_0}\right)^2\int_0^1(1-\eta)^n\eta\, d\eta + \left(\frac{\delta}{r_0}\right)\int_0^1(1-\eta)^n d\eta$$

The integrals can be evaluated and combined with equation (6.5) to give:

$$\left(\frac{\delta}{r_0}\right)^2\int_0^1\left(\frac{r_0}{\delta}+\eta\right)\rho_1 h_1\, d\eta = \frac{9}{N^2}\cdot\frac{n^2}{(n+1)(n+2)} + \frac{3}{N}\cdot\frac{n}{(n+1)} \tag{6.6}$$

The index n is a shape parameter for the profiles, whose value is undetermined. The value of the outer integral is relatively insensitive to the value of n chosen, as shown in Table IV.

The case of $n = \infty$ is equivalent to a simple exponential profile extending to infinity.

Substituting equations (6.6) into equation (6.1), the energy equation finally becomes:

$$\int_0^1\rho_1 h_1 r_1\, dr_1 + \frac{9}{N^2}\cdot\frac{n^2}{(n+1)(n+2)} + \frac{3}{N}\cdot\frac{n}{(n+1)} = \frac{IV}{2\pi r_0^2\rho_0 u_0(h_0-h_\infty)} \tag{6.7}$$

The left hand side of this equation is a function of EI only, and using the universal characteristic, the radius r_o can be written in terms of EI and E.

Since the total current is independent of x, equation (6.7) reduces to a simple first order differential equation of the form,

$$V = f\left(\frac{dV}{dx}\right)$$

This can be solved in non-dimensional terms, to give a unique characteristic for the constant pressure axial flow arc.

Using Ohm's law, the arc radius can be expressed in electrical terms to give,

$$r_o^2 = \frac{I}{2\pi\sigma_o E \int_o^{'} \sigma_1 r_1 dr_1}$$

where the conductivity integral $\int_o^{'} \sigma_1 r_1 dr_1$ is shown in figure 14, the non-dimensional form of the universal radius characteristic. Equation (6.7) then becomes:

$$\int_o^{'} \rho_1 h_1 r_1 dr_1 + \frac{q}{N^2} \cdot \frac{m^2}{(m+1)(m+2)} + \frac{3}{N} \cdot \frac{m}{(m+1)} = \frac{V N 2\pi\sigma_o \left(\frac{h}{G}\right)_o}{\rho_o u_o I} \cdot \int_o^{'} \sigma_1 r_1 dr_1 .$$

This can be written in the form:

$$g(N) = \frac{V 2\pi\sigma_o \left(\frac{h}{G}\right)_o}{\rho_o u_o I} \quad , \tag{6.8}$$

where $g(N)$ represents the combined functions of N.
This has been calculated and is shown in figure 20 for the core alone, $m = 1$, and $m = \infty$.
The effect of the outer boundary is negligible for values of N greater than 10, and the difference between the curves for $m = 1$ and $m = \infty$ is small.

Differentiating equation (6.8) with respect to x gives:

$$g'(N)\frac{dN}{dx} = \frac{dV}{dx}\,\frac{2\pi\sigma_o\left(\frac{h}{C_p}\right)_o}{\rho_o u_o I}$$

or, in terms of N;

$$\frac{g'(N)}{N}\frac{dN}{dx} = \frac{4\pi^2\sigma_o\left(\frac{h}{C_p}\right)_o (h_o - h_\infty)}{\rho_o u_o I^2}$$

This can be integrated to give:

$$\int_\infty^N \frac{g'(N)}{N}\,dN = \frac{4\pi^2\sigma_o\left(\frac{h}{C_p}\right)_o^2 (h_o - h_\infty)\,x}{\rho_o u_o I^2},$$

which can be put in the form:

$$\frac{4\pi^2}{\int_\infty^N \frac{g'(N)}{N}\,dN} = N_u R_e P_r \qquad (6.9)$$

where $N_u = \dfrac{I^2}{\sigma_o\left(\frac{h}{C_p}\right)_o (h_o - h_\infty)\,x^2}$ Independent Nusselt No.

$R_e = \dfrac{\rho_o u_o x}{\mu_o}$ Reynolds No.

$P_r = \dfrac{C_{p_o}\mu_o}{k_o}$ Prandtl No.

These are the same non-dimensional parameters as those derived in the order of magnitude estimate of the energy equation in Section 5.1. The reference conditions for nitrogen are shown in Table V.

The integral $\int_\infty^N \frac{g'(N)}{N}\,dN$ was evaluated by approximating the function $g(N)$ by a number of simple power law segments, and the resulting solution for nitrogen is shown in figure 21. It can now be seen that for a particular gas, arcs in constant pressure axial flow can be represented by a single non-dimensional characteristic. Knowing the gas flow conditions and current, the voltage gradient distribution of a particular arc can readily be calculated from this characteristic.

6.1. Discussion of theory and comparison with measured arc characteristics:

The constant pressure flow arc characteristic shown in figure 21 displays the known features of axial flow arcs. For the steadily rising portion of the characteristic at high power gradients, the voltage gradient of an arc of fixed length and flow conditions is independent of current. Likewise, at constant current and length, the voltage gradient varies as the square root of the pressure, so long as the variation of the gas properties with pressure is small. These features are shown by King's results on figure 2 for arcs in constant pressure sonic flow at 1 and 10 atmospheres pressure. In this power range the arc is represented by the constant electrical conductivity model.

As the arc power is decreased, the slope of the characteristic decreases, giving a negative voltage gradient-current relationship. Down to 500 Watts/cm.($N = 10$), the solution is dominated by the contribution from the electrically conducting region of the arc. Under these conditions, the energy contained within the growing arc column above $4{,}000^{\circ}K$ is much greater than the freestream energy, and the voltage gradient is almost independent of the freestream temperature. At powers below 500 Watts/cm the outer thermal layer absorbs an increasing amount of heat and the electrically conducting region becomes dominated by radial heat conduction.

King's results make no reference to arc length and there appears to be little information on this aspect of arc behaviour. Holm, Kirschstein and Koppelmann [25] make one reference to this for an arc in constant pressure uniform flow, finding that the voltage gradient halved between arc lengths of 1 and 10 cms. In the shock tube experiments described in Chapter 8, the variation of voltage

gradient with arc length and flow velocity was examined in detail. Care was taken to minimise the electrode wake, and currents up to 48 amps at 1 and 2 atmospheres pressure were investigated.

Some of these results are shown on figure 21 and the complete results shown on a larger scale in figure 47, where they are compared with the theoretical solution. The variation of voltage gradient with arc current, length, pressure and flow velocity are all consistent with the theory.

The general shape of the theoretical arc characteristic is determined by the universal radius characteristic. This differs markedly for different gases, and to illustrate this, the radius characteristic for argon is shown on figure 13. The calculations for argon were supplied by Dr. Naylor [56]. The resulting arc characteristic is shown in figure 22, where it can be seen to differ considerably from that of the nitrogen arc. The reference conditions for argon are given in Table V. From these, and the argon arc characteristic it can be seen that for the same velocity and pressure, the voltage gradient of the argon arc is lower than the corresponding arc in nitrogen. Although there do not appear to be any published results for the constant pressure flow axial arc in argon, the free burning argon arc is known to have a low voltage gradient. Goldman [57] gives a voltage gradient of 3 to 5 v/cm for a 100 amp free burning argon arc, compared with King's [9] value of 10 v/cm for the 100 amp nitrogen arc.

Wutzke, Pfender and Eckert [58] have published the results of measurements on an argon arc in a relatively large diameter wind tunnel, in which the arc was well free of the walls. A mean voltage gradient of 4 v/cm was obtained for a 60 amp arc with a

flow velocity of 3×10^3 cm/sec at atmospheric pressure. Experiments in the shock tube suggested that with large diameter electrodes the arc has an almost linear voltage distribution, whose gradient is similar to that of an arc of about 2 cms length in undisturbed flow. Using this value of length, the arc of Wutzke, Pfender and Eckert is shown on figure 22, where it can be seen to lie close to the theoretical argon characteristic.

Figure 47, showing the nitrogen experimental results from the shock tube, also shows the effect of the outer layer shape parameter n on the final solution. Curves are shown for the electrically conducting core alone, $n = 1$ and $n = \infty$. It can be seen that within the range of the experimental results, the difference amounts to about 15% in power gradient. For gases such as CO_2 and SF_6 whose dissociation temperature lies below the limit for significant electrical conductivity, the outer thermal layer will assume greater importance as it now contains the dissociation energy. This will tend to increase the voltage gradient of such arcs at low powers.

Simple power laws can be used to represent the arc characteristics over limited power ranges, the exponent varying between 0.2 and 0.5. This accounts for the variety of laws quoted for variation of voltage gradient with pressure and for different gases.

7. THEORY OF THE AXIAL FLOW ARC WITH A LARGE PRESSURE GRADIENT

The case of an air or nitrogren arc expanding through a nozzle is of great practical interest to the circuit breaker designer. If, as a first approximation, viscous forces are neglected in comparison with pressure forces, the velocity distribution within the arc can be calculated from a simple momentum balance. If the flow Mach number is not much greater than unity, the kinetic energy of the flow can be neglected and the simple energy equation (5.9) can be used.

The simple one-dimensional momentum equation gives:

$$u^2 = \frac{2}{\rho}\int_0^x f(x)\,dx \tag{7.1}$$

where $f(x) = -\frac{dp}{dx}$, and ρ is the local density.

The flow has a stagnation point at the origin where u = 0 at $x = 0$, and the pressure distribution is assumed to be unchanged by the arc.

The simplified energy equation

$$2\pi\int_0^\infty \rho u(h_0 - h_\infty) r\,dr = IV,$$

becomes, on substituting for u from eqn. (7.1),

$$2\pi\left[2\int_0^x f(x)\,dx\right]^{\frac{1}{2}}\int_0^\infty \rho^{\frac{1}{2}}(h - h_\infty) r\,dr = IV$$

Non-dimensionalising by the gas properties at 4,000°K, this becomes:

$$\left[\int_0^x f(x)\,dx\right]^{\frac{1}{2}}\int_0^\infty \rho_1^{\frac{1}{2}} h_1 r_1\,dr_1 = \frac{IV}{2\pi r_0^2 (2\rho_0)^{\frac{1}{2}}(h_0 - h_\infty)} \tag{7.2}$$

Separating the enthalpy integral into the electrically conducting region and an outer layer:

$$\int_0^\infty \rho_1^{\frac{1}{2}} h_1 r_1\,dr_1 = \int_0^1 \rho_1^{\frac{1}{2}} h_1 r_1\,dr_1 + \left(\frac{\delta}{r_0}\right)^2\int_0^{\prime}\left(\frac{r_0}{\delta} + \eta\right)\rho_1^{\frac{1}{2}} h_1\,d\eta.$$

The core integral has again been calculated from the simple Elenbaas-Heller temperature profiles and is shown in figure 19 as a function of N. It's value can be seen to increase with increasing power input, due to the increase in velocity within the arc as the temperature increases.

As in the case of the constant pressure flow arc, the outer layer is represented by a simple power law distribution, and the heat conduction matched across the boundary. The outer layer distribution is written as:

$$\rho_1^{\frac{1}{2}} h_1 = (1-\eta)^m,$$

and the heat balance across the boundary can be written in non-dimensional terms to give,

$$\frac{\delta}{r_0} = \frac{m}{N}\left[\frac{dh_1}{d(\rho_1^{\frac{1}{2}} h_1)}\right]_{h_1=1}$$

For nitrogen, $\left[\frac{dh_1}{d(\rho_1^{\frac{1}{2}} h_1)}\right]_{h_1=1} \simeq 1.24$, and using this, the outer enthalpy integrals can be evaluated to give,

$$\int_0^\infty \rho_1^{\frac{1}{2}} h_1 r_1 dr_1 = \int_0^1 \rho_1^{\frac{1}{2}} h_1 r_1 dr_1 + \frac{1.54}{N^2}\cdot\frac{m^2}{(m+1)(m+2)} + \frac{1.24}{N}\cdot\frac{m}{(m+1)}. \qquad (7.3)$$

Expressing the radius in terms of the non-dimensional form of the universal radius characteristic, the energy equation finally becomes:

$$\left[\int_0^x f(x)dx\right]^{\frac{1}{2}} \frac{1}{E}\cdot\frac{\int_0^\infty \rho_1^{\frac{1}{2}} h_1 r_1 dr_1}{\int_0^1 \sigma_1 r_1 dr_1} = \frac{V\sigma_0}{(2\beta)^{\frac{1}{2}}(h_0 - h_\infty)}. \qquad (7.4)$$

This equation is of the form,

$$V = g(x).f(E).$$

Two special cases of this equation can be solved with relative ease. At high power gradients the function $f(E)$ can be approximated by a simple power law, and the energy equation can be solved for an arbitrary pressure distribution. For the case of a linear distribution of pressure gradient the equation can be solved directly without integration.

7.1. The high power arc with an arbitrary pressure distribution:

If the integrals of equation (7.4) are represented by the simple power law,

$$\frac{\int_0^\infty \rho_1^{\frac{1}{2}} h_1 r_1 dr_1}{\int_0^{r} \sigma_1 r_1 dr_1} = b N^{1-m}, \tag{7.5}$$

the energy equation can be put into the form:

$$VE^m = \beta \cdot g(x), \tag{7.6}$$

where $$\beta = \frac{b(2\rho_0)^{\frac{1}{2}}(h_0 - h_\infty)}{\sigma_0}\left[\frac{2\pi\left(\frac{h}{c_1}\right)_0 (h_0 - h_\infty)}{I}\right]^{m-1}.$$

Equation (7.6) can be integrated to give:

$$E = \left(\frac{m+1}{m} \cdot \beta\right)^{-\frac{1}{m}} \cdot g(x)^{\frac{1}{m}} \left[\int_0^x g^{\frac{1}{m}}(x)\, dx\right]^{-\frac{1}{m+1}}$$

which can be expressed in terms of Nusselt number N as:

$$N = b^{\frac{1}{m+1}}\left[\frac{I^2 \rho_0 g(x)}{4\pi^2\left(\frac{h}{c_1}\right)_0^2 \sigma_0 \left(\frac{\rho_0}{2}\right)^{\frac{1}{2}}(h_0 - h_\infty)}\right]^{\frac{1}{m+1}}\left[\frac{g^{\frac{1}{m}}(x)}{\int_0^x g^{\frac{1}{m}}(x)\, dx}\right]^{\frac{1}{m+1}}\left[\frac{m}{m+1}\right]^{\frac{1}{m+1}} \tag{7.7}$$

From equation (7.1),

$$g(x) = u_0\left(\frac{\rho_0}{2}\right)^{\frac{1}{2}}$$

where ρ_o and u_o are the local values of density and velocity at 4,000°K.

The right hand side of equation (7.7) can then be written in terms of local non-dimensional parameters to give the solution:

$$N = \left[\frac{Nu\, R_e\, P_n}{4\pi^2} \cdot \frac{b\,(\rho_o u_o^2)^{\frac{1}{2m}}\, x}{\int_o^x (\rho_o u_o^2)^{\frac{1}{2m}}\, dx} \right]^{\frac{1}{m+1}} \left[\frac{m}{m+1} \right]^{\frac{1}{m+1}} \tag{7.8}$$

For N > 1000, $\int_o^1 s_i n d_i = 0.7$ and from figure 19,

$b = 0.058$ and $m = 0.68$.

Thus for a known pressure distribution, the distribution of N along the arc can be obtained for a particular set of flow conditions.

If the analysis is further restricted to incompressible flow, and the variation of power along the arc length is small, an analogy exists between the arc voltage and the velocity potential of the flow. In this case,

$$\rho_o = \text{constant},$$

$$\text{and } m = 1.$$

With these assumptions equation (7.6) becomes:

$$VE = \beta \cdot g(x)$$

which can be arranged in the form,

$$\int_o^V V\,dV = \beta \int_o^x g(x)\,dx, \tag{7.9}$$

when m = 1, β reduces to:

$$\beta = \frac{b\,(2\rho_o)^{\frac{1}{2}}(h_o - h_\infty)}{\sigma_o}, \quad \text{and with} \quad g(x) = \left(\frac{\rho_o}{2}\right)^{\frac{1}{2}} u_o,$$

equation (7.9) becomes:

$$V^2 = \frac{2\,b\,\rho_o (h_o - h_\infty)}{\sigma_o} \int_o^x u_o\,dx. \tag{7.10}$$

From the fluid velocity potential ϕ which satisfies Laplace's equation $\nabla^2\phi = 0$, the axial component of velocity is given by:

$$u_o = -\frac{\partial \phi}{\partial x}.$$

From this,

$$\phi - \phi_{x=0} = -\int_o^x u_o \, dx,$$

and equation (7.10) reduces to:

$$V^2 = -\frac{2k\rho_o(h_o - h_\infty)}{\sigma_o} \cdot (\phi - \phi_{x=0}) \qquad (7.11)$$

where $\phi_{x=0}$ is the velocity potential at the origin.

Hence for incompressible flow, the arc voltage distribution can be obtained directly from velocity potential distributions. The value of k must be selected to suit the power range of the arc, which can be estimated from the solution given by equation (7.8).

7.2. Solution for a linear pressure gradient arc:

As discussed in section 4.3, the arc with a pressure gradient increasing linearly along the axis has a solution such that the voltage gradient is independent of the axial length. Cowley [51] shows that such a solution exists even when the full flow equations are used. Thus $E = \frac{V}{x}$, and the integral form of the energy equation can be solved directly over the whole power range.

Taking the linear pressure gradient distribution

$$f(x) = ax,$$

$$\left[\int_o^x f(x)\,dx\right]^{\frac{1}{2}} = x\left(\frac{a}{2}\right)^{\frac{1}{2}}$$

The energy equation (7.3) then becomes:

$$\frac{1}{E} \cdot \frac{\int_o^\infty \rho_i^{\frac{1}{2}} h_i r_i \, dr_i}{\int_o^{r_i} \sigma_i r_i \, dr_i} = \frac{V}{x} \cdot \frac{\sigma_o}{(\rho_o a)^{\frac{1}{2}}(h_o - h_\infty)}$$

Writing $\frac{V}{x} = E$, and expressing the result in terms of Nusselt number N,

$$\frac{1}{N^2} \cdot \frac{\int_0^\infty \rho_1^{\frac{1}{2}} h_1 r_1 dr_1}{\int_0^1 \sigma_1 r_1 dr_1} = \frac{4\pi^2 \sigma_0 \left(\frac{k}{C_p}\right)_0^2 (h_0 - h_\infty)}{I^2 (\rho_0 a)^{\frac{1}{2}}} \qquad (7.12)$$

From the momentum equation (7.1),

$$(\rho_0 a)^{\frac{1}{2}} = \frac{\rho_0 u_0}{x},$$

where u_0 is the local velocity at 4,000°K.

Equation (7.12) can be written in the form

$$Nu\, R_e\, P_r = 4\pi^2 N^2 \frac{\int_0^1 \sigma_1 r_1 dr_1}{\int_0^\infty \rho_1^{\frac{1}{2}} h_1 r_1 dr_1} \qquad (7.13)$$

The conducting integral is given by figure 14, and the enthalpy integral by equation (7.3). From these the solution can be calculated and is shown in figure 21, where it can be seen that the power loss from the nozzle arc is considerably greater than for the constant pressure flow case. In comparing the two cases it should be remembered that for the nozzle arc, the velocity at 4,000°K is approximately three times the cold flow velocity. The increased power loss from the nozzle flow arc is due to the increase in velocity in the high temperature region which gives a greatly increased enthalpy flow.

For the case of a nozzle with sonic exit conditions, increasing the current increases the arc temperatures, and hence the speed of sound and the enthalpy flow. The voltage gradient of such an arc with constant electrical conductivity

therefore increases slightly with increasing current, instead of remaining constant as for the constant pressure arc.

7.3. Comparison between the theory and experiment for arcs in nozzle flow:

Kirschstein and Koppelmann [26] and King [27] have published the results of detailed experiments on arcs in nozzle flow. The nozzle design is shown in figure 23 which also shows the measured flow distribution along the axis. The flow is of the 'divided blast' type, in which the gas flows into the annular space between the nozzles before dividing between the exits. By this means the arc is kept free of metal vapour and runs in pure gas. The flow distribution up to the sonic point approximates to the linear pressure gradient distribution of the theory and is taken as such. The published voltage gradients are also mean values between two voltage probes set at the sonic flow positions. The experimental measurements are shown in Table VI and compared with the theory on figure 21, where the Reynolds numbers are based on sonic flow conditions at 4,000°K. The agreement between the theoretical curve and the measurements is excellent at high power. At the highest powers the measurements fall slightly below the theory, although the results at different currents and pressures collapse to a single curve. Some deviation is to be expected, since in this region the theoretical curve involves an extrapolation of gas properties from 30,000°K to 50,000°K.

At low powers the experimental results of King [27] at 1 and 10 atmospheres pressure no longer collapse to a single curve, and they both lie above the theoretical curve. As shown in Chapter 5, departure from thermal equilibrium due to electric fields and radial temperature gradients is to be expected in this region.

8. SHOCK TUBE EXPERIMENTS

In order to test the theoretical model of the constant pressure arc a number of experiments have been carried out in this type of flow. The experiments were performed in a low Mach number shock tube with an axial arc held in the steady subsonic flow behind the initial shockwave.

The shock tube was found to be particularly suitable for this type of work, enabling the flow pressure and velocity to be varied independently. With subsonic flow behind the shock-wave, several milliseconds of steady flow were available for testing. Since the time constant of such gas blast arcs was known to be of the order of 100 microseconds, it was considered that the arc would reach steady state conditions within the flow time. By using a capacitor bank as a power source, the arc duration could be limited to the steady flow time. The short duration of the arc then made it possible to use small diameter electrodes without excessive erosion.

8.1. The shock tube:

The tube was 3 inches in diameter with a 10 ft driver section, a working section 10 ft from the diaphragm, and further 10 ft to delay the reflected shockwave. A double diaphragm system enabled the initial pressures to be accurately set, and the tube fired when required by releasing the pressure in a small space between the diaphragms. The layout of the shock tube and a block diagram of the associated electronics is shown in figure 24.

Shockwave speeds were measured by a pair of piezo-electric pressure gauges spaced 12 inches apart just before the working

section. After suitable amplification the output from these fired high speed trigger circuits which in turn operated a microsecond timer-counter. The signal from the first trigger circuit was also used to fire the arc initiation system after a suitable delay had been introduced. The accuracy of setting of the gauges in the mountings was ± 0.05 inches giving ± 0.4% error in the separation of 12 inches.

The gauge faces were 0.1 inches in diameter giving a shock transit time of 5 μsecs for a shock Mach number of 1.4. Typical gauge outputs reached full pressure in 5 to 7 μsecs at this Mach number and the trigger amplifiers fired within 1 μsec of the pressure traces starting to rise.

The working section was fitted with four $1\frac{3}{4} \times \frac{3}{4}$ inch Perspex windows and electrode bushings to isolate the tube from the electrical system. The electrodes were supported on aerofoil shaped struts, the downstream one being adjustable to a number of positions.

Power for the arc was provided by a pair of 5 kV capacitor banks, totalling 20 μF. These consisted of an oscillatory circuit and a resistance-capacitance circuit, connected in parallel to give about 2 milliseconds of D.C. current, followed by a sinusoidal decay to zero. With the maximum charging voltage of 5 kV this gave 48 amps for 2 milliseconds falling to zero after 5 milliseconds.

In the early stages of the work, described in reference 59, a plasma gun was used to initiate the arc. It was later found that with arc lengths greater than 4 cms excessive energy was

required to breakdown the electrode gap, causing large flow disturbances. The plasma gun was replaced by a fuse wire initiation system in which a spark gap was inserted between the H.T. electrode and the capacitor bank. A high voltage pulse, timed from the first shock speed measuring station, triggered the spark gap, blowing a fuse wire bridging the electrode gap. This system had the added advantage that the capacitor bank voltage was not applied to the measuring system until the instant the arc was struck. This enabled a low value resistance voltage divider to be used for measuring arc voltage. The divider used for the measurement was 100:1 ratio with 100 ohms in the lower end. The combined capacitance of the coaxial cable and oscilloscope amplifier was about 250 ppf. The response of this system was measured by replacing the electrode system with a vacuum switch. The voltage signal was recorded as the switch closed and was observed to fall from 5 kV to almost zero in about 20 μsecs. This was considered an adequate response time for the measurement of the main arcing voltages which were of the order of 100 volts.

The arc current was measured with a low inductance 0.05 ohm shunt of folded element construction having a frequency response up to 10 Mc/s. The downstream electrode was used as a common earth point for the system, and all mains supplies isolated from earth. The electrical circuit is shown in detail in figure 25 and the performance specifications of the individual pieces of electrical equipment shown in Table VII.

8.2. Performance of the shock tube:

The theory of the simple shock tube is well known, see for example reference 60, and only a brief description will be given here. The conditions behind a shockwave advancing into still gas are uniquely determined by the velocity of the wave front, and the conditions ahead of the wave. Across the shock wave there are step changes in velocity, pressure, and temperature. Following behind the shockwave is a second interface known as the contact surface, which represents the original position of the diaphragm. The pressure and velocity are continuous across the contact surface but there is a drop in temperature to below the initial condition. This is because the gas behind the contact surface has expanded from room temperature in the high pressure section. If a different gas is used in the high pressure section, there is a change in gas at the contact surface. The operation of the shock tube for ideal flow conditions is shown as a wave diagram in figure 26, which also shows the distribution of the flow parameters at a particular instant in time. In practice, the operation is complicated by viscous effects, which cause a boundary layer to build up on the tube walls behind the moving shock. This slows down the advancing shockwave, at the same time speeding up the contact surface until, if the tube is long enough they reach the same velocity. Under these conditions the running time reaches a maximum.

Mirels [61,62] has studied this effect for the two cases of laminar and turbulent boundary layer flow. He shows that the contact surface speeds up in order to make good the mass flow deficit caused by the stationary boundary layer.

The running time between the arrival of the shockwave and the contact surface was measured with a thin film heat transfer gauge mounted along the stagnation line of a probe on the tube centre line. These measurements are shown in figure 27 together with calculations based on the ideal theory, and Mirels [62] turbulent boundary layer theory. Although the latter is not strictly valid at low shock Mach numbers, it gives a good estimate of the running time. Mirels's figures indicate that for Ms = 2 the boundary layer has grown to about one third of the tube diameter by the end of the running time, whilst for Ms = 1.3 it is only about one tenth of the diameter. Thus for shock Mach numbers approaching 2 the flow behind the shock will tend to be non-uniform.

Once the shock Mach number is known, conditions behind the wave can be calculated from the Rankine - Hugoniot relations. The changes in flow across the shockwave are shown as a function of shock Mach number in figure 28. By selecting suitable values of initial pressure and shock speed, the flow velocity can be varied whilst keeping the pressure constant. This introduces a different freestream temperature for each velocity. The theory indicates that the arc voltages should be almost independent of the freestream temperature and this temperature change provides an additional parameter against which to check the theory.

8.3. High speed photography:

High speed photography proved to be a most valuable tool and two types of camera were used as an aid to understanding arc behaviour. Direct photography with a "Fastax" high speed cine camera enabled the whole current cycle to be photographed up to the rate of 16,000 pictures/sec.

The second camera used was an 'Imacon' image converter camera giving either 10^5 or 10^6 pictures/second. A number of separate pictures appear on the same film, the images being successively displaced to avoid overlapping. A typical film taken at 10^5 pictures/second is shown in figure 17 where the arc is arranged diagonally in order to make maximum use of the screen area. By this means up to 18 individual pictures can be obtained.

The voltage wave forms used to switch the electron beam are derived from oscillatory capacitor discharges. These wave-forms decay with time, causing the exposure of successive frames to increase. This decay also causes the pictures to overlap towards the end of the film. A slight fault developed with this camera and the image movement compensation was not correct, making alternate pictures blurred on some of the films.

8.4. Method of obtaining arc voltage distributions:

Due to the small diameter of the arcs investigated and their sensitivity to flow disturbances, it was not possible to use probes to measure the voltage distribution of a single arc. This had to be deduced from total voltage measurements on a succession of arcs of different lengths. As pointed out by King [9], care must be exercised in interpreting these as the voltage distribution of a single arc. If the arc has extensive non-uniform regions at both anode and cathode, the successive arc voltages do not give the correct voltage distribution for short arc lengths. If, however, one of the non-uniform regions is small compared with the arc length the resulting distribution is close to that of a single arc.

Photographs of the arc in the shock tube, figure 35, showed that there was no visible contraction of the arc at the downstream electrode. The measurements of a number of arcs of different lengths were thus taken to represent the voltage distribution of a single arc.

The theory of Chapter 6 shows that the column of the constant pressure axial flow arc is not uniform, but grows slowly in a downstream direction. This increase in diameter is accompanied by a fall in voltage gradient. The theoretical curve of figure 21 suggests that over a small power range, the voltage gradient distribution can be represented by a simple power law. To obtain the voltage gradient distribution, a logarithmic plot was made of the arc column voltages against arc length. These were found to approximate to power law relationships, and the voltage gradient distributions were then obtained by differentiation. A value of 20 volts was taken as the combined anode and cathode voltage drops and subtracted from the total arc voltage to obtain column voltage. This was the value obtained with almost zero arc gap and agrees with the earlier measurements of reference 59. In most cases the electrode drops were only a small proportion of the total column voltage. For the majority of the tests the upstream electrode was the cathode, as this gave the steadiest arc voltage records and least electrode erosion.

8.5. Attainment of steady state arcing conditions:

In view of the relatively short duration of the D.C. current pulse it was necessary to test whether the arc reached a steady state within the available arcing time. Since convection plays a significant part in the energy balance, the time to reach steady state conditions was expected to be of the order of the flow time

over the arc length. The flow speed varied between 10^4 and 3×10^4 cm/sec, which with arc lengths between 0.5 and 5 cms, gave transit times of between 16 and 500 μsecs. The arc was considered to be representative of the steady state when the arc voltage-current characteristics were independent of peak current for a particular set of conditions.

Tests were carried out at two different frequencies, one giving 1 msec of D.C. current and the other 2 msec of D.C. current. Voltage-current characteristics were measured for different peak currents for both circuits. Figure 29 shows the voltage-current characteristics of a 3.5 cm long arc at a flow speed of 9×10^3 cms/sec and 2 atmospheres pressure. It can be seen that for the higher frequency circuit there is a marked dependence of the characteristics on peak arc current. For the lower frequency circuit the voltage-current characteristics for two values of peak current are similar. The higher frequency measurements were carried out for air, whilst the lower frequency tests were done in nitrogen. The low dissociation temperature of oxygen, and the subsequent retention of the narrow core down to low currents gives the arc core a faster time constant in air than in pure nitrogen.

The lower frequency circuit was considered adequate for the main investigation in nitrogen. At each flow condition, tests were carried out with 50 and 20 amps peak current. The current at which the voltage-current characteristics of the two peak currents differed appreciably was taken to be the lowest value for which the arc could be considered as steady state.

8.6. The effect of electrode design on arc behaviour:

The main problems encountered in this work were those of providing stable flow conditions in the arc, and finding a satisfactory downstream electrode design. As shown in reference 59, the downstream arc root tends to be blown along the downstream electrode by the gas flow, and then short across to the electrode tip. This gives the arcing voltage a series of sawtoothed irregularities and makes voltage gradient measurement difficult since the exact arc length is not known.

The shape shown in figure 30 was developed to overcome this arc shorting problem. The electrode itself is a streamlined aerofoil in the form of a swept forward wing made from pure tungsten. The inward flow along the wing surface keeps the arc in the centre, and the double current feed minimises the magnetic forces. The wing section is reduced in thickness at the centre to cause as little flow disturbance as possible. This system eliminated the arc shorting problem, providing that the upstream region of the arc was stable.

The design of the upstream electrode also proved to be of great importance in obtaining reliable results. In order to record the true effect of changes in gas flow on the arc, the upstream electrode should be small compared with the arc diameter, so that the arc is not running within the electrode wake. Because of the small diameter of the arc, this is difficult to achieve in practice, since too small an electrode results in burning which introduces disturbances into the arc.

To determine the effect of the electrode wake on the arc, three upstream electrode designs were tested and these are shown

in figure 30. The voltage distributions obtained with system number 1 are shown in figure 31 and contrary to the theoretical model are almost linear, as were those of the initial experiments of reference 59 obtained with 0.32 cm diameter electrodes. The results with the second electrode system are shown on figure 32 where the voltage gradient can be seen to decrease along the length of the arc. The third electrode, number 3, was even further reduced in size, but due to its fragile nature only a limited number of tests were performed. These are also shown on figure 32 for 4.8 cm and 0.8 cm arc lengths, and there is no significant difference from the results obtained with electrode number 2. The measurements at 0.8 cm arc length showed occasional disturbances, probably caused by bursts of electrode material, as this showed signs of melting. These comparisons suggested that the second electrode system was small enough for the arc to be free of wake effects, except at low currents, and was used for the main test programme.

The effect of the wake on the arc voltage distribution can be explained as follows. Within the wake, and particularly close to the electrode, the flow velocity is less than the freestream velocity, returning to this value further downstream. If the arc lies within this region it will experience an accelerating flow and the downstream portions of the arc will experience more convection than the upstream region. This tends to raise the voltage gradient of the downstream region, giving an almost linear voltage distribution.

Having eliminated the major wake effects, it was found that the arc was subject to instability unless great care was exercised in shaping the upstream electrode itself. For the range of flow conditions investigated, the Reynolds number of the upstream electrode

length varied between 2.5×10^5 and 10^6. This is the critical Reynolds number range for transition from laminar to turbulent flow over the length of the electrode. This flow stability problem is illustrated in figure 33 which shows two electrode tips, one of which (a), produced violent instability with certain flow conditions, whilst the other, (b) gave a stable arc. It can be seen that the latter has eroded evenly, leaving a small conical tip on the electrode.

Figure 34 shows image converter photographs of arc instability with electrode (a) for two flow conditions. The lower Reynolds number condition shows a complex disturbance and break up of the arc. This probably originates from an unstable flow separation from the rear of the electrode. At the higher Reynolds number the arc has taken on a turbulent appearance. The measured arc voltage with this turbulent condition was little different than with a stable arc, except that it was not so steady. Figure 35 shows sections from a "Fastax" cine film taken with electrode (b). The arc remains quite steady over the first 1.5 cms of length with a slight snaking action over the rear half. The conical shape of the downstream end is caused by the hot gas blowing over the downstream electrode and is not part of the arc proper.

It was also found that the timing of the arc initiation with respect to the shockwave influenced arc stability. If the arc was initiated too soon before the shock arrived, the arc tended to bow sideways and with the longer arc lengths it was several hundred microseconds before the voltage settled down to a steady value. Satisfactory results were obtained when the spark gap was initiated about 100 microseconds before the arrival of the shockwave. An oscilloscope record of the arc voltage during the initiation period is shown in figure 36, together with image converter camera pictures

of the fuse blowing. Initially, the wire resistance increases slowly due to heating, followed by a rapid rise in voltage as the wire melts and after about 100 microseconds the arc forms.

This arc is initially small in diameter, and it expands to a steady diameter in the flow. The shockwave was timed to reach the upstream end of the arc just after the peak in the voltage trace. The onset of the shockwave makes little change on the voltage record in the early stages of arc development where the voltage is already high. This contrasts with the sudden rise in arc voltage if the arc is allowed to become fully developed before the shockwave reaches it. This was the case in the work with the plasma gun initiation system, where the arc burnt for some time in the still gas [59].

Due to the short duration of the arc, the electrodes do not reach a steady temperature during the test and this can influence the cathode mechanism. Thoriated tungsten was used as the upstream electrode in order to reduce the temperature required for thermal emission. For certain tests with 20 amps peak current a sudden drop of about 8 volts occurred during the D.C. arcing period. This drop is possibly due to a change from a field type cathode mechanism to a thermal emission mechanism as the electrode heats up. A voltage record showing this effect is shown in figure 37. The voltage change is only significant for short arc lengths and only occurred in a few cases.

A similar increase of about 8 volts was found when the polarity was reversed. The cathode then becomes the downstream electrode, and the arc root was continually swept over the surface which remained relatively cool.

8.7. The effect of flow conditions on arc voltage distribution:

Having obtained a satisfactory electrode system, and established that the arc was reasonably free of wake effects, the arc voltage distribution was determined for a number of flow conditions. By a suitable choice of initial conditions, shock Mach numbers were selected such that the absolute pressure behind the shockwave remained at 2 atmospheres, whilst the flow velocity was varied. This value of pressure was chosen because the corresponding pressure differences gave reliable operation of the double diaphragm system over the required Mach number range. These conditions and the resulting flow, are shown in Table VIII. It was felt that the gas properties would be sufficiently close to those at 1 atmosphere for the theoretical calculations to be valid. For comparison a set of results was taken at one atmosphere pressure with a velocity such that the arc Reynolds number was the same as for one of the 2 atmosphere conditions.

The arc current and voltage were measured for 7 arc lengths between 0.5 and 6 cms at each flow condition. For lengths up to 2 cm, two tests were taken at each setting and three or more tests repeated for the longer lengths. The majority of tests were done with about 50 amps peak current with a fewer number of arc lengths repeated at 20 amps peak. This was found to be the lowest current at which satisfactory fuse blowing was obtained with arc lengths greater than 2 cms.

Typical current and voltage records are shown in figure 38 and it can be seen that the arcing voltages are reasonably free of disturbances. The slight downward deflection in the centre of the voltage trace is due to a weak shockwave reflected from a join at the downstream end of the working section.

With the particular circuit used for the arc power supply, the R - C element which supplies current in the early part of the cycle, acts as a shunt capacitance across the arc at current zero. This slows down the voltage recovery transient after current zero and prevents the series spark gap re-igniting and the electrode then falls rapidly to earth potential. The oscilloscope is triggered before the arc is struck and the records show zero levels immediately before and after the test, providing a check on any drift in the oscilloscope zeros.

Having obtained a set of records, current and voltages were measured throughout the current cycle. In this analysis, the minimum points of the small variations in arcing voltage were taken, it being assumed that this corresponded to the minimum arc length between the electrodes. Voltage - current characteristics were then plotted for each arc length, and a smooth curve drawn, again through the minimum region of the points, figures 39 to 41. This date was considered satisfactory as long as the points from the 50 and 20 amps peak current coincided. For the highest shock Mach number of 1.8 the useful data were limited to the D.C. period of current by arrival of the contact surface.

The arc column voltage - length distributions are shown as logarithmic plots in figures 42 to 45. These can be approximated by simple power law distributions of the form

$$V = a_1 x^{m_1}$$

The voltage gradient distribution can be obtained by differentiation to give

$$E = a_1 m_1 x^{m_1 - 1}$$

The values of a_1 and m_1 obtained in this manner are shown in Table IX.

The values of the index m_2 found in these experiments are less than 1, indicating that the voltage gradient decreases with increasing arc length, as predicted by the theory. This is confirmed by the photographs of the arc shown in figure 35, where at low currents the luminosity can be seen to decrease along the length of the arc. At the higher current the photographs are over exposed and the effect is not so clear. In general it was found that the value of the index decreased with increasing arc power as predicted by the theory. Figure 46 shows m_2 as a function of power gradient.

The results have finally been reduced to non-dimensional form and are compared with the theoretical curve in figure 47. The agreement with the theory can be considered to be satisfactory, the results collapsing with a maximum scatter of $\pm$ 10% with most of the points within $\pm$ 5%.

The variation of power gradient with current, velocity, and arc length are all consistent with the theoretical model, the rates of change of power input with these parameters increasing as the overall power gradient increases. For all the flow conditions the points for the maximum current lie slightly above the others. This may be an electrode effect, the lower current arcs lying within the wake and being slightly sheltered from the main flow. Likewise, the voltage gradients increase slightly more rapidly with velocity than predicted, again possibly due to a narrowing of the wake as the flow velocity increases.

These last two features are displayed to a somewhat greater degree by the results obtained by Rowe[28] from a similar shock tube experiment. His experiments were carried out at 1 atmosphere pressure, but with larger electrodes (0.32 to 0.16 cms dia.) and consequently the

arc is influenced to a greater extent by the electrode wake. The voltage distributions were linear, as were the results of figure 31 with similar sized electrodes. Figure 32 compares these results (electrode No.1) with those of the final electrode system, and it can be seen that the mean voltage gradient of the arc with the larger electrode is the same as the wake free results at about 2 cms arc length.

In figure 48, Rowe's results (Table X) have been reduced to non-dimensional form using a characteristic arc length of 2 cms. The collapse of the data is not so good as the present results, but still lies close to the theoretical characteristic. As noted earlier, the discrepancies here are similar to those in the present experiments, but more pronounced.

The high voltage gradients of arcs in forced convection have often been attributed to turbulent heat transfer. Frind[30] has carried out measurements on arcs confined in long tubes under conditions of both laminar and turbulent flow. It was found that the arcs in turbulent flow had voltage gradients about five times greater than those in laminar. However, in order to achieve turbulent flow, the mass flow had to be increased by a factor of 70. As has been shown in the present work, high mass flow rates in themselves lead to increased voltage gradients.

In the shock tube, either laminar or turbulent flow arcs could be obtained under the same freestream condition by slight changes in electrode design. The photographs in figure 34 show an arc in turbulent flow generated by the upstream electrode wake. The voltages of these arcs did not differ appreciably from those of laminar flow arcs under the same freestream conditions. The theoretical analysis shows that the voltage gradient arises mainly from the increasing energy flux through

the growing electrically conducting column, and not from large conduction losses across its boundary. If the components of velocity introduced by the turbulence are small, compared with the freestream, the mean overall energy balance will be unchanged.

9. CONCLUSIONS

(1) A study of existing theories of cylindrical nitrogen arc columns shows that there is a close similarity between the radii of arcs with different forms of radial heat loss. This includes those with an appreciable proportion of radiation loss and with radial convection losses. This similarity takes the form of an almost unique relationship between the arc power gradient EI, and the radius characteristic $E\pi o$. This relationship can be calculated from the simple Elenbaas-Heller equation containing radial conduction as the only form of heat loss. This enables the radius of an arc to be expressed in terms of voltage gradient and current alone, without considering in detail the energy exchange mechanisms within the electrically conducting column.

(2) A simplified theoretical model of the steady state axial flow arc has been developed which shows that each particular flow geometry can be represented by a unique non-dimensional arc characteristic. The model is based on an integral form of the flow equations and the flow is considered to be laminar throughout. The arc is divided into two regions, the electrically conducting core and an outer thermal layer. The latter is represented by a simple power law distribution of gas properties, and by matching certain of the boundary conditions the energy content of the layer is related to the local power gradient. Using the arc radius characteristic described in (1), the radius of the electrically conducting core can be expressed in terms of voltage gradient and current alone and the overall energy balance reduces to a simple first order differential equation.

It is shown that this method of solution is insensitive to the actual shape of the temperature profiles. This is important where the outer layer is concerned as the shape of the profile has to be selected in an arbitrary manner. The solution gives the dependent Nusselt number of the arc, defined as:

$$N = \frac{EI}{2\pi \left(\frac{h}{c_p}\right)_o (h_o - h_\infty)}$$

as a unique function of the non-dimensional group.

$$\frac{\rho_o u_o I^2}{\left(\frac{h}{c_p}\right)_o^2 (h_o - h_\infty) \sigma_o x}$$

The reference conditions, denoted by the subscript o are taken at 4,000°K which is selected as the boundary of the electrically conducting arc column.

Theoretical solutions are presented in figure 21 for two special cases of the nitrogen flow arc; constant pressure, uniform velocity flow, and flow with a linearly increasing pressure gradient along the axis. The latter is of particular interest to the circuit breaker designer as it represents an arc in a nozzle flow closely approaching those used in practice. Using the curves of figure 21, the voltage gradient of a nitrogen arc in either of these flow situations can be calculated for given values of arc current and length, gas velocity and density.

In general it is found that the solutions are dominated by the electrically conducting region. In the case of the constant pressure flow arc, the velocity remains constant across the arc area and the required increase in energy flux is obtained by an increase in arc core diameter.

For the particular nozzle flow shown, $\frac{u_e}{x}$ is constant, the arc diameter remains unchanged, and the increase in energy flux arises from the increase of flow velocity with arc length. The pressure gradient causes the flow velocity of the heated gas to increase above the freestream value, giving an increase in energy flux compared with the constant pressure flow case.

Since the energy gradients are accounted for by the region above 4,000°K, it follows that little of the arc energy losses can penetrate beyond this temperature, and therefore convection must assume a dominant role in the outer parts of the electrically conducting core. The heat is thus carried back into the interior of the arc and is finally carried away in an axial direction. The importance of the radius characteristic described earlier lies in the fact that when convection is important within the electrically conducting core, its radius can still be expressed in terms of arc voltage gradient and current alone.

The theoretically calculated arc characteristics show good agreement with measured arc voltage gradients and account for the known features of arcs in axial flow. The high energy losses of arcs in nozzle flow can thus be accounted for entirely on the basis of laminar flow processes, and it is not necessary to introduce the concept of turbulence to explain them.

Over limited power ranges, the solutions can be represented by simple power laws whose indices vary from 0.6 for the nozzle arc, down to 0.2 for the low power constant pressure flow arc. In the high power range the theoretical solutions confirm the generally accepted rules that the voltage gradient is independent of current, and increases approximately as the square root of the

pressure. The solutions also show that as long as the thermal energy of the main flow is small compared with that of the electrically conducting arc column, the arc voltage gradient is independent of the temperature of the main flow.

Using a shock tube, the constant pressure d.c. axial flow arc has been investigated experimentally between 400 and 2,000 Watts/cm. Voltage distributions along the arc axis were obtained for the following flow conditions:-

flow velocity cm/sec	static pressure atmos.
9×10^3	2
2×10^4	2
3×10^4	2
2×10^4	1

The measured arc characteristics showed good agreement with the theoretical solution, although great care was necessary to minimise the effect of the upstream electrode wake.

The linear pressure gradient solution has been compared with published measurements up to 4.5×10^5 Watts/cm, and good agreement obtained for powers above 5×10^3 Watts/cm. Below this level the published measurements of King [27] at 1 and 10 atmospheres pressure no longer collapse to a single curve, although the 1 atmosphere results follow the theory down to 2×10^3 Watts/cm. Estimations of the requirements for thermal equilibrium suggest that these may be violated with the high electric fields and small diameters of low current nozzle arcs.

(3) The shock tube has proved an excellent tool for the investigation of electric arcs in constant pressure axial flow. With suitable electrode design, stable laminar flow arcs with velocities up to 3×10^4 cm/sec at 2 atmospheres pressure can be obtained, whose arc voltages are reproducible to $\pm$ 5%. By slight changes in electrode design either laminar or turbulent flow can be produced within the arc for the same freestream conditions. The arc voltages recorded under turbulent flow conditions were similar to those with laminar flow, except for a greater scatter in the results. The limits for laminar arc flow appear to be set by the design and Reynolds number of the upstream electrode rather than the arc itself.

10. Suggestions for Further Work

The ease with which the flow conditions can be controlled and the repeatability of the arc voltage measurements suggest that the shock tube would be an ideal tool for the investigation of the dynamic arc near current zero. It was shown in section 8.5 that with suitable combinations of current cycle time and gas flow, the arc voltage deviated from the d.c. characteristic, reproducing voltage records similar in shape to those of a gas blast circuit breaker approaching failure conditions. The point in time at which this deviation occurred depended strongly on the flow transit time along the arc. An investigation into the separate effects of velocity and pressure on the behaviour of the dynamic arc would be of great interest, as unlike the steady state arc, their effects are expected to differ considerably.

The success of the theoretical model in predicting the d.c. arc characteristics suggests its extension to the dynamic arc case. At low currents it was found that the outer thermal layer plays an increasingly important part in the energy balance. This is expected to play a significant part in the energy balance of the dynamic arc as the current approaches zero. In the present theory the extent and shape of the temperature profile of the outer layer is not well predicted and some experimental evidence would provide a useful guide.

Rowe[28] has used a pulsed ruby laser to obtain shadowgraphs of an axial flow arc in which the self luminosity of the arc was removed by filters. Although the general quality of the pictures was poor, they indicated the extent of the hot flow. With an

improvement in the optical technique much information about the flow could be obtained in this way.

It is a simple matter to change the working gas in the shocktube, and as this is confined to the low pressure section, relatively small quantities are consumed on each test. The steady state arc theory confirms that the voltage gradient of an arc in argon is considerably lower than that in nitrogen and some additional tests in argon would provide a useful check on the accuracy of the theory.

APPENDIX I

Computer programme for the solution of the fully developed arc column

Yos[33] presents a computer programme for integrating the cylindrical arc column, including the transparent radiation term.

The energy equation

$$\frac{1}{r}\frac{d}{dr}\left(r k \frac{dT}{dr}\right) + \sigma E^2 - P = 0$$

is integrated to give:

$$2\pi r k \frac{dT}{dr} + 2\pi\int_0^r \sigma E^2 r\, dr - 2\pi\int_0^r P r\, dr = 0 \qquad A_1.1$$

This equation is solved by dividing the arc into a number of annular elements of equal temperature difference. The elemental increments of electrical input, radiation, and conduction are defined as follows:-

$$dF = 2\pi \sigma_i E_i^2 r_i\, dr$$

$$dG = 2\pi P_i r_i\, dr$$

$$dQ = 2\pi\, d\left[r_i k_i \left(\frac{dT}{dr}\right)_i\right]$$

where the subscript i denotes the i^{th} element. The integrated quantities then become,

$$F_N = \sum_{T=T_c}^{T=T_N} 2\pi \sigma E^2 r\, dr$$

$$G_N = \sum_{T=T_c}^{T=T_N} 2\pi P r\, dr$$

$$Q_N = \sum_{T=T_c}^{T=T_N} 2\pi\, d\left[r k \frac{dT}{dr}\right]$$

Equation $A_1.1$ can then be written as,

$$Q_N = -(F_N - G_N)$$

The notation used in the programme differs in parts from the rest of the thesis and a separate list is given before the programme.

The programme computes the increment in radius, required to give a fixed temperature change ΔT. The gas properties are calculated at the midpoint of the temperature difference, T_{ii} The radial increment is given by,

$$\Delta r_N = r_N - r_{N-1} = \frac{2\pi r_{ii} k_{ii} \Delta T}{F_{ii} \quad G_{ii}} \qquad A_1.2$$

where the subscript ii denotes quantities evaluated at the midpoint temperature, T_{ii}. For small values of Δr_N

$$\Delta r_N = \frac{2\pi r_{ii} k_{ii} \Delta T}{0.5\left[F_N - G_N + F_{N-1} - G_{N-1}\right]}$$

As a first approximation

$$r_{ii} \simeq r_{N-1} + 0.5\,\Delta r_{EST.}$$

$$F_N \simeq F_{N-1} + 2\pi \sigma_{ii} E^2 r_{ii} \Delta r_{EST.}$$

$$G_N \simeq G_{N-1} + 2\pi P_{ii} r_{ii} \Delta r_{EST.}$$

where $$\Delta r_{EST.} = \frac{2\pi r_{N-1} k_{ii} \Delta T}{F_{N-1} - G_{N-1}}$$

The programme calculates the increment Δr_N and compares it with the estimated value $\Delta r_{EST.}$. The initial estimated value is then replaced by the new value Δr_N and the process repeated until the required accuracy is attained. This is expressed by the condition

$$\Delta r_N - \Delta r_{EST} > RTOL$$

where $RTOL$ is the symbol for the required tolerance.

Having found the radius increment the following quantities are calculated:-

$$r_N = r_{N-1} + \Delta r_N$$

$$F_N = F_{N-1} + 2\pi \sigma_{ii} E^2 r_{ii} \Delta r_{EST.}$$

$$G_N = G_{N-1} + 2\pi P_{ii} r_{ii} \Delta r_{EST.}$$

$$T_N = T_c - N(\Delta T).$$

u_{ii} sonic, $H_N = H_{N-1} + 2\pi \rho_{ii} u_{ii} h_{ii} r_{ii} \Delta r_{EST.}$

u_{ii} sonic, $M_N = M_{N-1} + 2\pi \rho_{ii} u_{ii} r_{ii} \Delta r_{EST.}$

$u_{ii} = 1$, $H_N = H_{N-1} + 2\pi \rho_{ii} h_{ii} r_{ii} \Delta r_{EST.}$

$u_{ii} = 1$, $M_N = M_{N-1} + 2\pi \rho_{ii} r_{ii} \Delta r_{EST.}$

In order to use the programme in its modified form for the calculation of the convection modified profiles of Appendix III, an additional input constant is required. This is the convection constant, $C = \frac{2 v_\infty}{r_0} \frac{dr_0}{dx}$, and using this, the radiation term is replaced by the term:

$$\frac{2 v_\infty}{r_0} \frac{dr_0}{dx} \left[h \int_0^r \rho r \, dr - \int_0^r \rho h r \, dr \right].$$

This becomes:

$$\frac{2 v_\infty}{r_0} \frac{dr_0}{dx} \left[h M_N - H_N \right]_{u_{ii} = 1.}$$

and is calculated once the increment in radius has been found.

SOLUTION OF FULLY DEVELOPED LAMINAR ARC COLUMN

A. IDENTIFICATION

Computer : KDF 9

Program No. : HBB414Ø

Title : Electric Arc

B. GENERAL DESCRIPTION

Purpose : From a table of gas constants, voltage and central temperature the conditions at each temperature step are calculated until the wall temperature is reached.

INPUT : (a) Gas constant table.

n; number of rows in table.

Temperature	σ mhos/cm	h w/cm/°K	P w/cm³	ρ gm/cm³	u cm/sec.	h Joules/gm.
T_1	σ_1	h_1	P_1	ρ_1	u_1	h_1
T_2	.	.	.	.	.	.
	.	.	.	.	.	.
T_n	σ_m	h_m	P_m	ρ_m	u_m	h_m

(b) T; number of central temperatures

T_1; T_2; T_3; ..... T_T;

E; number of voltage gradients

E_1; E_2; E_3; ..... E_E;

deltat; temperature step.

TW; wall temperature

unmark; =1 if u is constant 1;

=Ø if u is taken from tables;

=2 if both methods wanted;

conv; =1 if conversion applied;] Replaces radiation

=Ø no conversion applied;] by convection

RTOL; tolerance on radii calculations

FGTOL; tolerance on F - G

Marker; =1; if printing required at each step, otherwise $\emptyset$; -1; End data marker. If more data is to be input (a & b) delete -1 on all sets except last.

OUTPUT

WALL TEMPERATURE T_W

CENTRE TEMPERATURE T_1

VOLTAGE GRADIENT E

The output, for each voltage gradient at each temperature is produced using OUT-8 Stream 30.

T deg K	Radius R cm	Power input F Watts/cm	Radiation G Watts/cm	Enthalpy flow H u sonic, Watts	Mass flow M u sonic, gm/sec	Enthalpy flow H u = 1 Watts	Mass flow M u = 1 gm/sec
T_1	R_1	F_1	G_1	H_1	M_1	H_1	M_1
$T_1 - T$							
$T_1 - 2\ T$							
.							
.							
.							
T_L	R_L	F_L	G_L	H_L	M_L	H_L	M_L

where T_L is such that $T_L - T < T_W$

If printing at each step is not requested, only the row beginning T_L is printed.

C. METHOD OF USE

The program is in KALGOL and is stored on the POST MAST tape.

The call tape takes the form

```
K
HBB414Ø--KPU;
PROGAREA 38ØØ;
IN 8.
OUT L. →
```

VARIABLES

IDENTIFIER	TYPE	USE
rtol	real	Accuracy tolerance in radii
tw	real	Wall temperature
deltat	real	Temperature step
rest	real	Estimated step in radius
sig	real	Column 2 in gascon array
k	real	Column 3 in gascon array
pr	real	Column 4 in gascon array
pi	real	= 3.14159
ti	real	Temperature at mid point of laminar
r	real	Radius at mid point of laminar
r calc	real	Calculated step in radius
fgtol	real	Tolerance on f - g
rho	real	Column 5 in gascon array
u	real	Column 6 in gascon array
h	real	Column 7 in gascon array
rhoe	real	Constants used in calculation of enthalpy and mass flow
ue	real	
he	real	
c	real	Constant used in ga + equation, = $2\frac{\nu_\infty}{r_0}\frac{dr_0}{dx}$
fi	integer	Integer output format
fr	integer	Real output format
nt	integer	Number of rows in gascon array
i	integer	Controlled variable in for loops
j	integer	
n	integer	
a	integer	Current array position of ta, ra, fa, ga, ha and ma

VARIABLES (Cont'd.)

IDENTIFIER	TYPE	USE
b	integer	Previous array position of ta, ra, fa, ga, ha and ma
c	integer	Temporary store for a
t	integer	Number of central temperatures
ne	integer	Number of voltage gradients
	integer	Controlled variable in for loops
d	integer	Loop counter (1-30)
itd	boolean	Print marker. All rows printed if itd = true
conv	boolean	ga + marker. Extra added on to ga(a) if conv = true
ha	array	1:2 Present and previous enthalpy values
ma	array	1:2 Present and previous mass flow values
ta	array	1:2 Present and previous temperatures
fa	array	1:2 Present and previous joule heating
ra	array	1:2 Present and previous radius
ga	array	1:2 Present and previous radient energy loss
gascon	array	1:nt, 1:7 Array which holds gas constants
tc	array	1:t Array for holding central temperatures
e	array	1:ne Array for holding voltage gradients

BLOCK STRUCTURE

```
begin library AØ, A6
    procedure interp
    begin for a given temperature locates next row in gascon array
        Calculate proportion of step for interpretation
        Calculate sig, k, pr, rho, u, h at required temperature
    end interp
    Declare real, integer, boolean and array.
    Open read and write streams.  Declare output formats
    Declare pi
L:  Read nt.  If -ve got to FINISH
    begin Declare gascon array.
        Read gas constants table
        Read number of central temperatures
        begin Declare temperatures array
            Read central temperatures
            Read number of voltage gradients
            begin Declare voltage array
                Read voltage gradients
                Read temperature step
                Read wall temperature and print
                Read rhoe, ue and he, rtol + fgtol, print option
                For each voltage at each temperature
                begin Print central temperature and voltage gradient
                    Define array positions a = 1, b = 2
                    Laminar temperature = central temperature
                    Calculate temperature at middle & outside of laminar
                    Procedure interp
                    Calculate inside laminar radius, joule heating,
                    radient energy loss, enthalpy and mass flow.
                    Print heading.  If print option
                    begin Print inside temperature, radius, joule,
                        heading, radient energy loss, enthalpy & mass
                    end
```

BLOCK STRUCTURE (Cont'd.)

```
        If joule heating - energy loss  fgtol go to FAILI
L4.     Reverse array positions a & b (i.e. next laminar)
        Calculate temperature at middle and outside
        Procedure interp
        Estimate radius step.  Loop count = 0
L3.     Calculate middle radius
        Calculate outside joule heating and energy loss
        If difference   fgtol go to FAILI
        Calculate radius step
        If real c - rest  rtol
        begin rest = rcalc.  Loop count + 1
              If loop count   30 go to FAIL2
              Go to L3
        end
        Calculate outside joule heating, energy loss
        enthalpy and mass flow
        If print option or last temperature
        begin Print temperature, radius, joule heating
              energy loss, enthalpy and mass flow
        end
CALCULATIONS:  If temperature - temp step   wall temp
        go to L4
PRINT: go to L5
FAILI: Print message
FAIL2: Print message and partial results
L5:     end
        go to L
    end
  end
end
FINISH : close streams
end
```

```
begin
library
          comment A6,A14,A30;
procedure interp(gascon,sig,k,pr,rho,u,h,t,nt);
value t,nt;
real sig,k,pr,t,rho,u,h;
integer nt;
array gascon;
begin real factor;
     integer i;
     for i:=1 step 1 until nt do
     if t<gascon[i,1]then goto L;
     i:=nt;write text(30,[2"=*]);
          write(30,format([-d.ddd␣nd]),t);write text(30,[[e]
                                                        1]);
          L:factor:=(t-gascon[i-1,1])/(gascon[i,1]-gascon[i-1
                                                        ,1]);
     sig:=factor×(gascon[i,2]-gascon[i-1,2])+gascon[i-1,2];
     k:=factor×(gascon[i,3]-gascon[i-1,3])+gascon[i-1,3];
     pr:=factor×(gascon[i,4]-gascon[i-1,4])+gascon[i-1,4];
     rho:=factor×(gascon[i,5]-gascon[i-1,5])+gascon[i-1,5];
     u:=factor×(gascon[i,6]-gascon[i-1,6])+gascon[i-1,6];
     h:=factor×(gascon[i,7]-gascon[i-1,7])+gascon[i-1,7];
end interp;
```

```
            real rtol,tw,deltat,rest,sig,k,pr,pi,
                        ti,r,rcalc,fgtol,rho,u,h,rhoe,ue,he,C,u2;
            integer fi,fr,nt,i,j,n,a,b,c,t,ne,l,d,umark;
            boolean itd,conv;
            array ha,ma,ha2,ma2,ta,fa,ra,ga[1:2];
open(20);open(30);
fi:=format([sss-ddddddddd]);fr:=format([s-d.dddd₁₀-nd]);
write text(30,[return*to*joyce*rowe[p]]);
pi:=3.14159235659;
            L:write text(30,[[c]]);
                copy text(20,30,[??]);
                write text(30,[[c]]);
                nt:=read(20);if nt<0 then goto FINISH;
begin array gascon[1:nt,1:7];
for i:=1 step 1 until nt do
for j:=1 step 1 until 7 do
gascon[i,j]:=read(20);
t:=read(20);
    begin array tc[1:t];
    for i:=1 step 1 until t do
    tc[i]:=read(20);
    ne:=read(20);
            begin array e[1:ne];
            for i:=1 step 1 until ne do
            e[i]:=read(20);
            deltat:=read(20);
            tw:=read(20);write text(30,[*wall*temperature]);
            write(30,fr,tw);
```

```
        umark:=read(20);
        if read(20)=1 then
             begin conv:=true;C:=read(20);
        write text(30,[[2c10s]conduction*and*convection[c]]);
             write text(30,[[c10s]convection*constant*=*]);
             write(30,format([-d.dddd##nd]),C);
             end else
             begin conv:=false;
write text(30,[[2c10s]conduction*and*radiation*only[c]]);
             end;
             if umark=2 and conv then
             begin write text(30,[[c]values*of*umark*and
             *conv*incorrect[p]]);goto L;
             end;
             rtol:=read(20);fgtol:=read(20);
             if read(20)=1 then itd:=true else itd:=false;
             for j:=1 step 1 until t do
             for l:=1 step 1 until ne do
begin write text(30,[[2c]centre*temperature]);
             write(30,fr,tc[j]);
write text(30,[[2c]**voltage*gradient]);write(30,fr,e[l]);
             a:=1;b:=2;
             ta[b]:=tc[j];
             ti:=ta[b]-5;ta[a]:=ta[b]-10;
             interp(gascon,sig,k,pr,rho,u,h,ti,nt);
             if umark=1 then u:=1 else if umark=2 then
                  begin u2:=u;u:=1;
                  end;
                  ra[a]:=sqrt(40xk/(e[l]↑2xsig-pr));
                  fa[a]:=pixra[a]↑2xe[l]↑2xsig;
                  ga[a]:=pixra[a]↑2xpr;
                  ha[a]:=rhoxuxhxra[a]↑2xpi;
                  ma[a]:=rhoxuxra[a]↑2xpi;
```

```
                if umark=2 then
                    begin ha2[a]:=rhoxu2xhxra[a]↑2xpi:
                    ma2[a]:=rhoxu2xra[a]↑2xpi;
                    end;
                if umark=0 then
                write text(30,[[c50s](u*sonic*from*tables)])else
                write text(30,[[c50s](u*constant*=1)]);
if umark=2 then write text(30,[[10s](u*sonic*from*tables)]);
                write text(30,[[2c64s]mass]);
                if umark=2 then write text(30,[[21s]mass]);
            write text(30,[[c20s]power[10s]enthalpy[5s]flow]);
            if umark=2 then write text(30,[[7s]enthalpy[5s]flow]);
                write text(30,[[c10s]radius[5s]input[5s]]);
                if conv then write text(30,[convection])else
                write text(30,[radiation*]);
                write text(30,[[3s]flow[15s]]);
                if umark=2 then write text(30,[[5s]flow]);
            write text(30,[[c5s]t[11s]r[11s]f[11s]s[11s]h[11s]m]);
            if umark=2 then write text(30,[[11s]h[11s]m]);
            write text(30,[[c3s](deg.k)[7s](cm)[5s]
            (watts/cm)[2s](watts/cm)
                [4s](watts)***(gms/sec)]);
if umark=2 then write text(30,[[4s](watts)[5s](gms/sec)]);
                write text(30,[[2c]]);
```

```
        if itd then
        begin
        write(30,fr,ta[a]);write(30,fr,ra[a]);
        write(30,fr,fa[a]);write(30,fr,ga[a]);
        write(30,fr,ha[a]);write(30,fr,ma[a]);
        if umark=2 then
    begin write(30,fr,ha2[a]);write(30,fr,ma2[a]);
            end;
            write text(30,[[c]]);
        end;
        if fa[a]-ga[a]<fgtol then goto FAIL1;
        L4:c:=a;a:=b;b:=c;
    ti:=abs(ta[b]-0.5xdeltat);ta[a]:=ta[b]-deltat;
        interp(gascon,sig,k,pr,rho,u,h,ti,nt);
    if umark=1 then u:=1 else if umark=2 then
        begin u2:=u;u:=1;
        end;
        rest:=(2xpixra[b]xdxdeltat)/(fa[b]-ga[b]);
        d:=0;
        L3:r:=ra[b]+0.5xrest;
        fa[a]:=fa[b]+2xpixsigxe[1]↑2xrxrest;
        ga[a]:=ga[b]+2xpixprxrxrest;
```

```
            if conv then ga[a]:=C*ha[b]-C*h*ma[b];
            if fa[a]-ga[a]<fgtol then goto FAIL1:
rcalc:=2*pi*r*l*deltat/(0.5*(fa[a]-ga[a]+fa[b]-ga[b]));
            if abs(rcalc-rest)>rtol then
            begin rest:=rcalc;
            d:=d+1;if d>30 then goto FAIL2;
            goto L3;
            end;
            ra[a]:=ra[b]+rcalc;
            ha[a]:=2*pi*rho*u*h*rest*r+ha[b];
            ma[a]:=2*pi*rho*u*r*rest+ma[b];
            if umark=2 then
            begin
            ha2[a]:=2*pi*rho*u2*h*r*rest+ha2[b];
            ma2[a]:=2*pi*rho*u2*r*rest+ma2[b];
            end;
            if itd or ta[a]-deltat<tu then
            begin write(30,fr,ta[a]);write(30,fr,ra[a]);
            write(30,fr,fa[a]);write(30,fr,ga[a]);
            write(30,fr,ha[a]);write(30,fr,ma[a]);
            if umark=2 then
                begin
            write(30,fr,ha2[a]);write(30,fr,ma2[a]);
                end;
                    write text(30,[[c]]);
            end;
```

```
                CALCULATIONS:
                    if ta[a]-deltat≥tw then goto L4;
                    PRINT:goto L5;
                    FAIL1:write text(30,[[2c]F-G diverges]);
              write(30,fr,fa[a]);write(30,fr,ga[a]);goto L;
              FAIL2:write text(30,[[2c]RADIUS*NOT*CONVERGING]);
              write(30,fr,rcalc);write(30,fr,rest);write(30,fr,ra[a]);
                    write(30,fr,ra[b]);
                    L5:end;
                    goto L;
              end;
              end;
              end;
              FINISH:close(20);close(30);
end
```

APPENDIX II

The derivation of the energy equation in integral form

The method of solution adopted for the axial flow arc equations utilises the equations of motion in integral form. The derivation of this form of the equations is given in standard text books [54,55], but is presented here for the energy equation, as the same mathematical techniques are employed for the arc model of Appendix III.

The continuity equation,

$$\frac{\partial(\rho u r)}{\partial x} + \frac{\partial(\rho v r)}{\partial r} = 0$$

on integration gives,

$$\rho v = -\frac{1}{r}\int_0^r r \frac{\partial(\rho u)}{\partial x}\, dr. \qquad A_2 \cdot 1$$

Substituting this into the energy equation

$$\rho u \frac{\partial h}{\partial x} + \rho v \frac{\partial h}{\partial r} = \frac{1}{r}\left(r \frac{k}{c_p} \frac{\partial h}{\partial r}\right) + \sigma E^2$$

and integrating, gives:

$$\int_0^\infty \rho u r \frac{\partial h}{\partial r}\, dr - \int_0^\infty \frac{\partial h}{\partial r}\left[\int_0^r r \frac{\partial(\rho u)}{\partial x} dr\right] dr = \left[r \frac{k}{c_p} \frac{\partial h}{\partial r}\right]_0^\infty + E^2 \int_0^\infty \sigma r\, dr. \qquad A_2 \cdot 2$$

From considerations of symmetry, $\frac{\partial h}{\partial r} = 0$ at r = 0, and the boundary condition of zero heat flow at infinity gives $r \frac{\partial h}{\partial r} = 0$ at $r = \infty$.

Hence: $\left[r \frac{k}{c_p} \frac{\partial h}{\partial r}\right]_0^\infty = 0$

Integrating the term $\int_0^\infty \frac{\partial h}{\partial r}\left[\int_0^r r \frac{\partial(\rho u)}{\partial x} dr\right] dr$ by parts,

$$\int_0^\infty \frac{\partial h}{\partial r}\left[\int_0^r r \frac{\partial(\rho u)}{\partial x} dr\right] dr = \left[\int_0^r dh\right]_0^\infty \cdot \left[\int_0^r r \frac{\partial(\rho u)}{\partial x} dr\right]_0^\infty - \int_0^\infty \left[\int_0^r dh\right] r \frac{\partial(\rho u)}{\partial x} dr.$$

which, with the boundary conditions

$$h = h_c \text{ AT } r = 0 \text{ AND } h = h_\infty \text{ AT } r = \infty$$

becomes:

$$\int_0^\infty \frac{\partial h}{\partial r}\left[\int_0^r r \frac{\partial(\rho u)}{\partial x} dr\right] dr = \int_0^\infty (h_c - h) r \frac{\partial(\rho u)}{\partial x} - (h_c - h_\infty)\int_0^\infty r \frac{\partial(\rho u)}{\partial x} dr$$

Substituting this into the energy equation and using Ohm's Law in the form:

$$2\pi E^2 \int_0^\infty \sigma r \, dr = E I$$

equation (A_2.2) reduces to the form:

$$2\pi \frac{d}{dx}\int_0^\infty \rho u (h - h_\infty) r \, dr = I \frac{dV}{dx}$$

where the voltage gradient E is written as $\frac{dV}{dx}$.

This can be integrated to give:

$$2\pi \int_0^\infty \rho u (h - h_\infty) r \, dr = I V \qquad A_2.3$$

where V is the column voltage measured from the origin.

In a similar manner the momentum equation (5.1) can be written as:

$$\frac{d}{dx}\int_0^\infty \rho u (u - u_\infty) r \, dr = -\frac{dh}{dx} \qquad A_2.4$$

APPENDIX III

The electrically conducting column of the constant pressure axial flow arc, including convection.

In section 5.1, an order of magnitude estimation showed that the convection terms assumed considerable importance within the electrically conducting regions of the arc. This is now examined in greater detail to determine the effect of convection on the temperature profiles and energy flows. The arc is represented by a model which allows for the displacement effect of heat addition at constant pressure. The streamlines are derived from this displacement effect and the local convection heat transfer found.

The model is approximate, since the convection terms are derived from the assumption that the temperature profiles are locally similar. The slopes of the isothermals are taken to be proportional to the slope of the edge of the conducting region, the slope of this bounding isothermal is then regarded as a known quantity and becomes part of an overall convection constant. The model is similar to the transpiration cooled arc (section 4.3), the slope of the bounding isothermal being equivalent to a radial in-flow.

From the solution of the momentum equation $u = u_\infty$, and the continuity equation, the convection terms in the energy equation can be calculated in terms of $\frac{dr_0}{dx}$, the slope of the bounding isothermal.

Taking the energy equation in the form

$$\rho u \frac{\partial h}{\partial x} - \rho v \frac{\partial h}{\partial r} = \frac{1}{r} \frac{\partial}{\partial r}\left(r \frac{k}{c_p} \frac{\partial h}{\partial r} \right) + \sigma E^2$$

the derivative $\frac{\partial h}{\partial x}$ can be written as:

$$\frac{\partial h}{\partial x} = \frac{\partial h}{\partial r} \cdot \frac{dr}{dx}$$

Assuming that $\frac{dr}{dx}$ is proportional to $\frac{dr_o}{dx}$, the axial convection term can be written:

$$\rho u \frac{\partial h}{\partial x} = - \rho u_\infty \frac{r}{r_o} \frac{dr_o}{dx} \cdot \frac{\partial h}{\partial r} \qquad A_3.1$$

The radial convection can be calculated from the continuity equation, as in Appendix II, to give:

$$\rho v = - \frac{1}{r} \int_o^r r \frac{\partial (\rho u)}{\partial x} dr .$$

Since $u = u_\infty$, this becomes:

$$\rho v = - \frac{u_\infty}{r} \int_o^r r \frac{\partial \rho}{\partial x} dr .$$

The density gradient $\frac{\partial \rho}{\partial x}$ also can be expressed in terms of $\frac{dr_o}{dx}$ to give:

$$\frac{\partial \rho}{\partial x} = - \frac{\partial \rho}{\partial r} \cdot \frac{r}{r_o} \cdot \frac{dr_o}{dx}$$

Substituting this into the continuity equation, the radial mass flow becomes:

$$\rho v = \frac{u_\infty}{r r_o} \cdot \frac{dr_o}{dx} \int_o^r r^2 \frac{\partial \rho}{\partial r} dr .$$

Integrating by parts,

$$\rho v = \frac{u_\infty}{r r_o} \frac{dr_o}{dx} \left[\rho r^2 - 2 \int_o^r \rho r \, dr \right] . \qquad A_3.2$$

Substituting from equations $(A_3.1)$ and $(A_3.2)$, the energy equation now can be written in the form:

$$- 2 \frac{u_\infty}{r_o} \cdot \frac{dr_o}{dx} \cdot \frac{dh}{dr} \int_o^r \rho r \, dr = \frac{d}{dr} \left(r \frac{k}{c_p} \frac{dh}{dr} \right) + \sigma E^2 r \qquad A_3.3$$

Convection is represented by the term on the left hand side of this equation, and $\frac{v_o}{r_o} \frac{dr_o}{dx}$ represents the component of axial flow per unit area normal to the bounding isothermal.

If this quantity is regarded as a constant, the equation can be solved as a function of radius only, and the effect of convection on a particular profile studied.
If this equation is integrated again, it can be put into the form used by Yos [33] for the numerical solution of the conduction equation with radiation.

Integrating across the radius equation ($A_3.3$) becomes:

$$2\frac{u_\infty}{r_0}\cdot\frac{dr_0}{dx}\int_0^r \frac{dh}{dr}\left[\int_0^r \rho r\,dr\right]dr = \left[r\frac{k}{c_p}\frac{dh}{dr}\right]_0^r + E^2\int_0^r \sigma r\,dr.$$

Integrating $\int_0^r \frac{dh}{dr}\left[\int_0^r \rho r\,dr\right]dr$ by parts,

$$\int_0^r \frac{dh}{dr}\left[\int_0^r \rho r\,dr\right]dr = h\int_0^r \rho r\,dr - \int_0^r \rho h r\,dr,$$

and the energy equation finally becomes:

$$-2\frac{u_\infty}{r_0}\cdot\frac{dr_0}{dx}\left[h\int_0^r \rho r\,dr - \int_0^r \rho h r\,dr\right] = \left[r\frac{k}{c_p}\frac{dh}{dr}\right]_0^r + E^2\int_0^r \sigma r\,dr. \qquad A_3.4$$

The convection term on the left hand side is now equivalent to the radiation term $\int_0^r \rho r\,dr$. of Yos's form of the conduction - radiation equation (Appendix I), and the same numerical technique can be used for solution. By replacing radiation with convection, it should be possible to correlate the results of such solutions with the similarity variables of the radiation - conduction arc of section 4.2.

The programme of Appendix I has been used to calculate the temperature profiles of 10,000°K arcs with various values of the convection constant, $C = 2\frac{u_\infty}{r_0}\frac{dr_0}{dx}$ The results for a 10 v/cm arc are shown in figure $A_3.1$, where it can be seen that the effect of convection is to extend the lower temperature regions. These

profiles are plotted in terms of the similarity radius X. In practice, arcs with a large amount of convection have high voltage gradients, so that the actual physical radius of an arc is reduced by convection.

The extended outer regions only carry a small proportion of the electrical input and the central temperature - power input relationship remains close to that of the simple conduction arc. For large values of the convection constant the temperature gradient becomes zero at a point in the profile. At this point all the heat is convected back into the arc. As no convection boundary condition is specified in the numerical programme the conduction becomes zero at some unspecified temperature. In practice, this only happens within the electrically conducting region when an unrealistic value of the convection constant is used, as in the case of C = 1000 with E = 10 v/cm.

Figure $A_3.2$ shows the distribution of total power input and convected power across a particular 10,000°K profile. The voltage gradient of 25 v/cm and the convection constant of 1000 represents flow conditions of 10^4 cm/sec and 1 atmosphere pressure, with a value of $\frac{dr_o}{dx}$ of 0.03.

The similarity radius X_o is close to that of the simple conduction arc, confirming the use of the universal radius characteristic for this arc. The value of the slope of the bounding isothermal, $\frac{dr_o}{dx}$ is so small that such an arc would have the appearance of a uniform column unless exceptionally good photographs were available.

Although this model could be used as a basis for the solution of the complete axial flow arc, this would probably entail as much computation as a full numerical solution.

REFERENCES

1. Finkelnburg, W. — Electric arcs and thermal plasma. Handbuch der Physik, Vol. XXII.

2. Ayrton, H. — The electric arc. London 1902.

3. Suits, C.G. — High pressure arcs in common gases in free convection. Physics Review, Vol.55 March 1939, pp.561-567.

4. Suits, C.G. Poritsky, H. — Application of heat transfer data to arc characteristics. Physics Review, Vol.55 March 1939, pp.1184-1191.

5. McAdams, W.H. — Heat transmission. McGraw-Hill 1933.

6. Elenbaas, W. — Similarity of high pressure discharges of the convection stabilised type. Philips Research Report Vol.1, No.5. 1946, pp. 339 - 359.

7. Rowe, R.D. — The theory of free convection arc columns. University of Oxford, Report No. 104568.

8. Wienecke, R. — Über das Geschwindigeitsfeld der Hochstromkohlebogensäule. Zeitschrift Für Physik, BD.143, 1955, pp.128 - 140.

9. King, L.A.
The voltage gradient of the free burning arc in air or nitrogen.
E.R.A. Report G/XT172, 1961.

10. Adams, V.W.
Guile, A.E.
Lord, W.T.
Naylor, K.A.
Correlation of experimental data for electric arcs in transverse magnetic fields.
Proceeding I.E.E. 114,(10) 1967, pp.1556 - 1558.

11. Lord, W.T.
An electric arc in a transverse magnetic field (A theory of an arc of low power).
R.A.E. Technical Report 67086. 1967.

12. Lord, W.T.
Correlation of voltage-current characteristics of wall-stabilised, free-burning and cross-flow arcs.
R.A.E. Technical Report 67087, 1967.

13. Yas'ko, O.I.
Correlation of the characteristics of electric arcs.
British Journal of Applied Physics Series 2, Vol. 2, 1969.

14. Stine, H.A.
Watson, V.R.
The theoretical enthalpy distribution of air in steady flow along the axis of a D.C. arc.
N.A.S.A. TN D-1331. 1962.

15. Chen, M.
Theoretical and experimental investigation of arc plasma generation technology.
A.S.D.-TDR-62-729 Vol.III W.A.D.C. 1962.

16. Weber, H.E. Growth of an arc column in flow and pressure fields.
Agardograph 84, Sept. 1964.

17. Skifstad, J.G. Analysis of the flow and heat transfer processes in a tube arc for heating a gas stream.
A.I.A.A. J. Vol.1, No.8. August 1963.
pp. 1906 - 1909.

18. Watson, V.R. Numerical calculations for the characteristics of a gas flowing axially through a constricted arc.
NASA TN D - 4042. 1967.

19. Dautov, G.Yu.
Zhukov, M.F. Some generalisations relating to the study of electric arcs.
Prikl.Mekh. I Tekh.Fiz No.2, 1965, pp.97 - 105.

20. Dautov, G. Yu.
Dudikov, Yu.S.
Zhukov, M.F.
Mustafin, G.M. Investigation of stabilised arc in the gas flow channel.
8th International Conference of Ionization Phenomena in Gases. Vienna 1967.
Ion and Plasma Sources Panel 6.2.
Plasma Jets 6.2.7.

21. Dautov, G. Yu.
Sazonov, M.I. Investigation of potential gradients in stabilised arcs.
8th International Conference on Ionization Phenomena in Gases. Vienna 1967.
Ion and Plasma Sources Panel 6.2.
Plasma Jets 6.2.8.

22. Grotian, W. Der Gleichstrom - Lichtbogen Grosser Bogenlänge.
Ann. Phys. (4) 47, 1915.

23. Aartz, C.J.M. Investigation of an arc discharge which is stabilised with a screw shaped stream of air.
Thesis, Eindhoven 1952.

24. Kirschstein, B.
Koppelmann, F. Photographische Aufnahmen Elektrischer Lichtbögen Grosser Stromstärke.
Wiss. Ver. Siemens Werken, Berlin. July 1934.

25. Holm, R.
Kirschstein, B.
Koppelmann, F. Überlick über die Physik des Starkstromlichtbogens mit besonderer Berücksightigung der Loschung in Hochleistungswechselstromschaltern.
Wiss. Ver. Siemens Werken, Berlin, March 1934.

26. Kirschstein, B.
Koppelmann, F. Der Elektrische Lichtbogen in Schnellströmendem Gas.
Wiss. Ver. Siemens Werken, Berlin. March 1937.

27. King, L.A. The voltage gradient of an arc column under forced convection in air or nitrogen.
E.R.A. Report 5072. 1964.

28. Rowe, R.D. The behaviour of an electric arc in a shock tube.
Thesis, D. Phil., University of Oxford. 1969.

29. Swanson, B.W.
Roidt, R.M.
Browne, T.E.
The Effect of gas dynamics and properties of SF_6 and air on short line fault interruption.
Westinghouse Electric Scientific Paper 69 - IE9 - Arcs - P3. August 1969.

30. Frind, G.
Electric arcs in turbulent flows, II.
General Electric Company.
A D 636 804 April 1966.

31. King, L.A.
Theoretical calculations of arc temperatures in different gases.
Colloquium Spectroscopicum Internationale VI.
Amsterdam 1956. Pergamon Press Ltd., London.

32. Wells, A.A.
Numerical calculations of the properties of axially symmetric arc columns.
R.A.E. Tech. Report 67076, 1967.

33. Yos, I.
Transport properties of nitrogen, hydrogen, oxygen and air to 30,000°K.
Avco Research Lab. Rad-TM-63-7. 1963.

34. Maecker, H.
Fortschritte in der Bogenphysik.
5th International Conference on Ionization Phenomena in Gases. Vol.II, Munich 1961.

35. Yos, I.
Evaluation of high temperature gas transport properties.
A V SSD - 0414 - 67 - R R.

36. Hermann, W.
Monterde-Garcia, A.
Bestimmung von Wirkungsquerschnitten aus aus Messungen an Zylindrischen Kaskabenbögen.
Zeitschrift Fur Physik 205, 1967. pp.313-327.

37. Schade, E.
Properties of nitrogen up to 25,000°K.
8th International Conference of Ionization Phenomena in Gases. Vienna 1967.

38. Spitzer, L.
Physics of fully ionized gases.
Interscience Tracts on Physics and Astronomy No.3.

39. Burhorn, F.
Wienecke, R.
Plasmazusammensetzung. Plasmadichte, Enthalpie und spezifische Wärme von Stickstoff, Stickstoffmonoxyd und Luft bei 1,3,10 und 30 atm. in Temperaturbereich zwischen 1000 und 30000°K.
Zeitschr. Für. Physikalische Chemie 215, 1960. pp.269 - 284.

40. Brinkmann, H.
An optical study of the electric arc.
Thesis, Utrecht, Amsterdam 1937.

41. Schmitz, G.
Schick, K.
An approximate integration of the Elenbaas-Heller Differential Equation.
Z. Naturforsch Vol. 10a. No.6, 1955. p.495.

42. Goldenberg, H.
Approximate solution of a non-linear differential equation giving the temperature distribution of the positive column of a static arc.
Brit. J. Appl. Physics, Vol.10, No.1, Jan. 1959. pp. 47 - 51.

43. Engel, A.V.
Steenbeck, M.
Electric gas discharges.
Berlin 1934.

44. Somers, P.J.
Investigation of an arc-discharge in nitrogen at increased pressure.
Thesis, Utrecht 1954.

45. Burhorn, F.
Temperaturmessungen am Wasserstabilisierten Hochleistungs Bogen.
Zeitschrift Für Physik Vol. 131, 1951. pp.28 - 40.

46. Marston, C.H.
Frind, G.
Miskovsky, V.
Schorn, A.M.
Radiation Heat Flux from High Pressure Air Arcs.
General Electric Space Sciences Laboratory.
R67 SD58. October 1967.

47. Allen, J.E.
Craggs, J.D.
High current spark channels.
Brit.J. Appl. Phys. Vol.5, No.12. Dec. 1954.

48. King, L.A.
Howes, J.A.
Material transfer in the welding arc.
Physics of the Welding Arc, A Symposium.
Institute of Welding, London 1962.

49. Foitzik, R.
Untersuchungen am Stabilisierten Elektrischen Lichtbogen (Wälzbogen) in Stickstoff und Kohlensäule bei Drücken von I bis 40 at.
Wiss. Veroff. Siemens-Konz. 19, 28. 1940.

50. Borovik, E.G.
Kantsedel, V.P.
Knyazen, Yu R.
Mitvin, R.
Petrenko, V.I.
Pulsed arc in argon at pressure up to 10^8 N/M^2 (1000 ATM).
Soviet Physics - Technical Physics Vol.12.
No. 4. Oct. 1967.

51. Cowley, M.
Programme for arc studies.
M.H.D. Group, University of Cambridge.

52. Schmitz, G.
Druxes, H.
Patt, H.J.
Zur Modelltheorie des Zylindersymmetrischen Lichtbogens mit Radialer Masseneinströmung.
Zeitschrift fur Physik 187, 1965. pp.271 - 289.

53. Eckert, E.R.G.
Transpiration cooling of a constricted electric arc heater.
A.I.A.A. J. Vol.5, No.4, April 1967.

54. Goldstein, S.
Modern developments in fluid dynamics.
Clarendon Press, Oxford 1943.

55. Schlichting, H.
Boundary layer theory.
McGraw-Hill Book Co. Inc. 1958.

56. Naylor, K.A.
Private communication.

57. Goldman, K.
Electric arcs in argon.
Physics of the welding arc. A Symposium.
Institute of Welding, London 1962.

58. Wutzke, S.A.
Pfender, E.
Eckert, E.R.G.
Study of electric arc behaviour with super-imposed flow.
AIAA J. Vol.5. No. 4, April 1967.

59. Topham, D.R.
A preliminary study of an axial electric arc in shock tube flow.
Loughborough University of Technology Report TT 6802. 1968.

60. Glass, I.I.
Hall, J.
Shock tubes.
U.T.I.A. Review No. 12. 1958.

61. Mirels, H.
King, W.S.
Series solutions for shock tube laminar boundary and test time.
A.I.A.A. J. Vol. No.5, May 1966.

62. Mirels, H.
Shock tube test time limitation due to turbulent wall boundary layer.
A.I.A.A. J. Vol.2, No.1. Jan. 1964.

TABLE I

Transition Currents for Arcs in Different Gases, after King [31]

GAS	CO_2	O_2	H_2	N_2
Dissociation Potential	4.3	5.084	4.477	9.762
90% Dissociation ^oK	3800	5110	4575	8300
Transition Current Amps	0.1	0.5	1.0	50

TABLE II

Conduction Arc with Radiation, after Wells [32]

EI W/cm	E V/cm	Λ_o cm	$E\Lambda_o$ Volts	T ^oK	Radiation %
10^4	10	0.77	7.7	15,600	30
10^4	20	0.35	7.0	18,300	8.4
10^4	30	0.23	6.9	19,400	3.8
10^4	40	0.18	7.2	19,400	2.3

TABLE III

Comparison Between Conduction and Transpiration Arc in H_2 after Eckert & Anderson [53]

EI W/cm	E V/cm	Λ_o cm	$E\Lambda_o$ Volts	T ^oK	Type
4,000	53	0.14	7.4	15,000	TRANS.
11,000	50	0.17	8.5	30,000	
3,500	34.2	0.21	7.0	15,000	COND.
9,500	30.7	0.25	7.7	30,000	

TABLE IV

Outer Thermal Layer Profile Shape Factor

m	$\frac{m^2}{(m+1)(m+2)}$	$\frac{m}{(m+1)}$
1	0.167	0.500
2	0.333	0.677
5	0.595	0.834
10	0.757	0.910
∞	1.000	1.000

TABLE V

Gas Reference Conditions

Gas Properties	Nitrogen	Argon
T ^{o}K	4000	4000
T ^{o}K	288	288
h_∞ Joules/gm	2.91×10^{2}	1.54×10^{2}
h_o Joules/gm	5.05×10^{3}	2.40×10^{3}
k_o Watts/cm ^{o}K	2.91×10^{-3}	1.2×10^{-3}
c_{p_o} Joules/gm ^{o}K	1.51	0.532
ρ_o gm/cm^3/atmos.	8.53×10^{-5}	1.10×10^{-4}
u_o (sonic) cm/sec	1.23×10^{5}	1.35×10^{5}
σ_o mhos/cm	100	100
N	$\frac{EI}{57.6}$	$\frac{EI}{31.8}$
N_u R_a P_r	$0.485 \times 10^{-4} \frac{\rho_o u_o I^2}{x}$	$0.875 \times 10^{-4} \frac{\rho_o u_o I^2}{x}$

TABLE VI

Nozzle Arc Experiments

Kirschstein & Koppelmann, reference 26, $x = 0.5$ cms

h. sonic Atmospheres	I Amps	E Volts/cm	EI W/cm	N	$N_u R_e P_r$
1	1000	101	1.01×10^5	1.76×10^3	1.19×10^7
2	1000	150	1.5×10^5	2.60×10^3	2.38×10^7
3	1000	170	1.7×10^5	2.96×10^3	3.57×10^7
4	1000	190	1.9×10^5	3.31×10^3	4.75×10^7
5	1000	210	2.1×10^5	3.66×10^3	5.95×10^7
5.5	1000	216	2.16×10^5	3.76×10^3	6.55×10^7
4	400	210	8.4×10^4	1.46×10^3	7.6×10^6
4	800	192	1.53×10^5	2.63×10^3	3.05×10^7
4	1200	184	2.20×10^5	3.82×10^3	6.85×10^7
4	1600	184	2.94×10^5	5.10×10^3	1.22×10^8
4	2000	184	3.68×10^5	6.40×10^3	1.90×10^8
4	2400	184	4.45×10^5	7.75×10^3	2.75×10^8

TABLE VI (Cont'd)

Nozzle Arc Experiments

King, reference 27, α = 0.5 cms

P_0 sonic Atmospheres	I Amps	E Volts/cm	EI W/cm	N	$N_u R_e P_r$
1	2	500	10^3	17.4	48
1	4	340	1.36×10^3	23.4	1.92×10^2
1	6	280	1.68×10^3	29.2	4.33×10^2
1	10	220	2.2×10^3	38.2	1.20×10^3
1	20	150	3.0×10^3	52	4.80×10^3
1	50	130	6.5×10^3	113	3.0×10^4
1	100	100	10^4	174	1.20×10^5
1	1000	100	10^5	1740	1.20×10^7
10	2	1500	3×10^5	51.8	4.80×10^2
10	4	1000	4×10^3	69.5	1.92×10^3
10	6	830	5×10^3	86.5	4.33×10^3
10	10	630	6.3×10^3	109	1.20×10^4
10	20	500	10^4	174	4.80×10^4
10	50	350	1.75×10^4	303	3.00×10^5
10	100	320	3.2×10^4	555	1.20×10^5
10	200	300	6.0×10^4	1040	4.80×10^6
10	1000	300	3.0×10^5	5200	1.20×10^8

TABLE VII

Equipment Specifications

OSCILLOSCOPE

Telequipment Type D53

Current Measurement Type 'G' Amplifier D.C. to 10 Mc/s

Voltage Measurement Type 'HD2' Amplifier D.C. to 25 Mc/s

TIMER - COUNTER

Racal Type S.A. 535 Range 2 μsec to 10^4 sec.

IMAGE CONVERTER CAMERA

Imacon, John Hadland (P.1.) Ltd.

10^5 or 10^6 pictures/sec.

8 pictures 15mm square

18 pictures with reduced picture width.

TABLE VIII

Shocktube test conditions
(Nitrogen)

Ms	h_∞ Atmos.	U_∞ cm/sec	T_∞ °K
1.2	2	9×10^3	316
1.4	2	2×10^4	362
1.8	2	3×10^4	435
1.4	1	2×10^4	362

TABLE IX

Shock tube Results (Nitrogen)

p_∞ = 2 Atmos.

u_∞ = 9×10^3 cm/sec

I Amps	a_2	m_2	Ey/cm $x = 1$cm	EV/cm $x = 5$cm	$N_u R_2 P_\infty$ $x = 1$cm	N $x = 1$cm	$N_u R P$ $x = 5$cm	N $x = 5$cm
20.0	50.1	0.820	41.0	30.7	354	14.2	71.5	10.6
25.0	46.2	0.800	37.0	26.9	555	16.1	112	11.7
31.6	42.2	0.800	33.6	24.3	887	18.4	177	13.4
48.0	36.7	0.825	30.2	22.8	2040	25.0	410	19.0

p_∞ = 2 Atmos.

u_∞ = 2×10^4 cm/sec

I Amps	a_2	m_2	Ey/cm $x = 1$cm	EV/cm $x = 5$cm	$N_u R_2 P_\infty$ $x = 1$cm	N $x = 1$cm	$N_u R_2 P_\infty$ $x = 5$cm	N $x = 5$cm
6.3	118	0.815	96	71.5	73	10.5	14.6	7.8
7.9	107	0.795	85	61.0	115	11.6	23.0	8.35
10.0	94.4	0.790	74.5	53.0	184	12.9	36.8	9.18
12.9	83.2	0.790	65.6	46.5	304	14.8	61.0	10.5
15.9	74.1	0.790	58.5	41.7	465	16.1	92.0	11.4
20.0	66.1	0.775	51.2	35.7	737	17.7	148	12.3
25.1	60.3	0.765	46.2	31.6	1160	20.2	232	13.8
31.6	56.2	0.755	42.3	28.5	1830	23.8	366	16.0
39.8	53.7	0.746	40.0	26.6	2920	27.0	584	17.9
46.8	52.8	0.738	39.0	25.6	4030	31.8	808	20.9

TABLE IX (Cont'd.)

Shock tube Results (Nitrogen)

p_∞ = 2 Atmos.

u_∞ = 3×10^4 cm/sec

I Amps	a_2	m_2	EV/cm $x=1$cm	EV/cm $x=5$cm	$N_u R_2 P_r$ $x=1$cm	N $x=1$cm	$N_u R_2 P_r$ $x=5$cm	N $x=5$cm
46.8	66.1	0.68	45	27	6080	36.4	1200	21.8

p_∞ = 1 Atmos.

u_∞ = 2×10^4 cm/sec

I Amps	a_2	m_2	EV/cm $x=1$cm	EV/cm $x=5$cm	$N_u R_2 P_r$ $x=1$cm	N $x=1$cm	$N_u R_2 P_r$ $x=5$cm	N $x=5$cm
15.9	55	0.840	46.2	30.6	223	12.7	44.5	8.42
20.0	50.7	0.790	40.0	26.5	354	13.9	70.7	9.9
25.0	46.2	0.780	36.0	23.8	553	15.6	111	11.0
31.6	42.7	0.755	32.2	21.3	885	17.7	177	11.9
45.7	39.8	0.745	29.6	19.6	1930	23.4	386	15.5

TABLE X

Shock tube Results (Nitrogen) at 1 Atmosphere Pressure

x = 2 cms. Rowe, reference 28.

u cm/sec	I Amps	E Volts/cm	$N_4 R_4 P_x$	N
1.49×10^4	10	51	36	8.9
"	20	36	144	12.5
"	50	23	900	20.0
"	100	18	3600	31.5
2.86×10^4	10	66	69	11.5
"	20	46	278	16.0
"	50	32	1720	27.8
"	100	24	6900	41.5
4.55×10^4	5	113	27.6	9.8
"	10	78	110.0	13.5
"	20	57	440.0	19.8
"	50	39	2760	34.0
"	100	32	11000	55.5
"	150	30	24000	78.0
7.05×10^4	5	130	42.7	11.3
"	10	90	171	15.5
"	20	67	700	23.3
"	50	45	4270	45.5

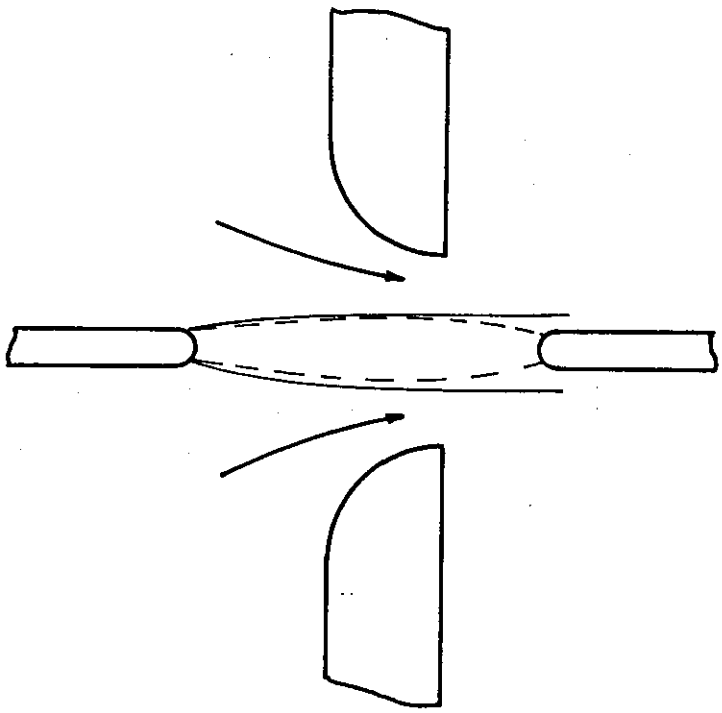

FIG.1. Schematic Drawing of a Gas Blast Circuit Breaker Arc

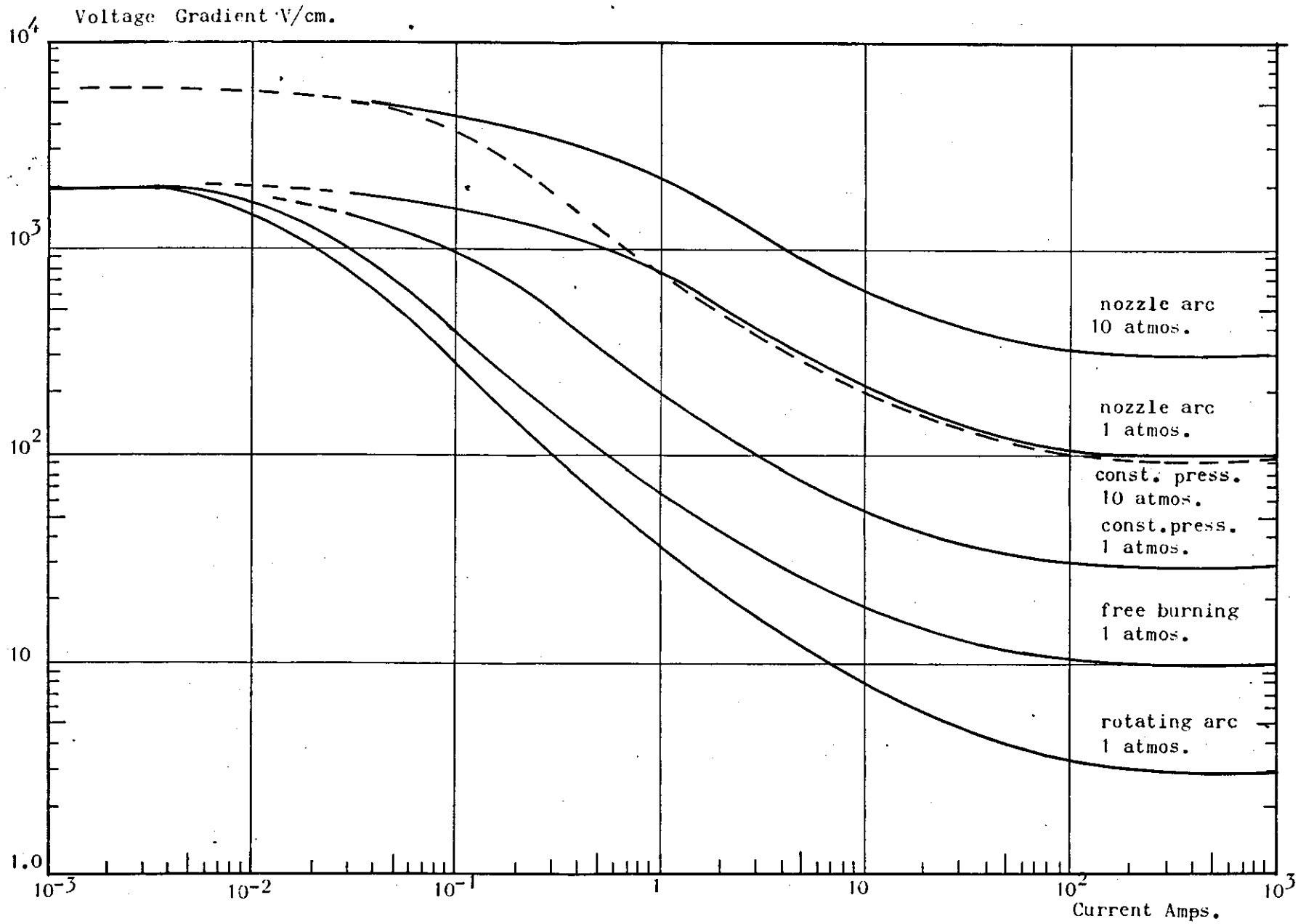

FIG. 2. Voltage Gradients of Arcs in Nitrogen (After King, 27)

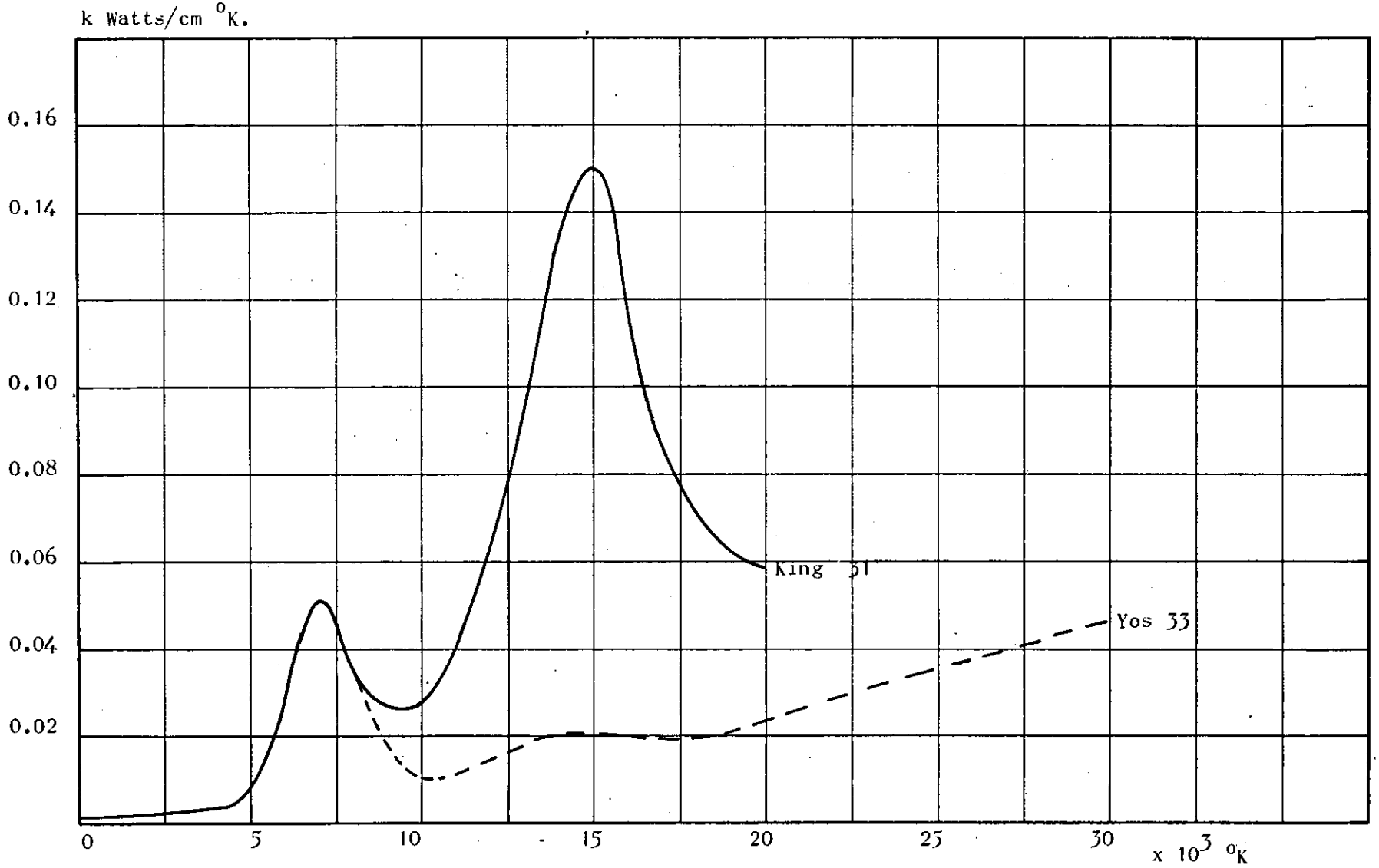

FIG.3. Thermal Conductivity of Nitrogen at 1 atmos. press.

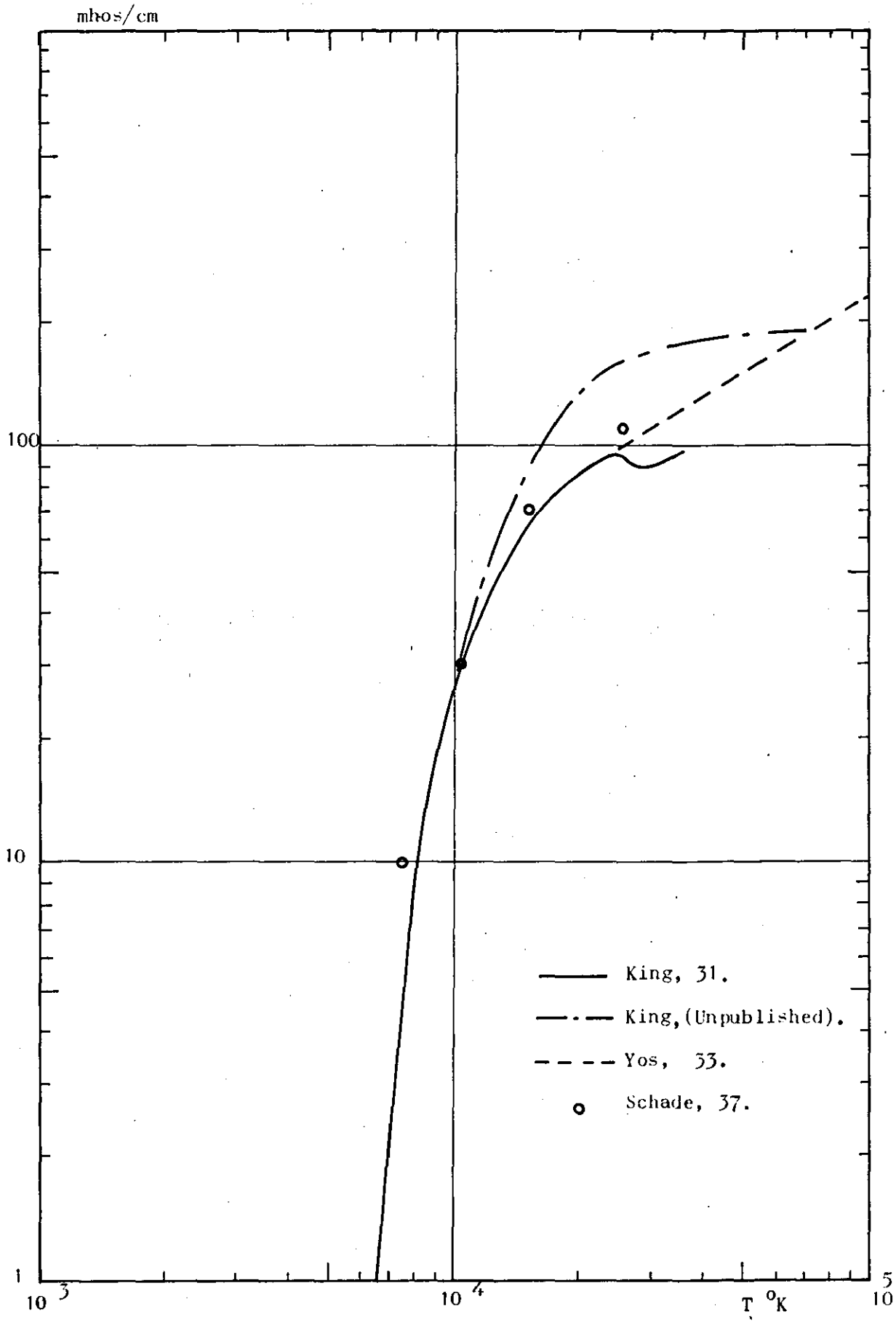

FIG.4. Electrical Conductivity of Nitrogen
1 Atmos. Press.

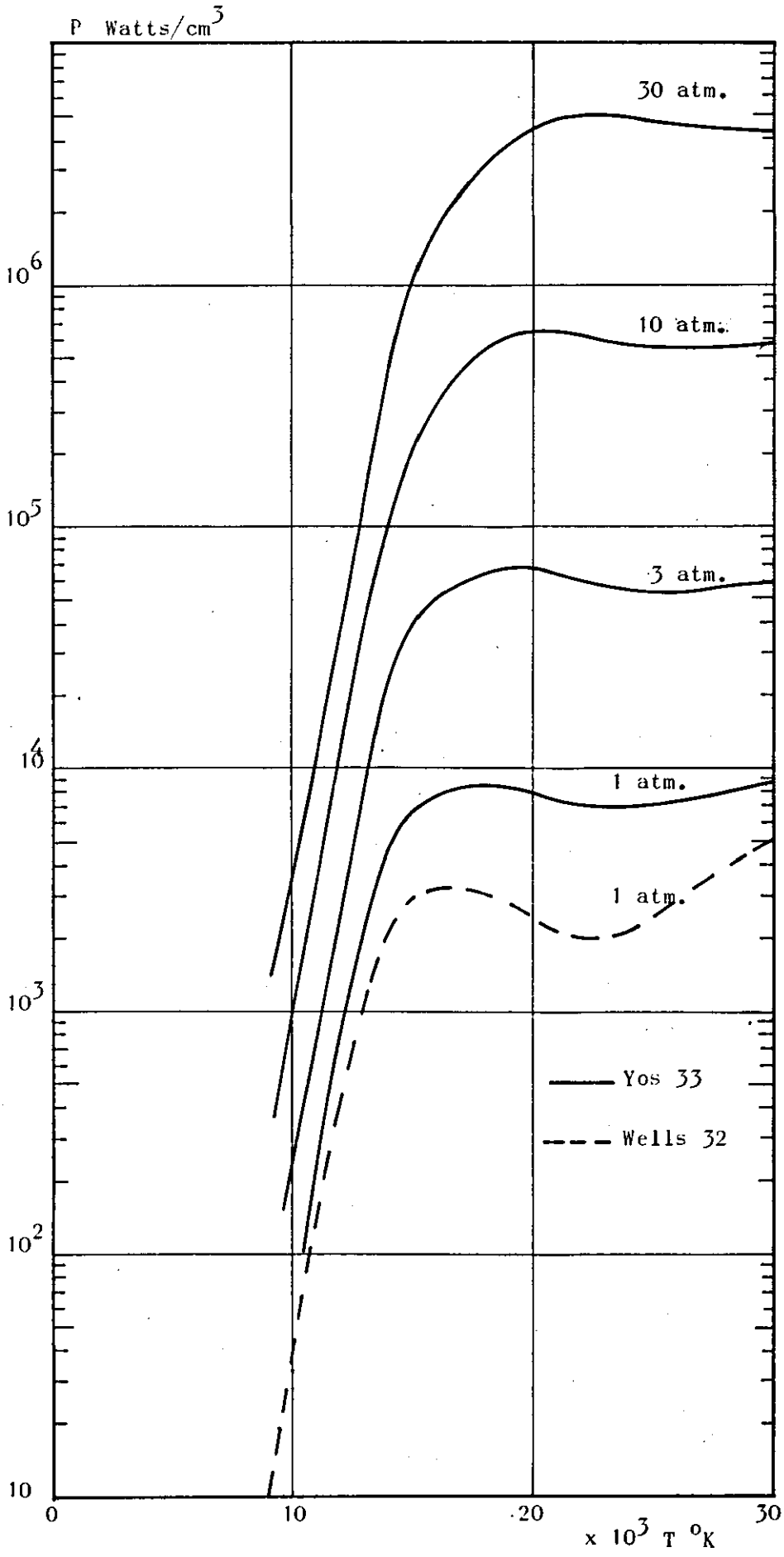

FIG.5. Radiation Properties of Nitrogen

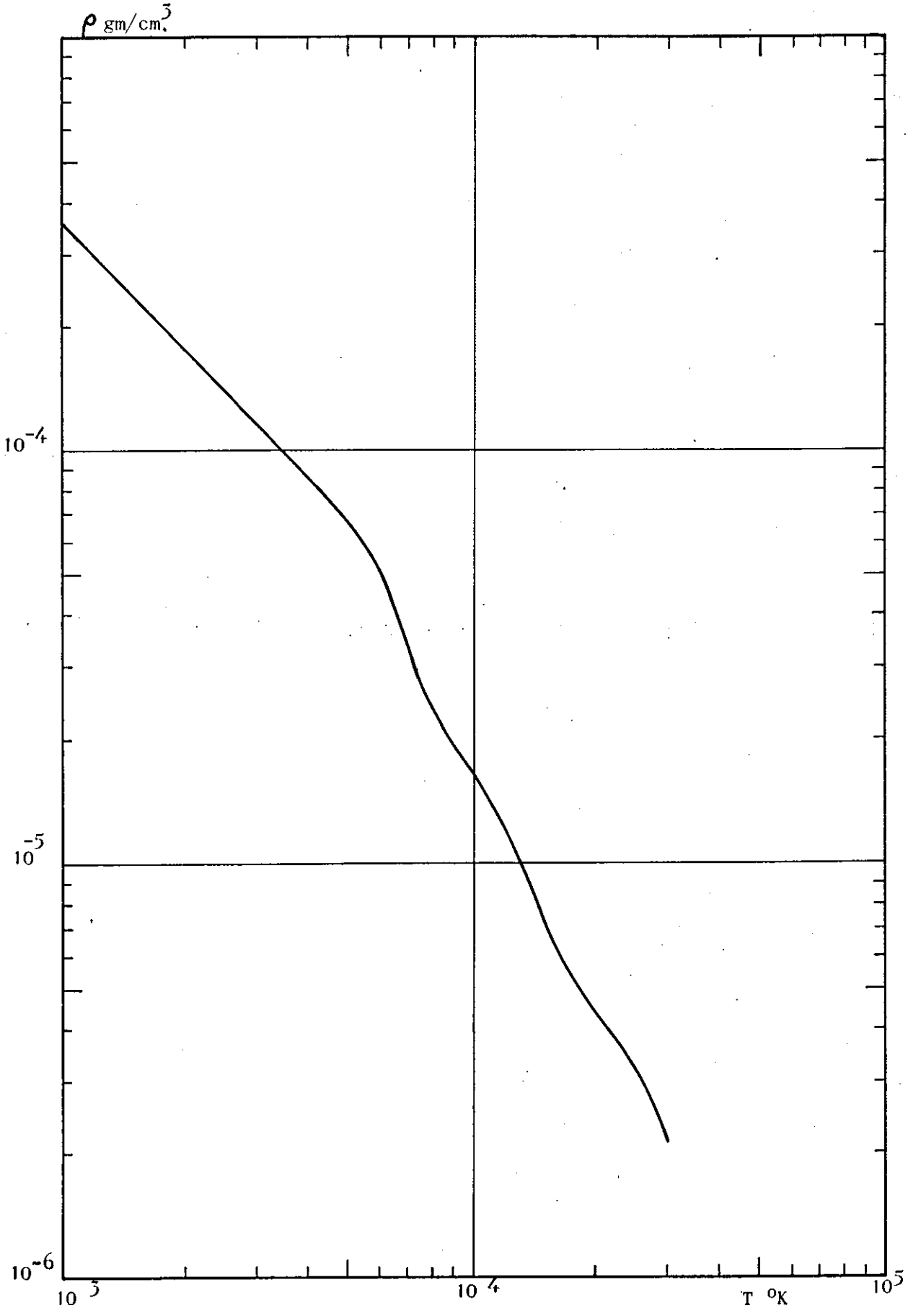

FIG. 6. Density of Nitrogen at 1 Atmos. Press.

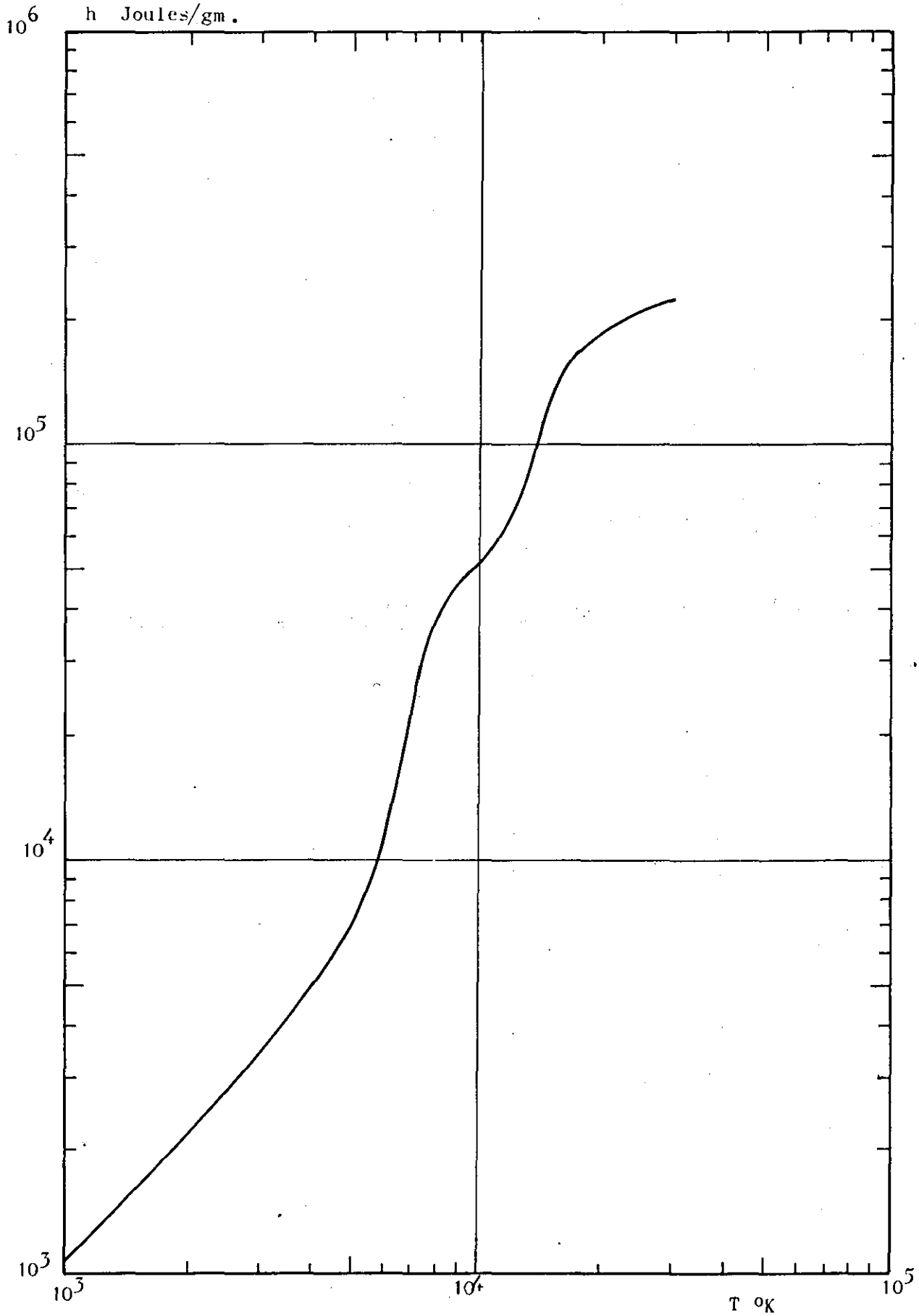

FIG. 7. Enthalpy of Nitrogen at 1 Atmos. Press.

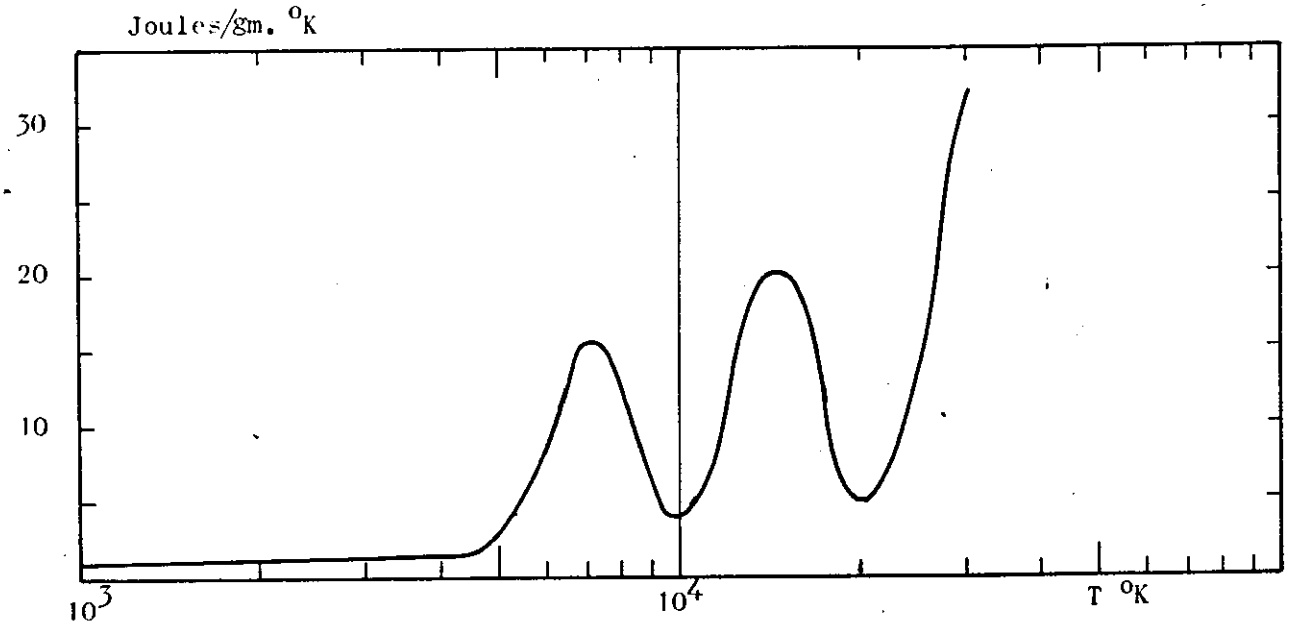

FIG.8. Specific Heat of Nitrogen at 1 Atmos.Press.

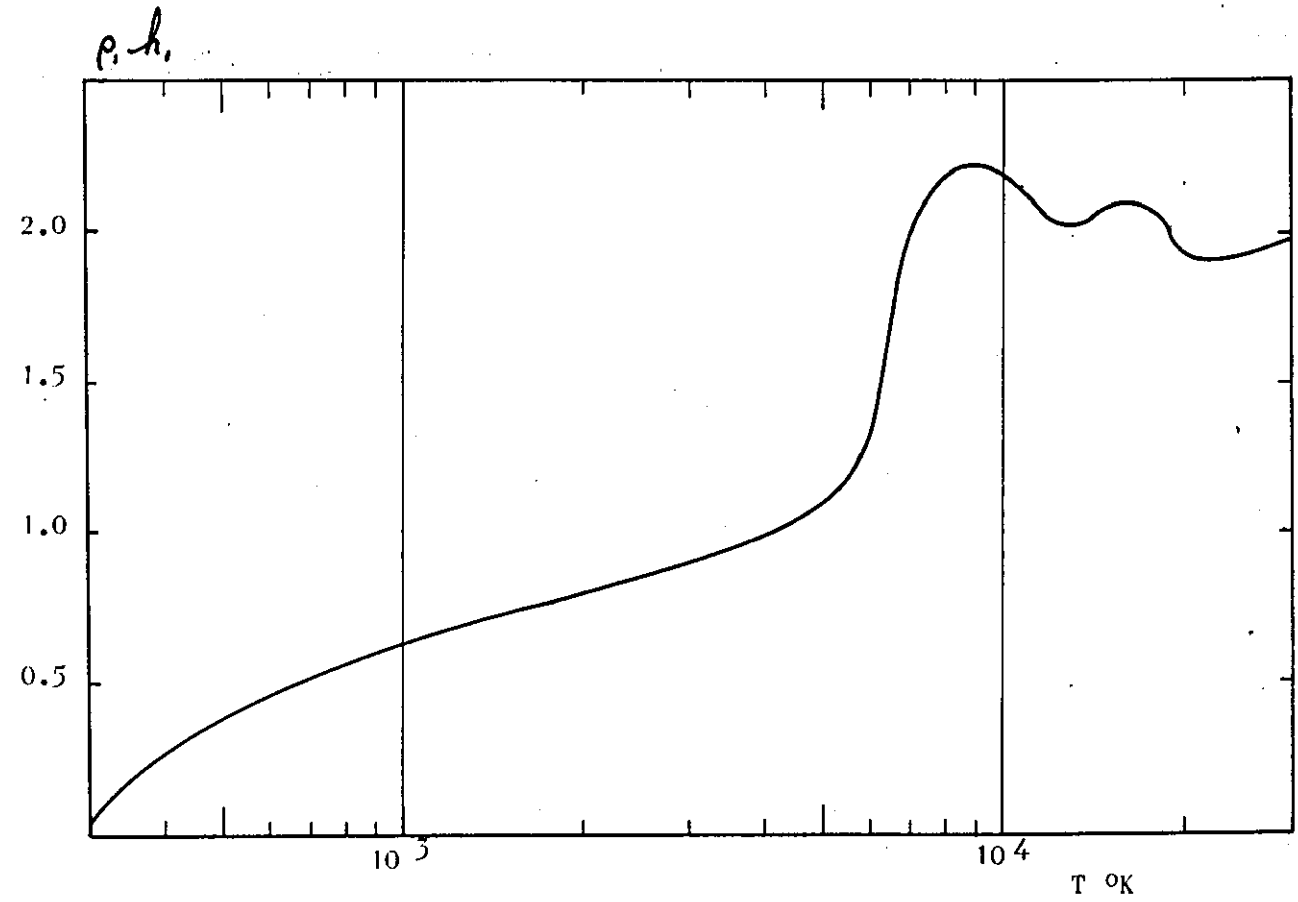

FIG. 9. Non-Dimensional Specific Enthalpy Difference

Nitrogen at 1 Atmos. Press. Normalised to 4000°K

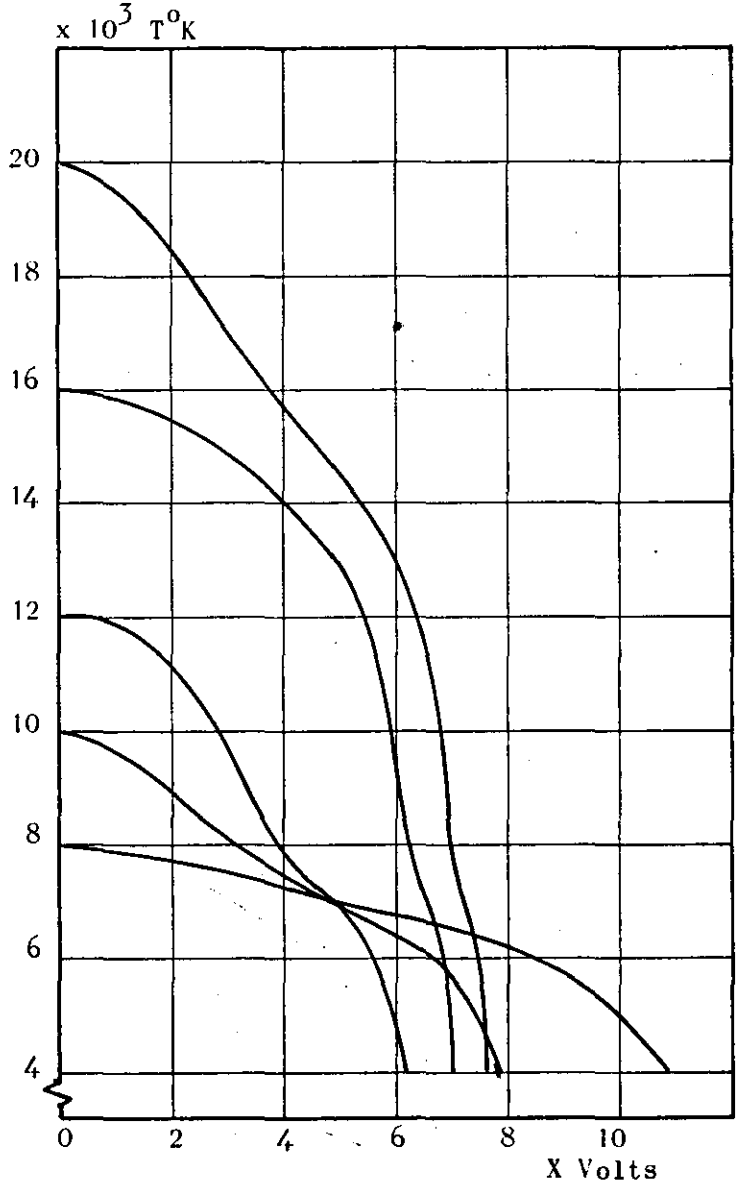

FIG.10. Nitrogen Arc Temperature Profiles Neglecting Radiation.

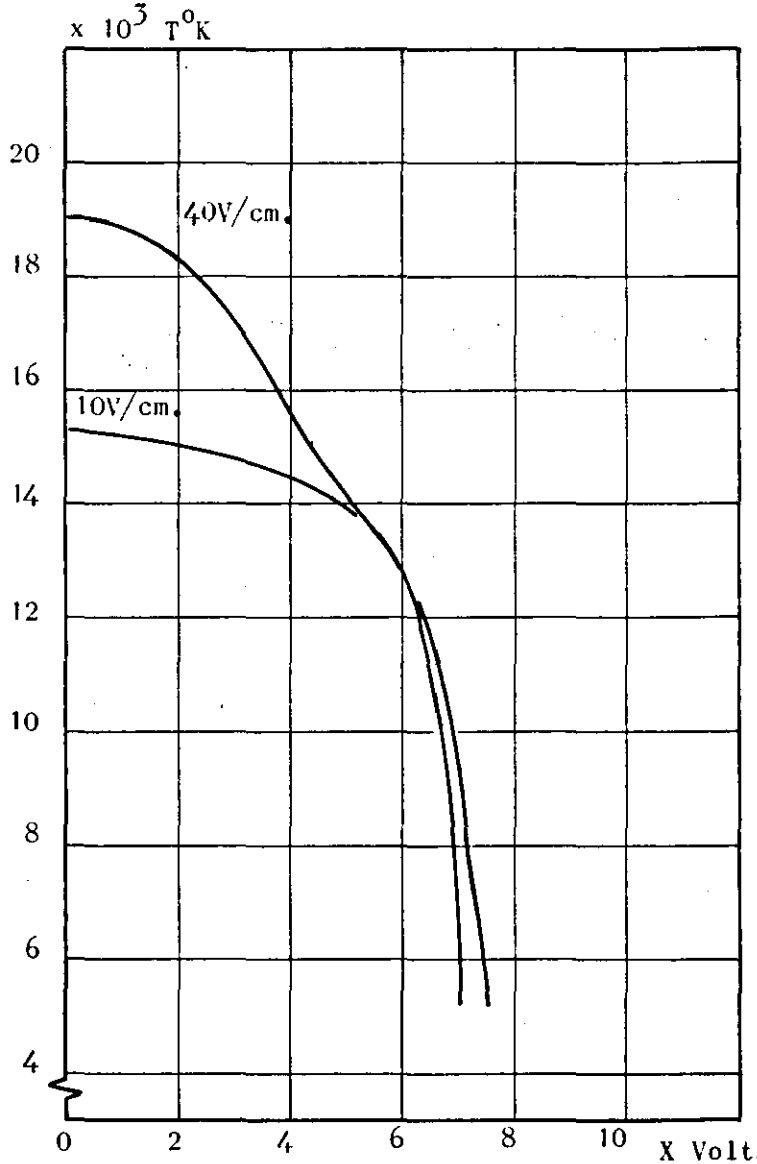

FIG.11. Nitrogen Arc Temperature Profiles 10^4W/cm. Including Radiation (After Wells 32)

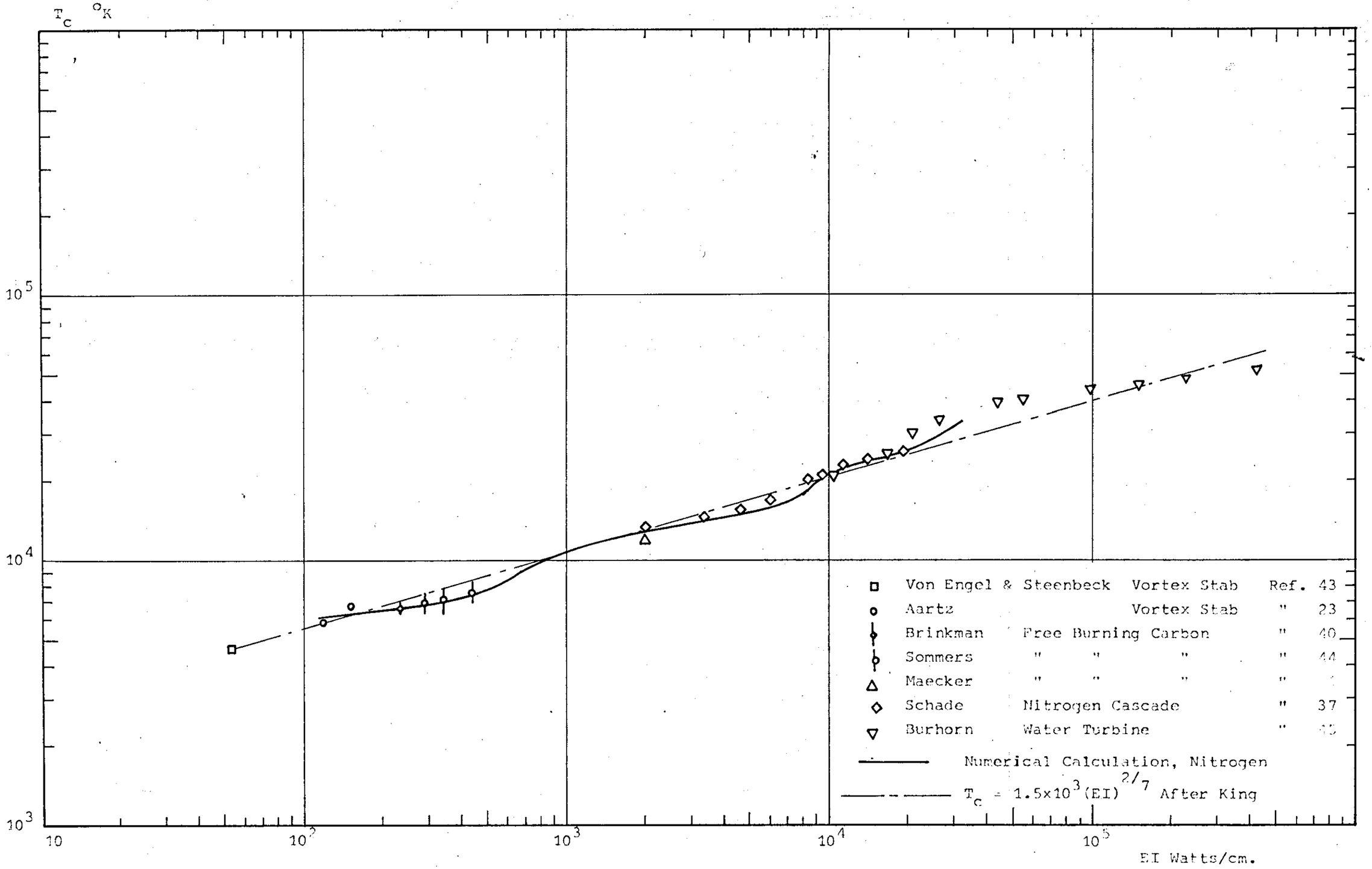

FIG. 12. Power Gradient-Central Temperature, Nitrogen.

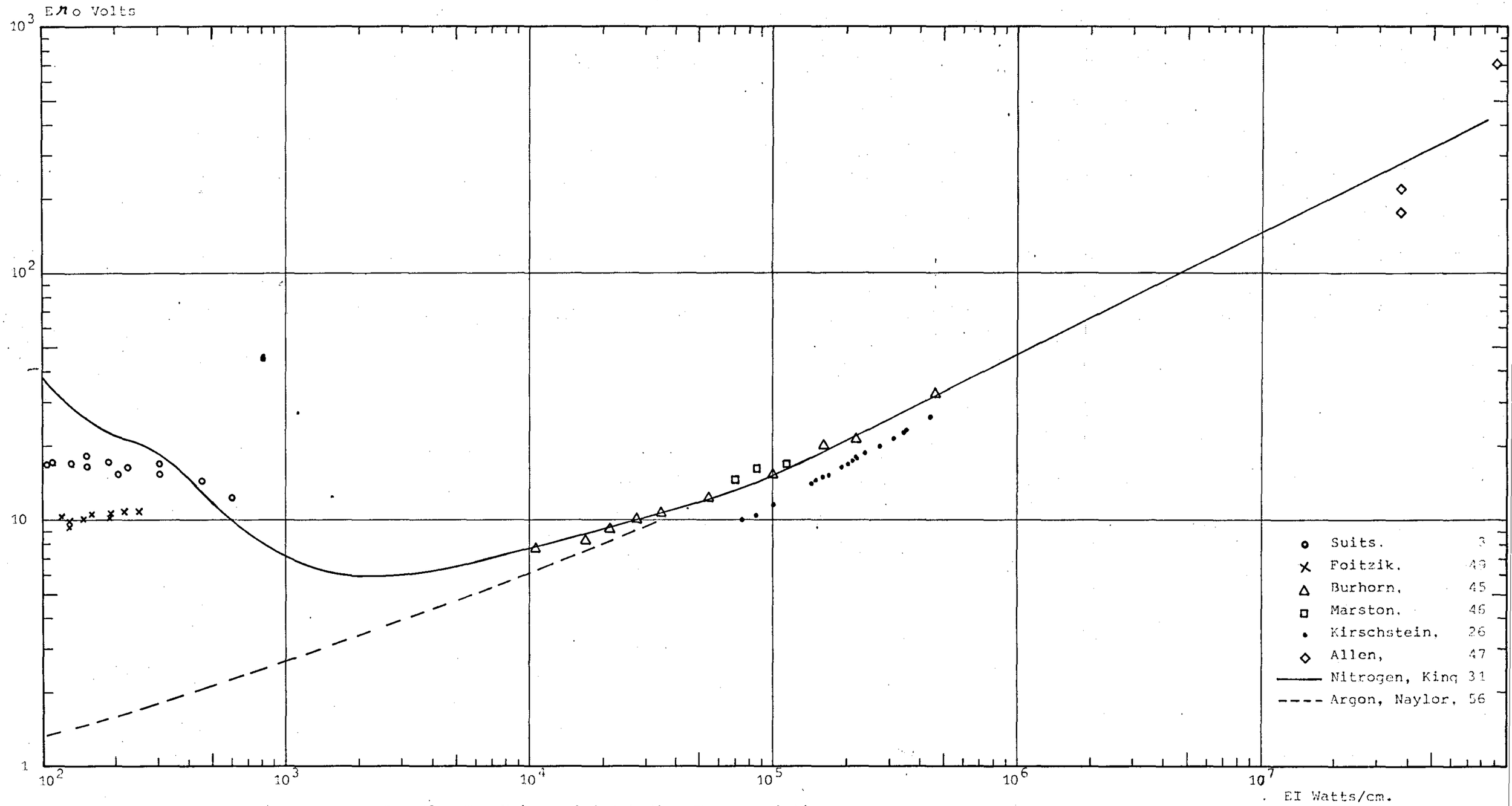

Fig. 12. The Universal Arc Ratio Characteristic.

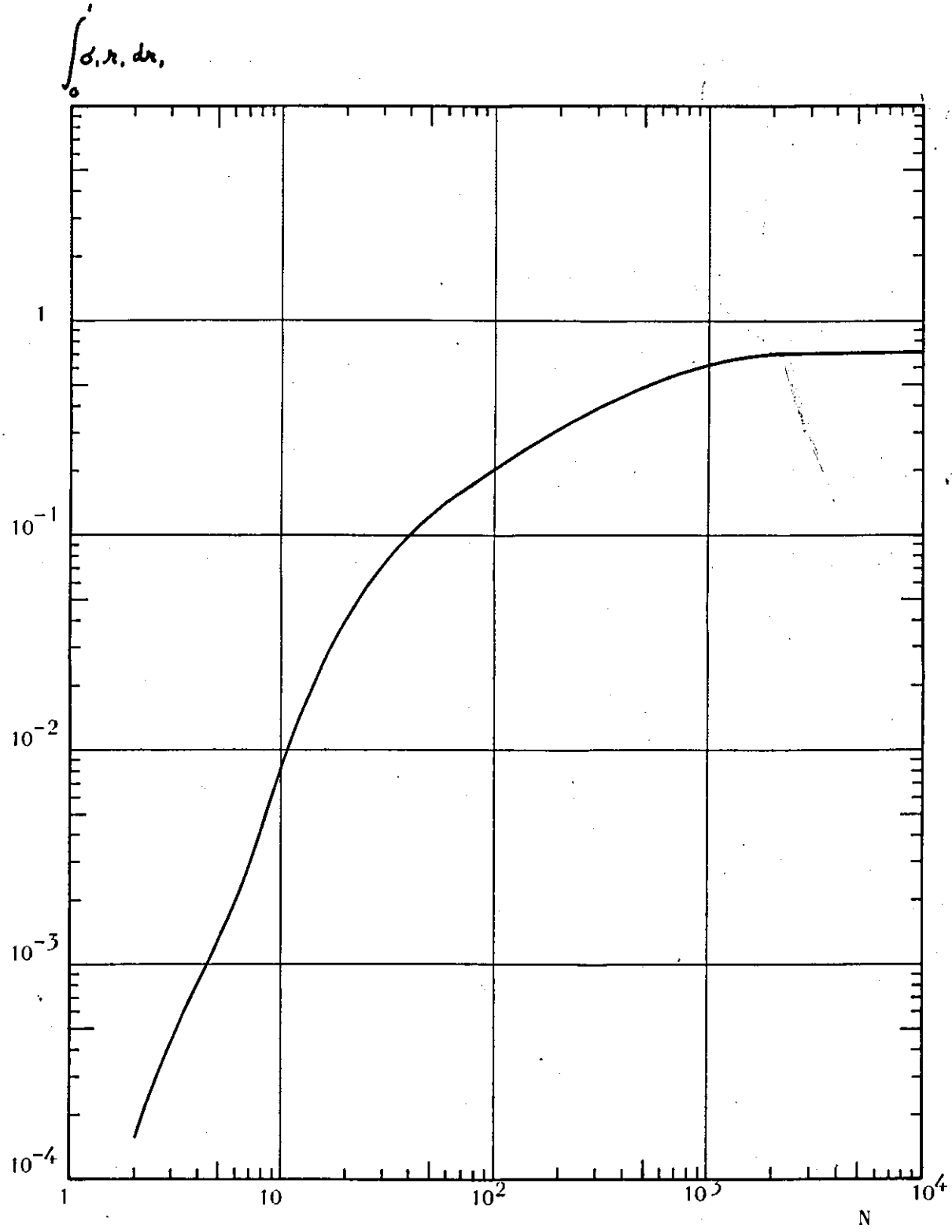

FIG. 14. Non-Dimensional Arc Radius Characteristic

For Nitrogen

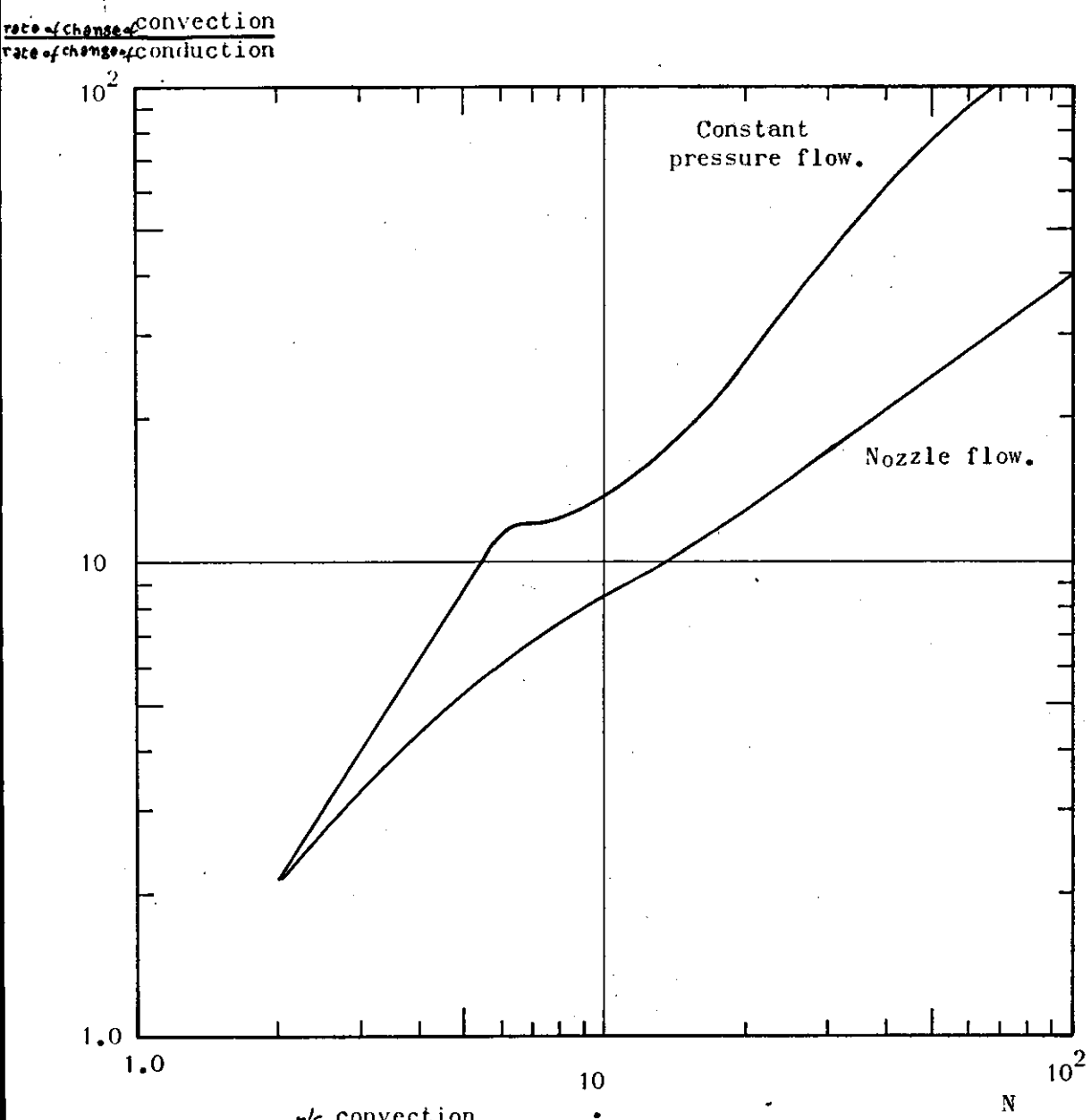

FIG. 15 $\frac{r/c.\text{convection}}{r/c.\text{conduction}}$ at 4000°K in a nitrogen arc.

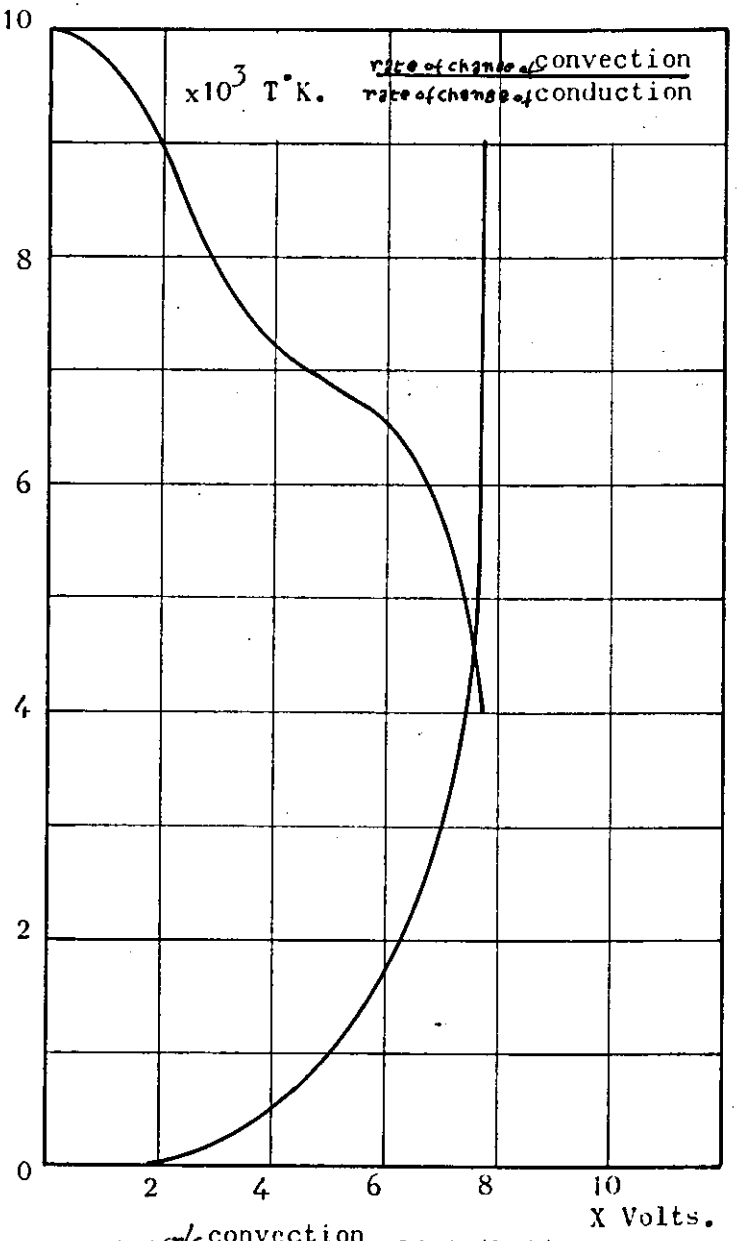

FIG. 16 $\frac{r/c.\text{convection}}{r/c.\text{conduction}}$, Distribution across a nitrogen arc.

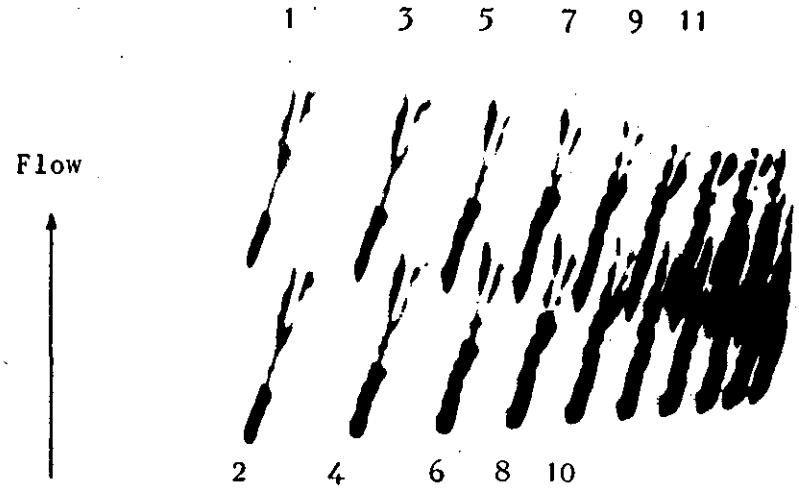

10^5 Pictures/sec. x = 2.8 cms.

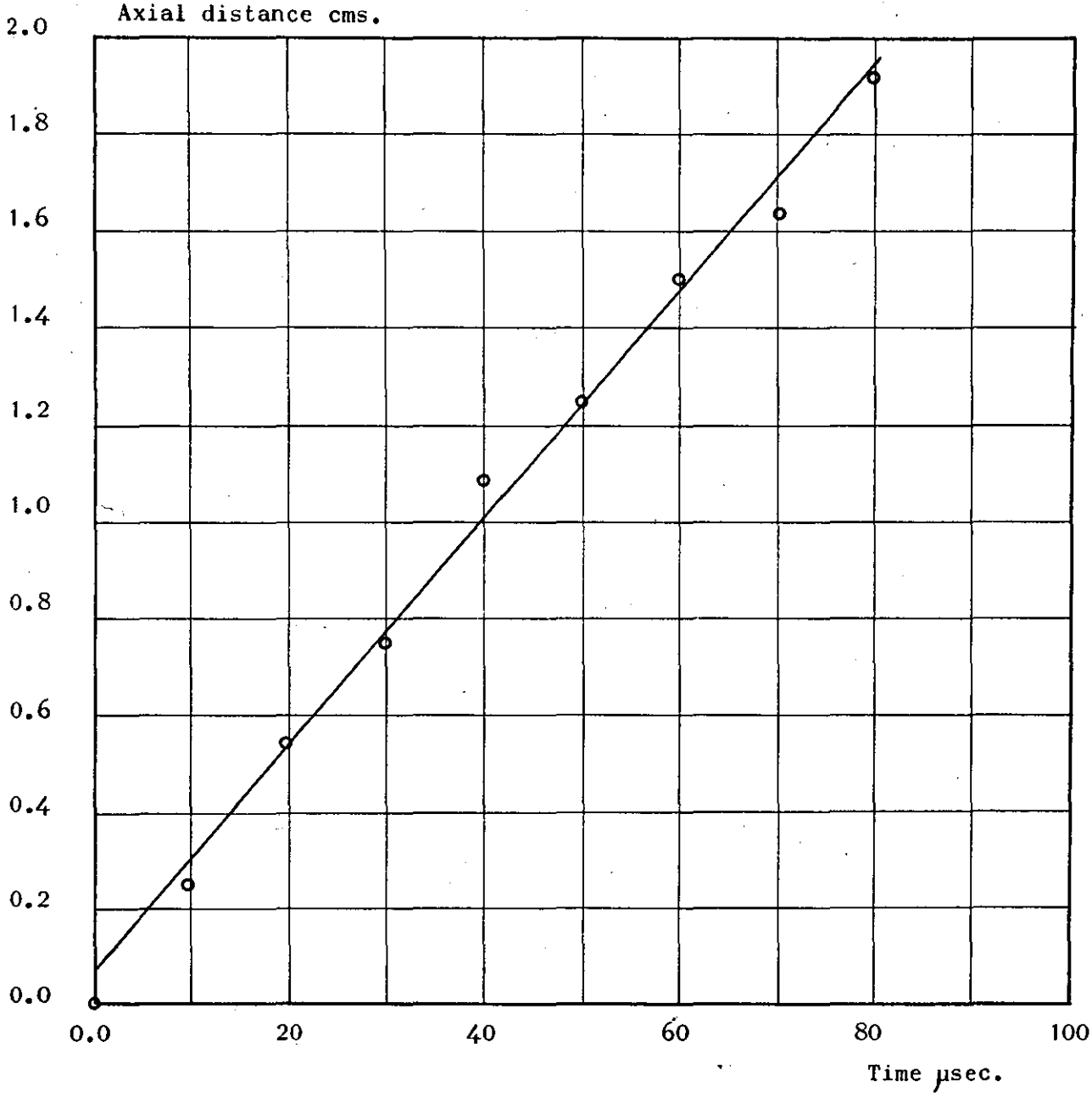

$u_\infty = 2.3 \times 10^4$ cm/sec. Vapour velocity 2.5×10^4 cm/sec.

FIG. 17. Measurement of Metal Vapour Velocity.

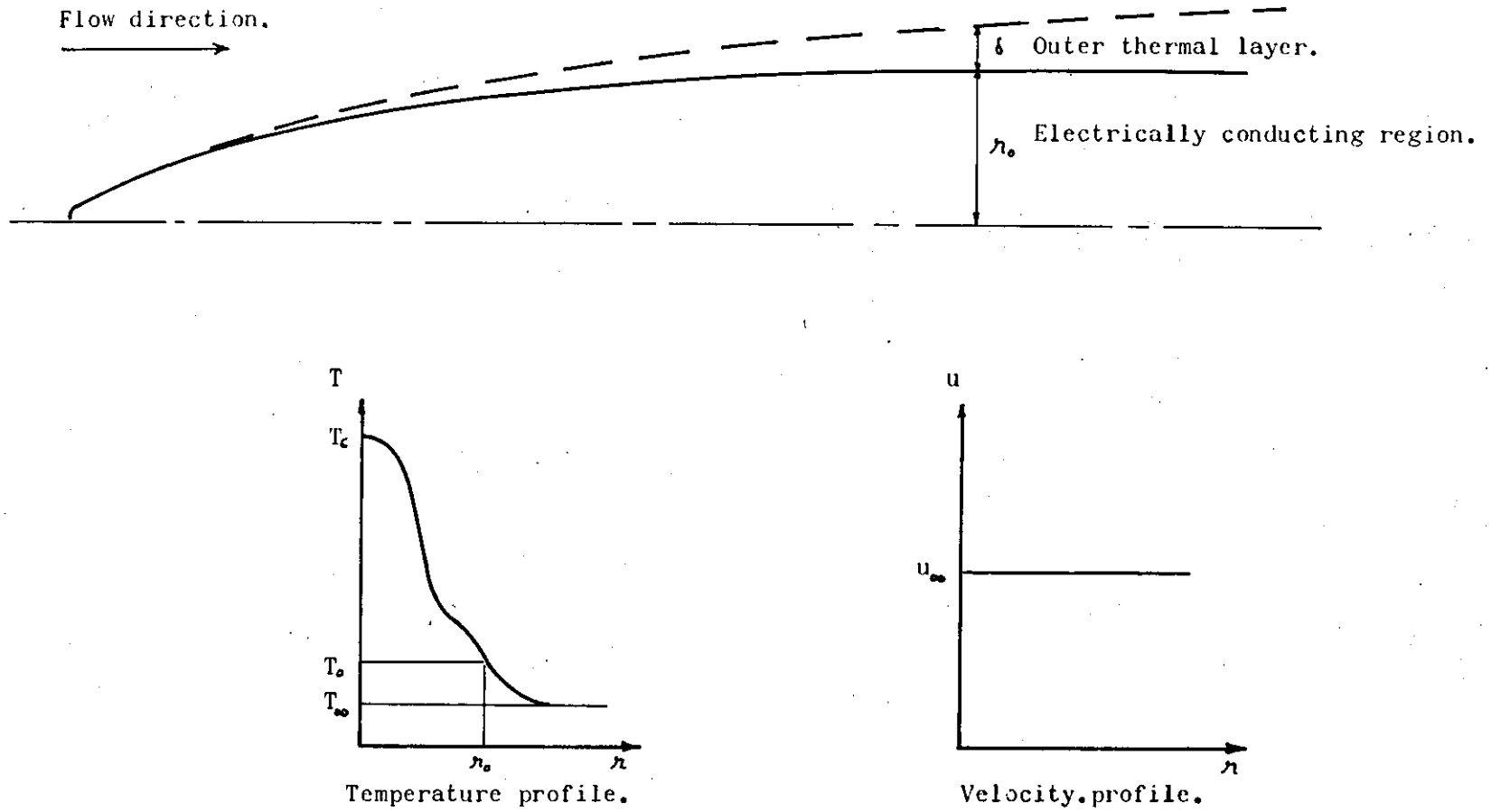

FIG.18. Model of Constant Pressure Flow Arc.

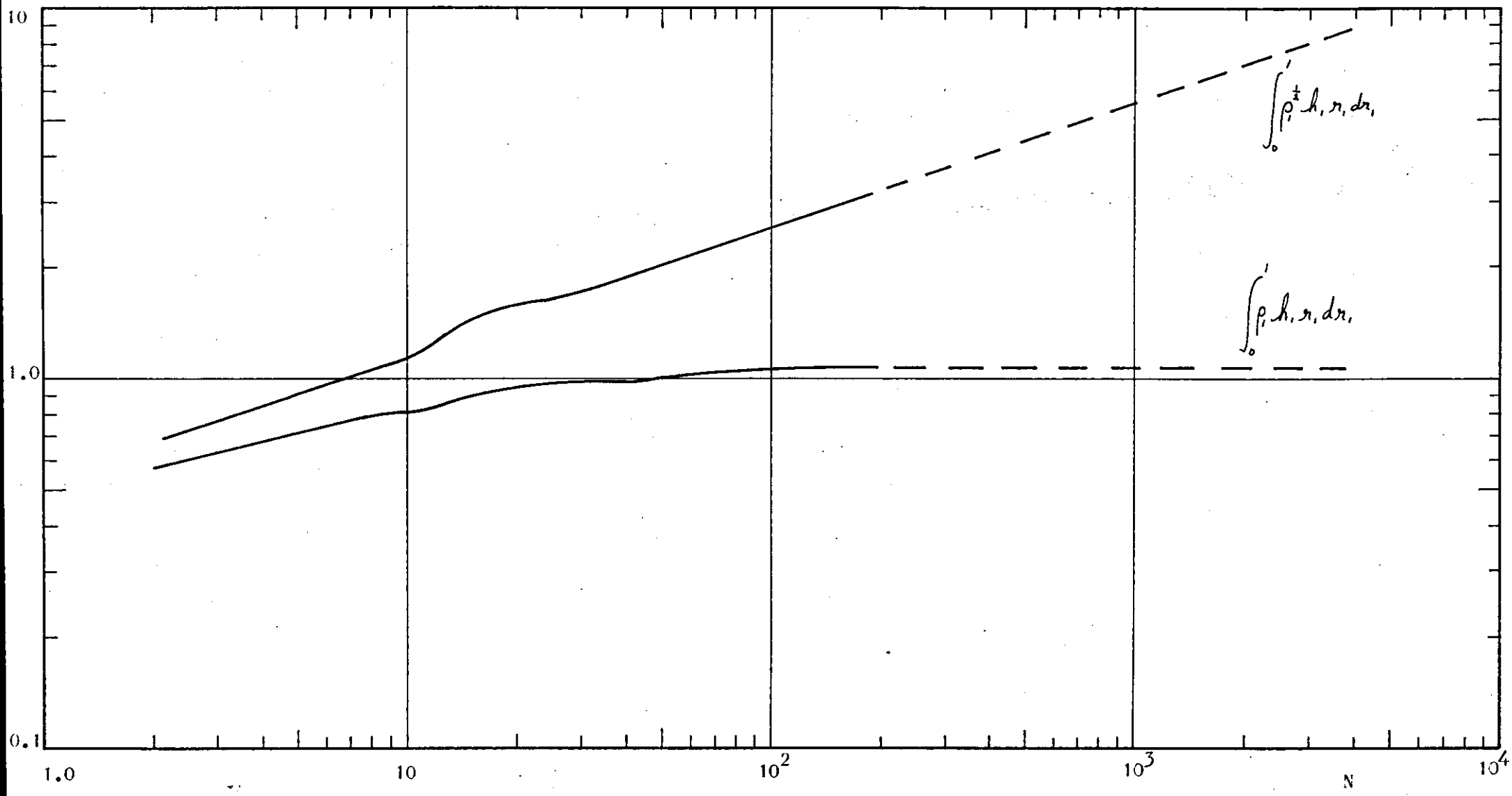

FIG.19. Non-dimensional Enthalpy Integrals for Nitrogen.

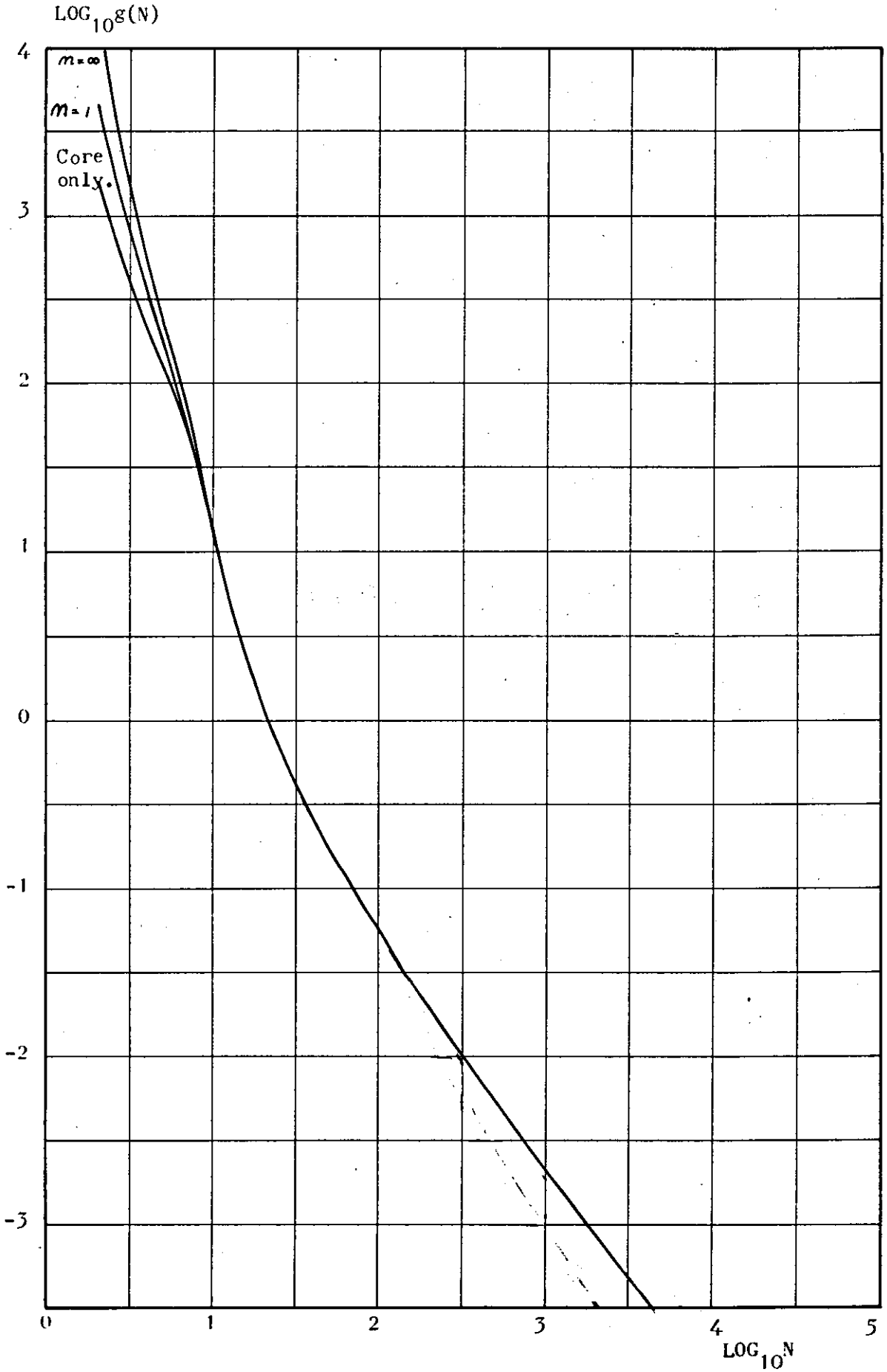

FIG.20. Overall Energy Function, g(N). Nitrogen.

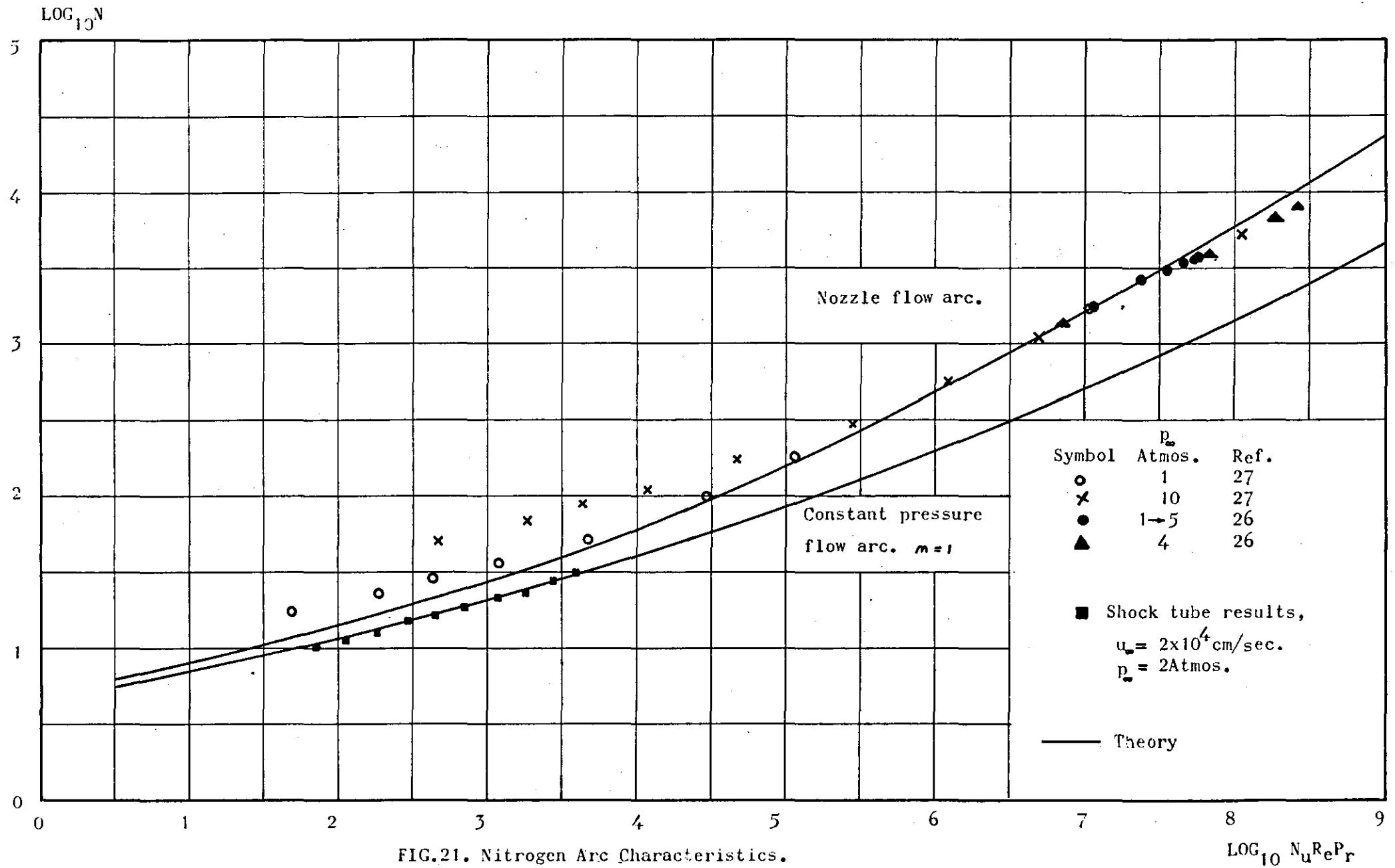

FIG.21. Nitrogen Arc Characteristics.

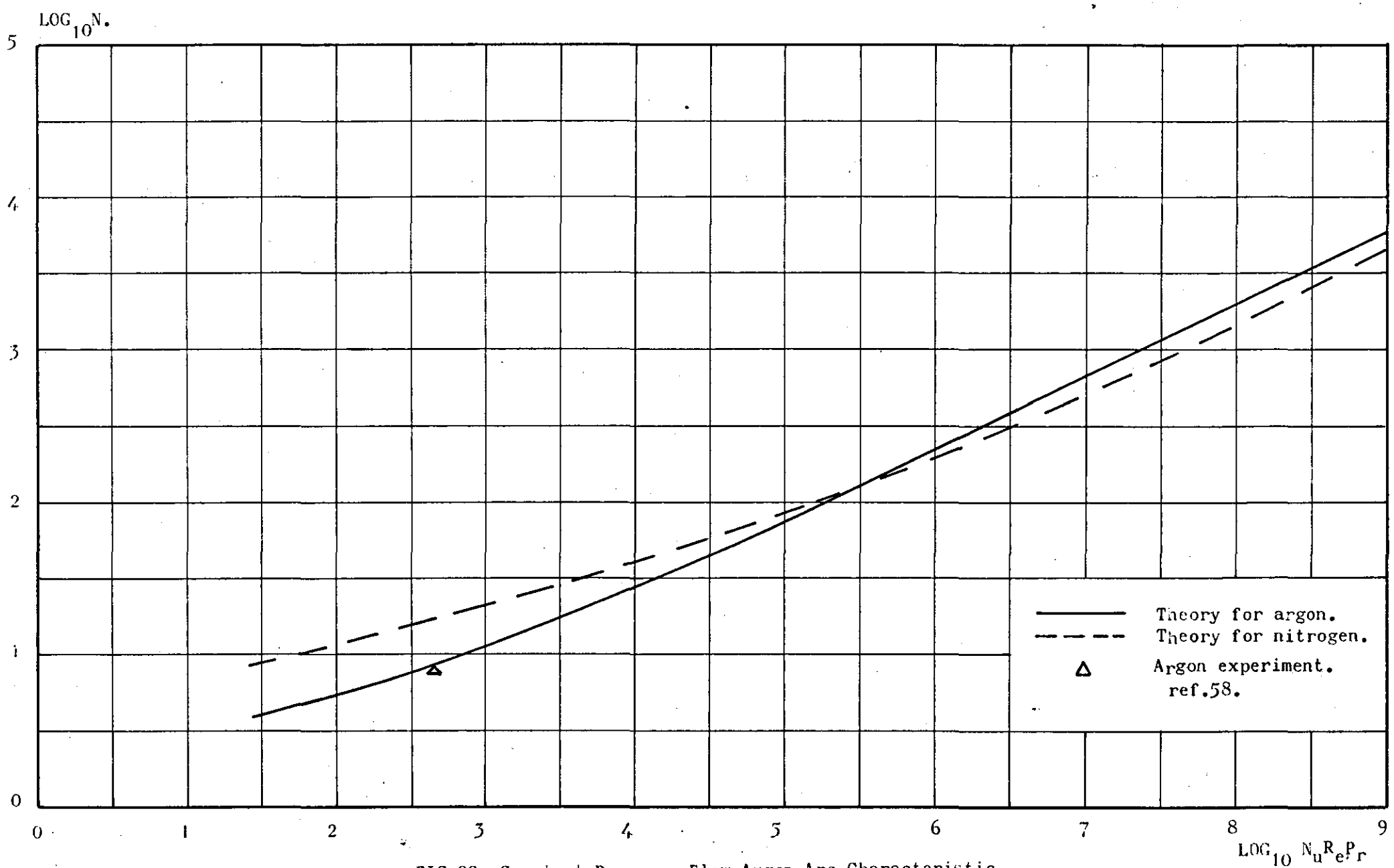

FIG.22. Constant Pressure Flow Argon Arc Characteristic

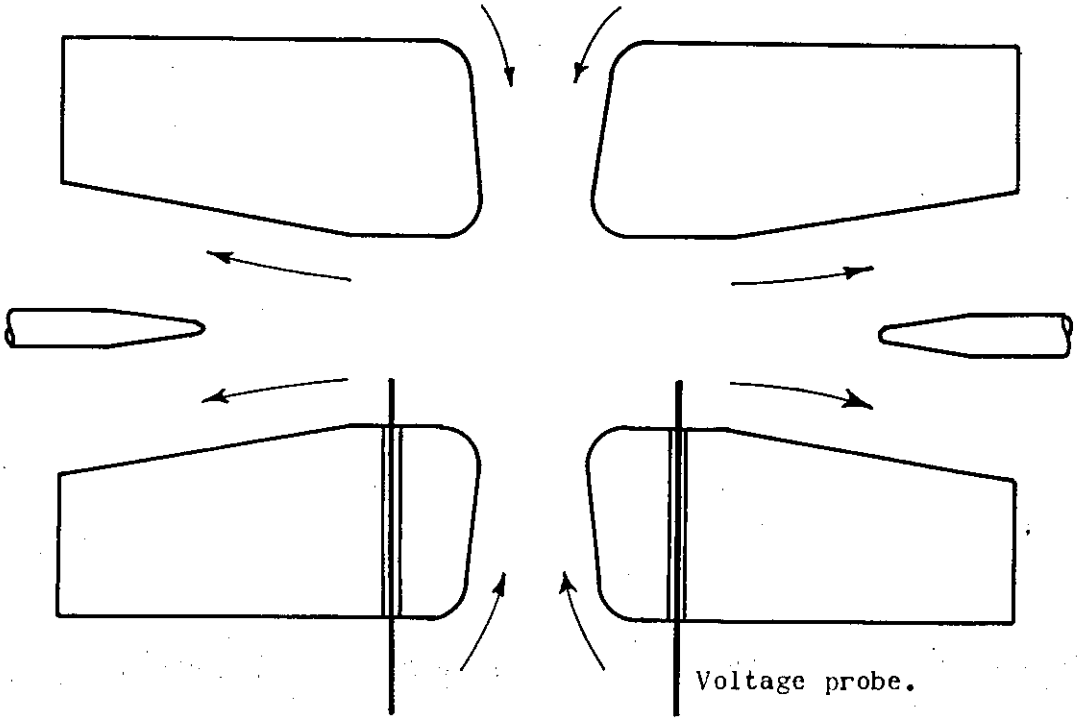

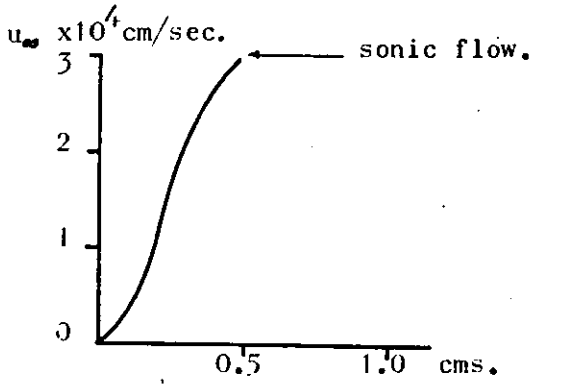

Flow velocity distribution.

FIG.23. Nozzle Arc Experiment. refs.26,27.

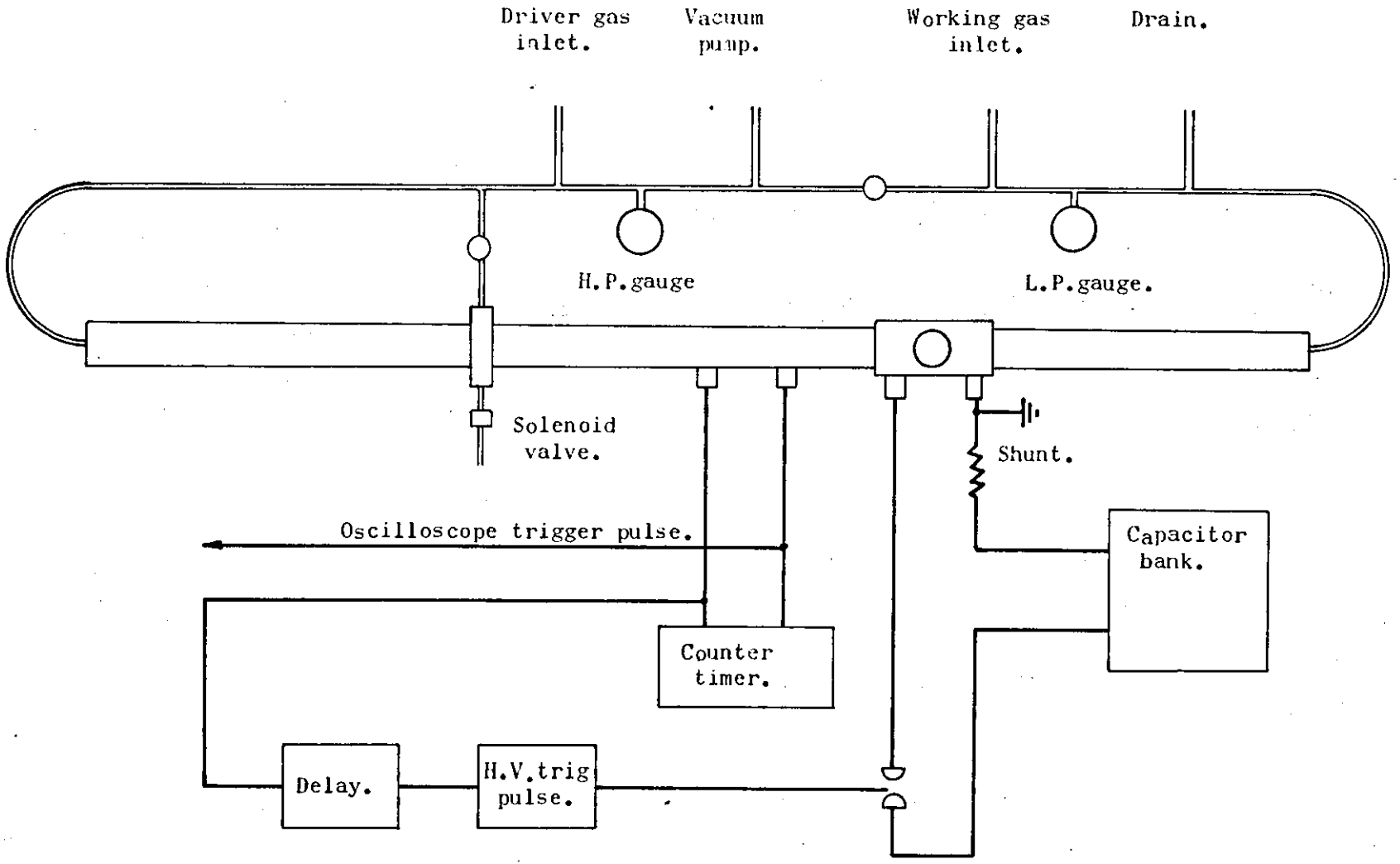

FIG.24. Shock Tube Layout.

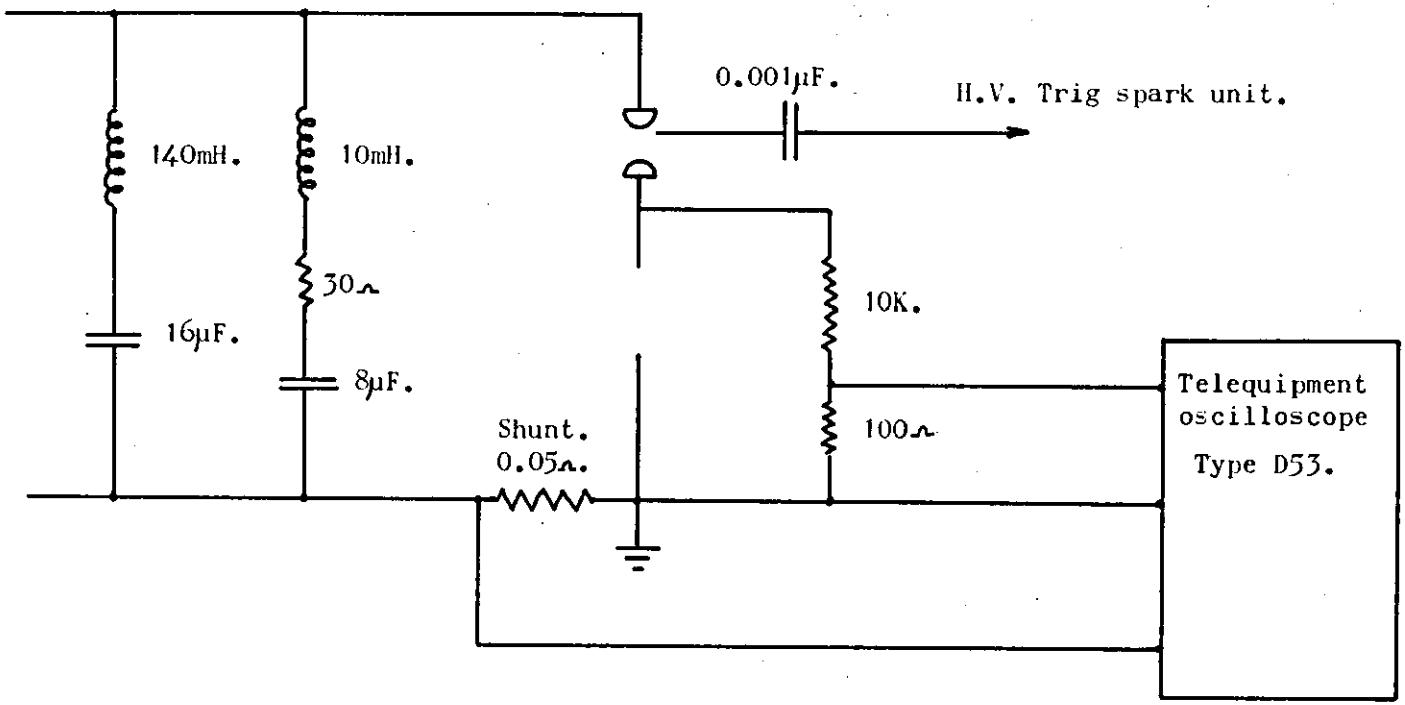

FIG.25. Main Circuit Diagram.

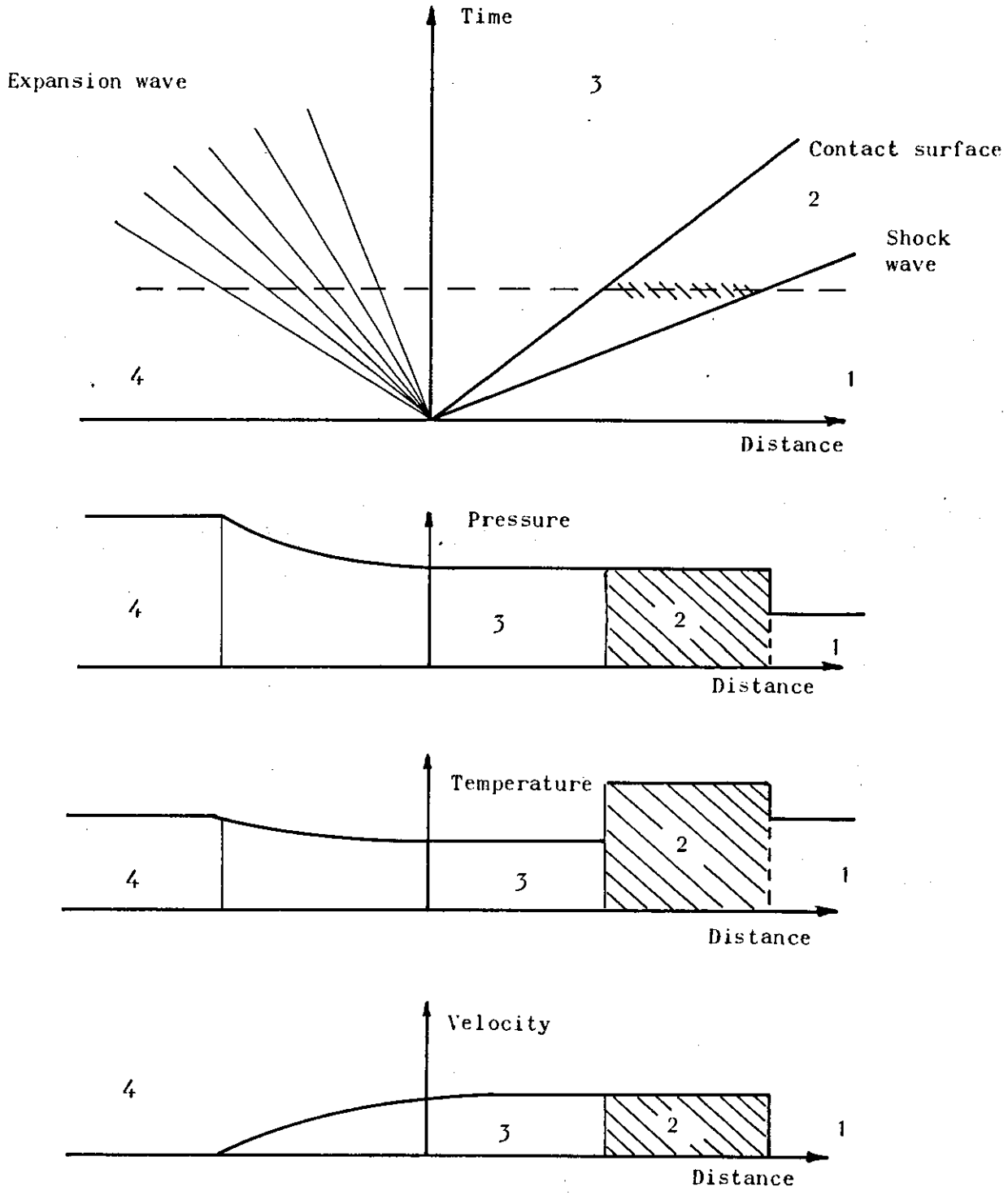

Fig. 26. Operation of Simple Shock Tube

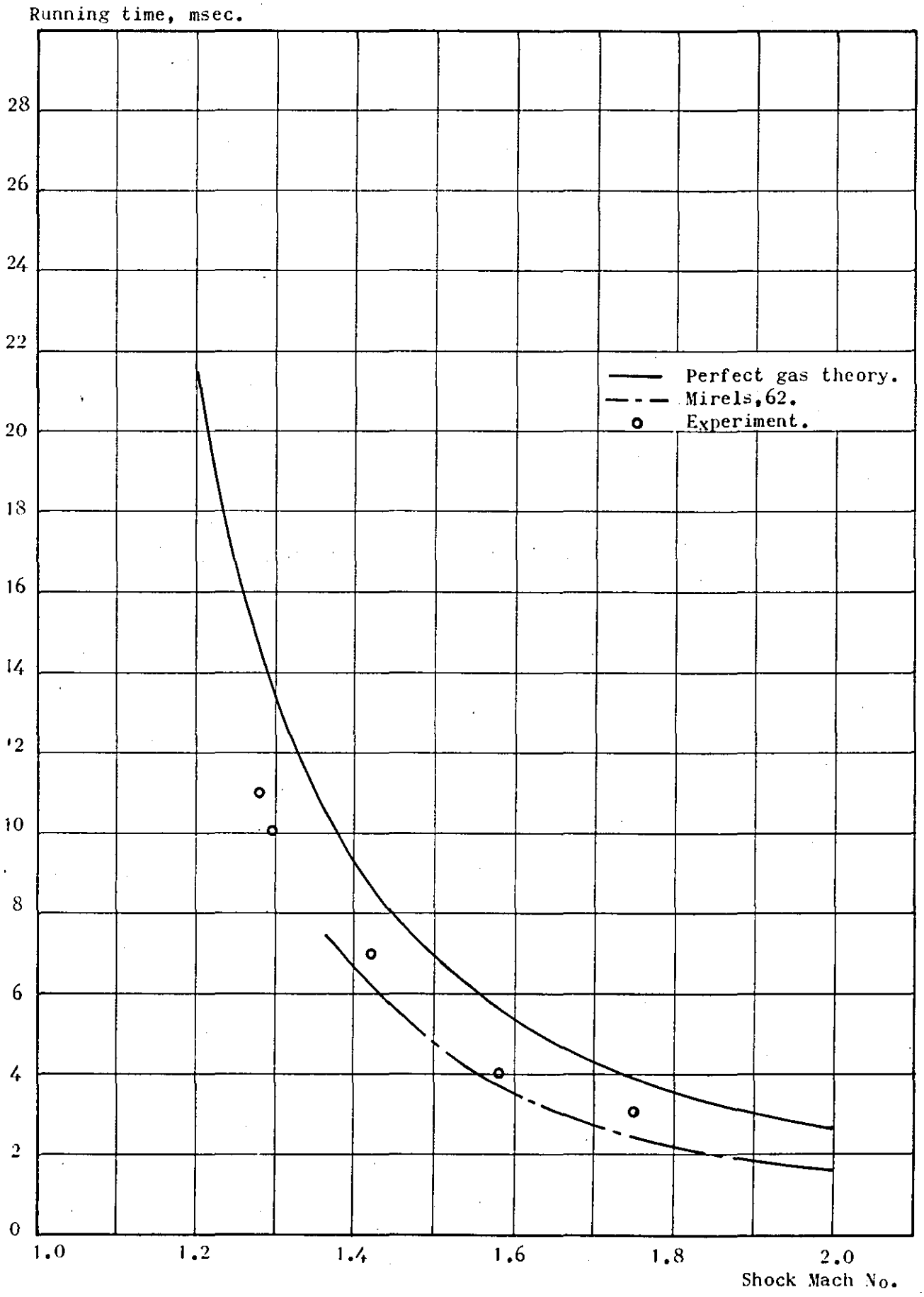

FIG. 27. Shock Tube Running Time.

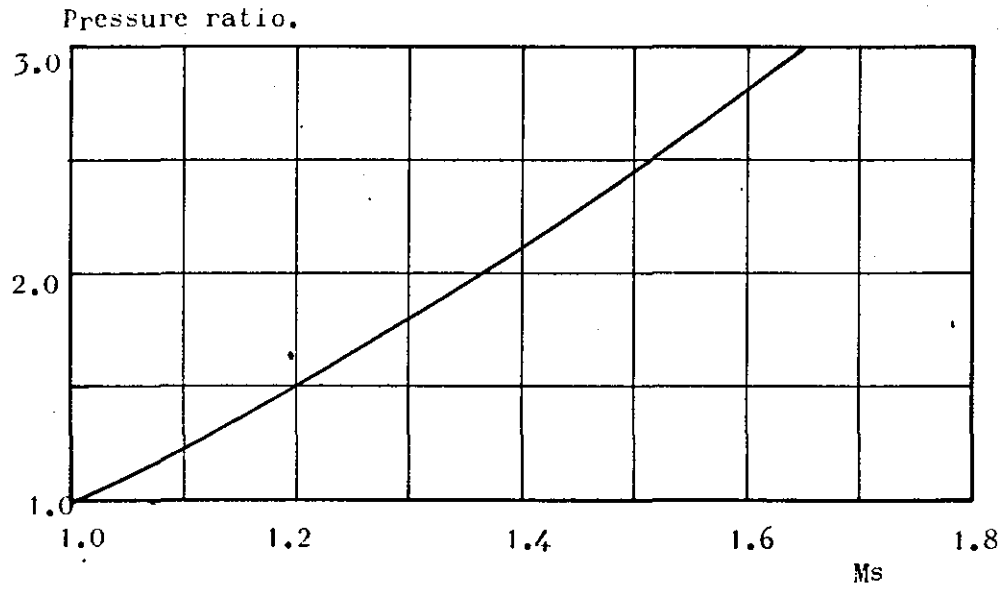

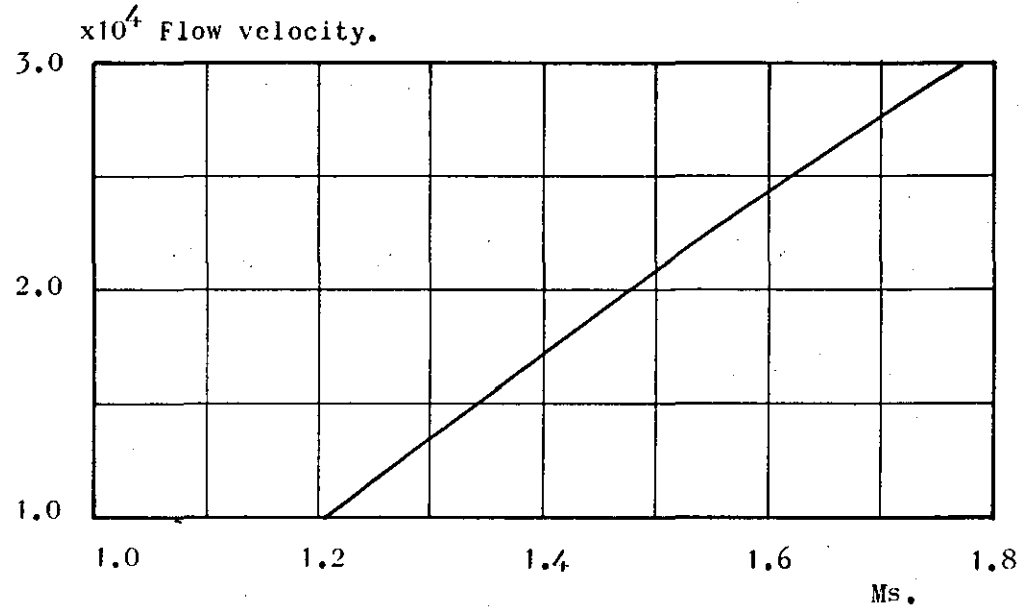

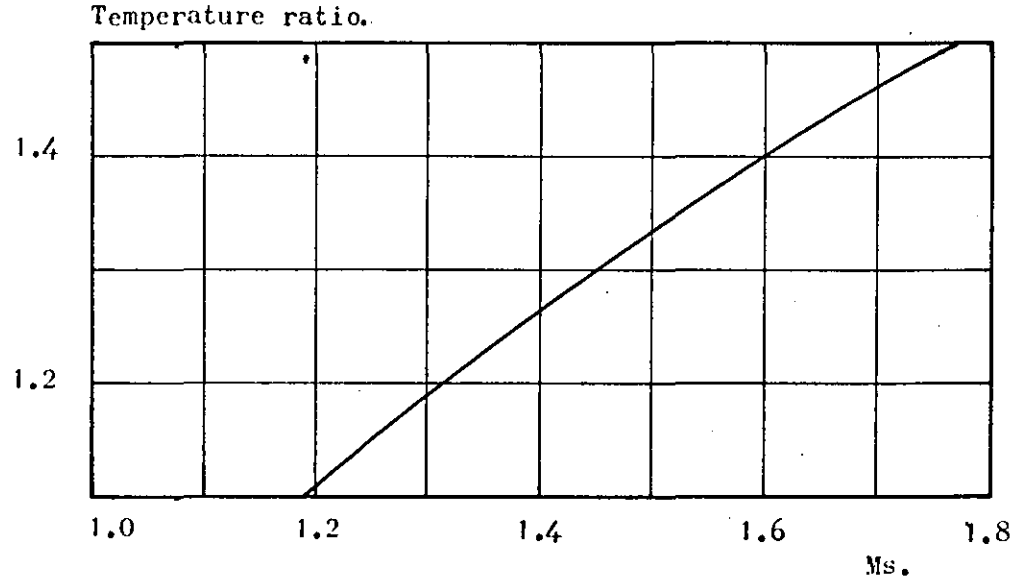

FIG.28. Conditions Across Shock Wave. $\gamma = 1.4$.

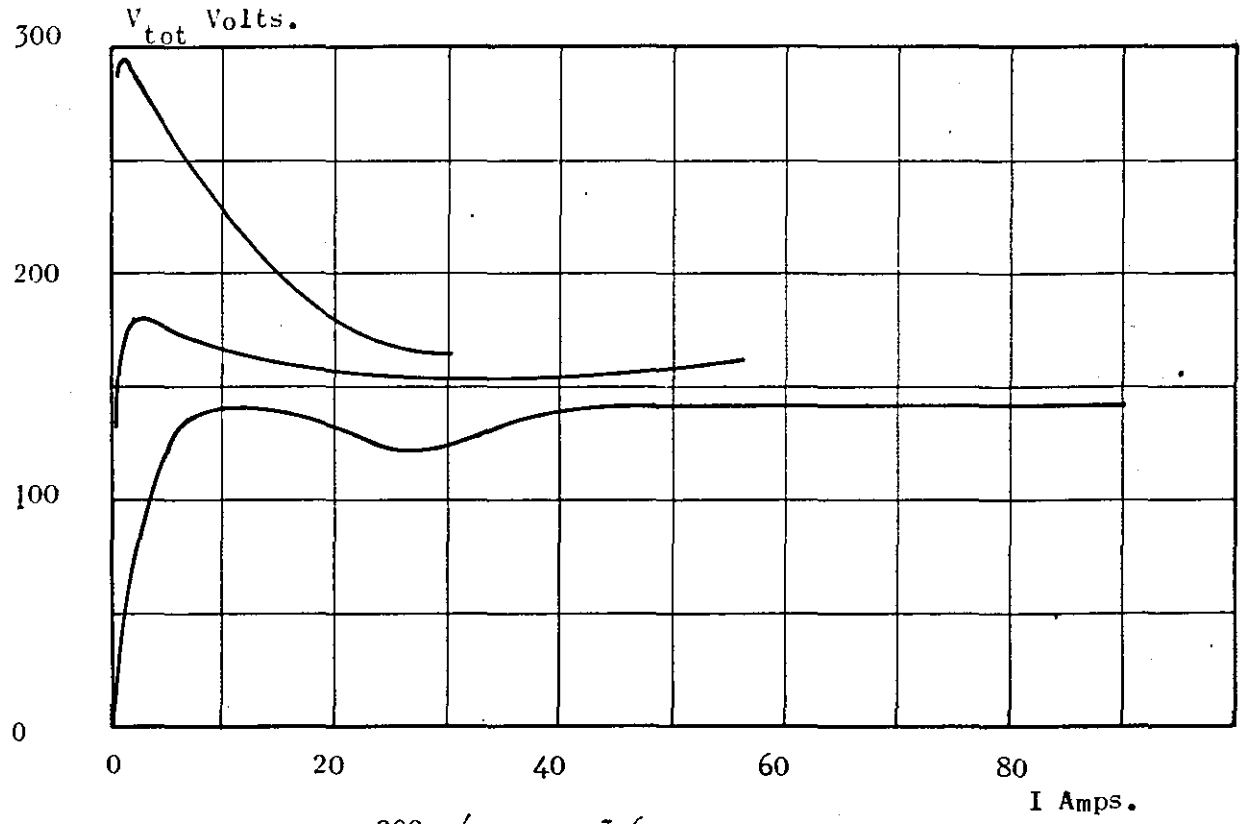

200 c/sec. $\varkappa$ =3.6 cms.

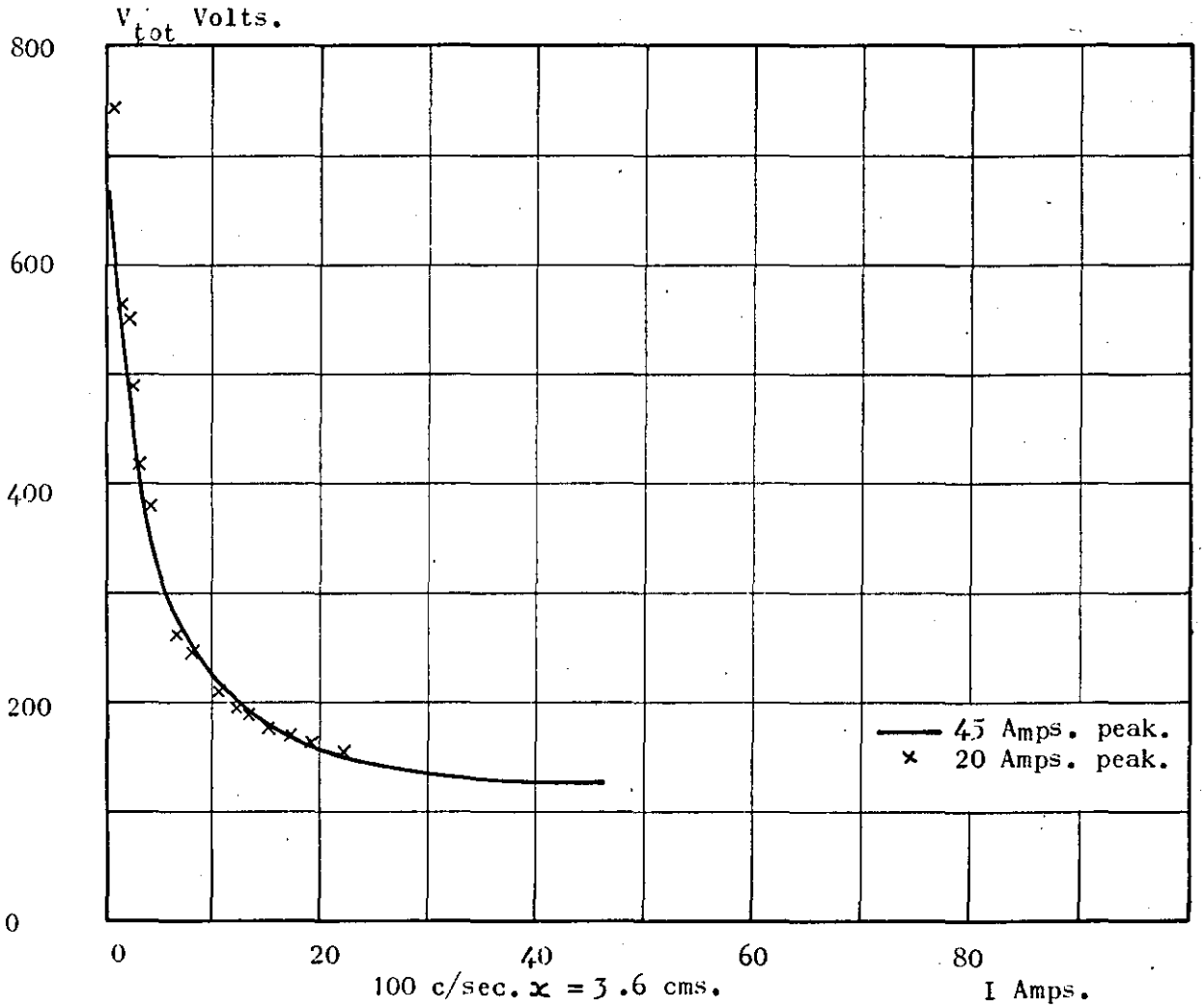

100 c/sec. $\varkappa$ = 3 .6 cms.

FIG.29. Effect of Peak Current on V— I Characterists.

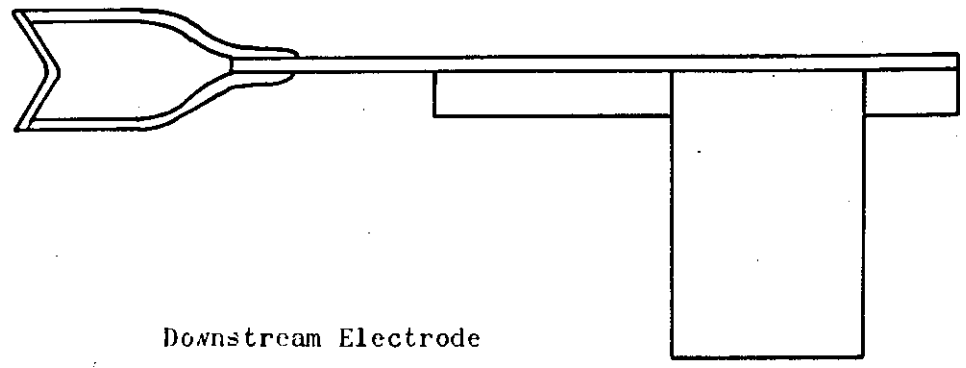

Downstream Electrode

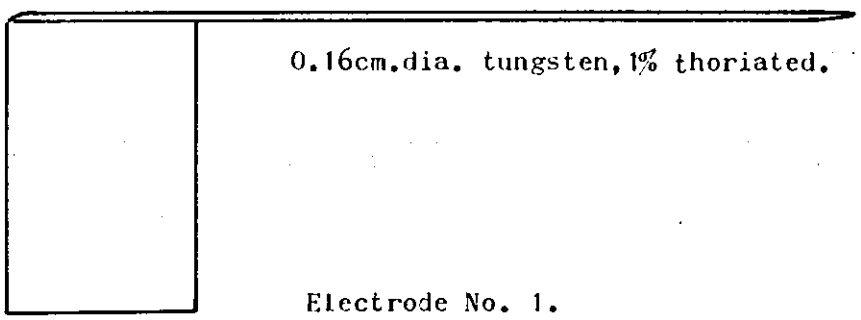

0.16cm.dia. tungsten, 1% thoriated.

Electrode No. 1.

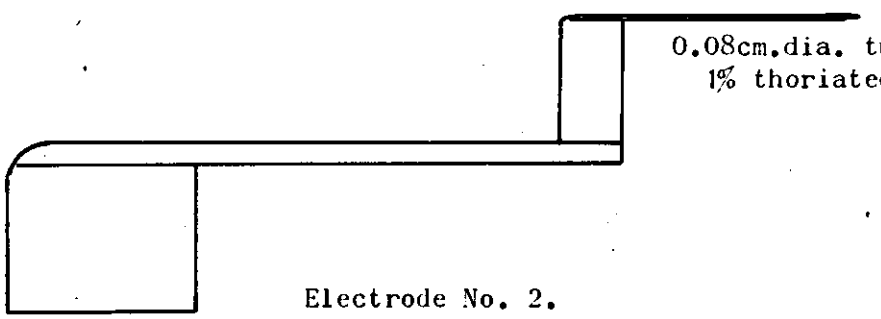

0.08cm.dia. tungsten,
1% thoriated.

Electrode No. 2.

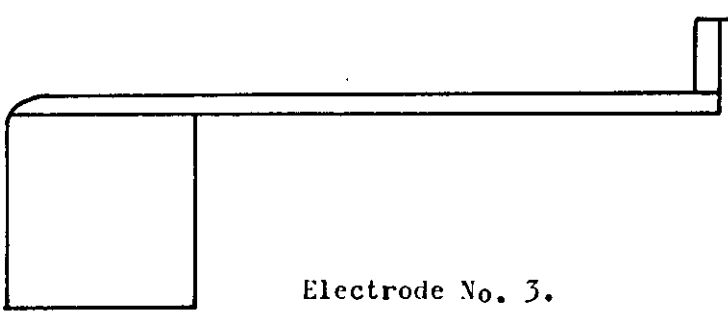

0.003cm.dia.
pure tungsten.

Electrode No. 3.

FIG.30. Electrode Systems Used, Full Scale.

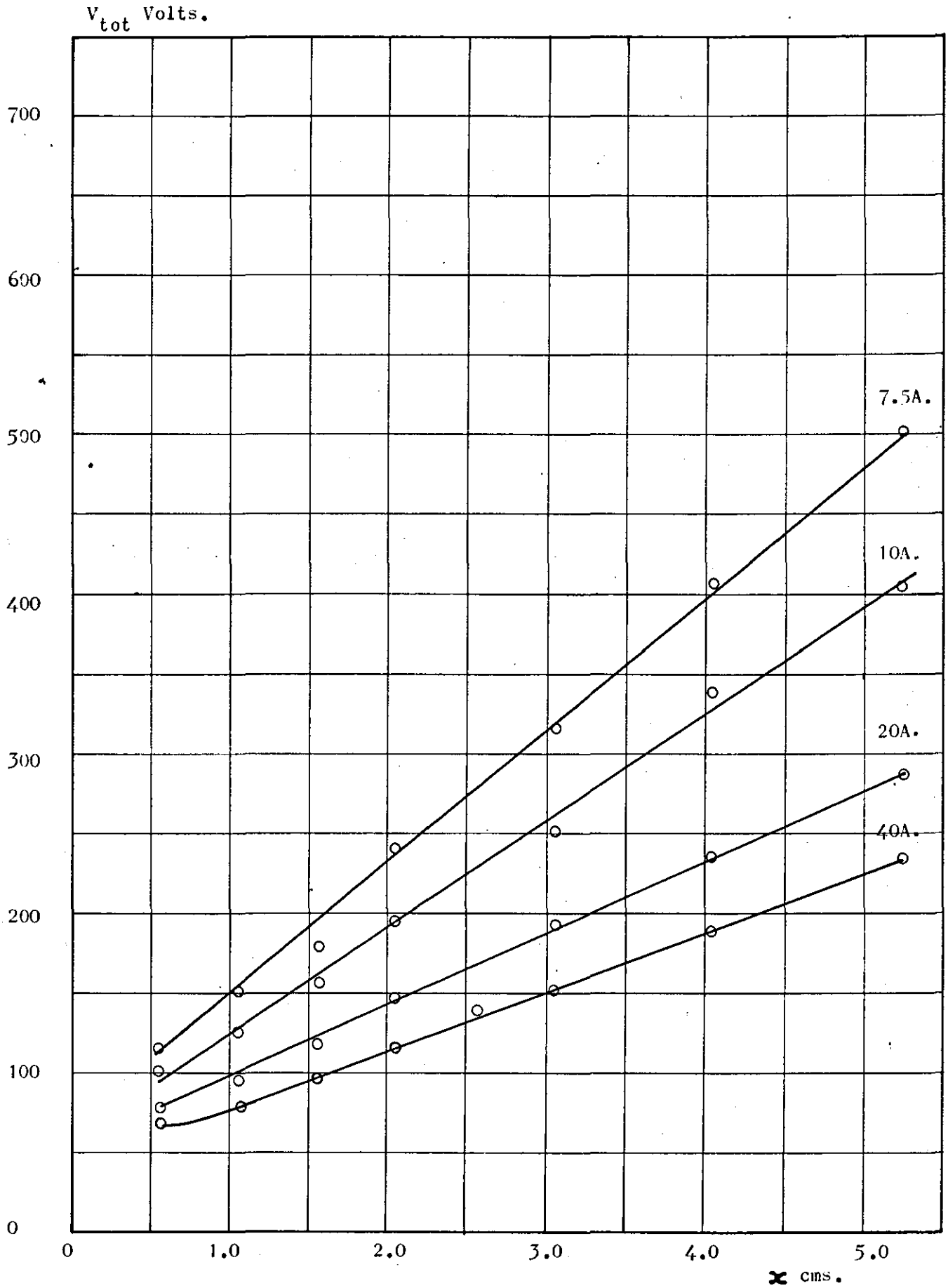

FIG.31. Arc Voltage Distributions, Electrode No.1.

$u_\infty = 2 \times 10^4$ cms/sec. 2 Atmos.press.

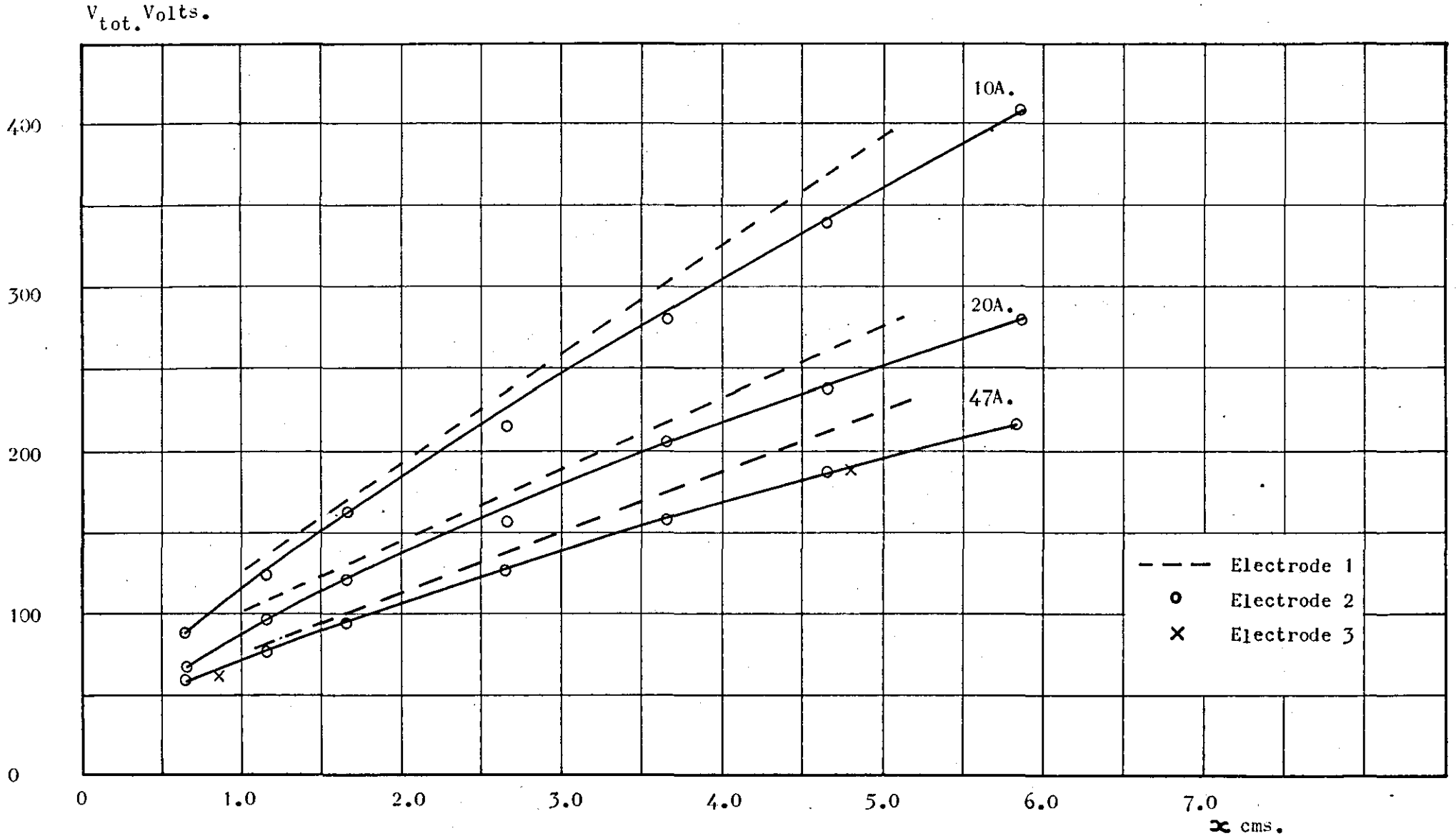

FIG.32. Arc Voltage Distributions, $u = 2 \times 10^4$ cms/sec. 2 Atmos.press.

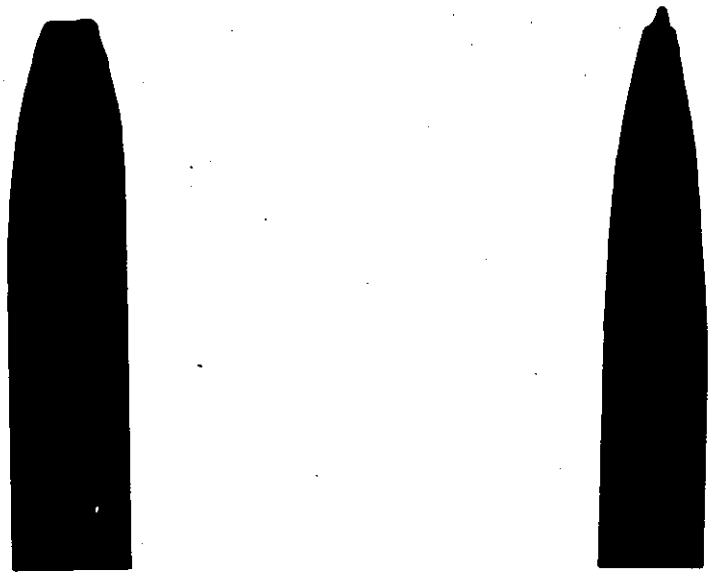

(a) (b)

FIG.33. Upstream Electrode Shapes. × 16 Mag.

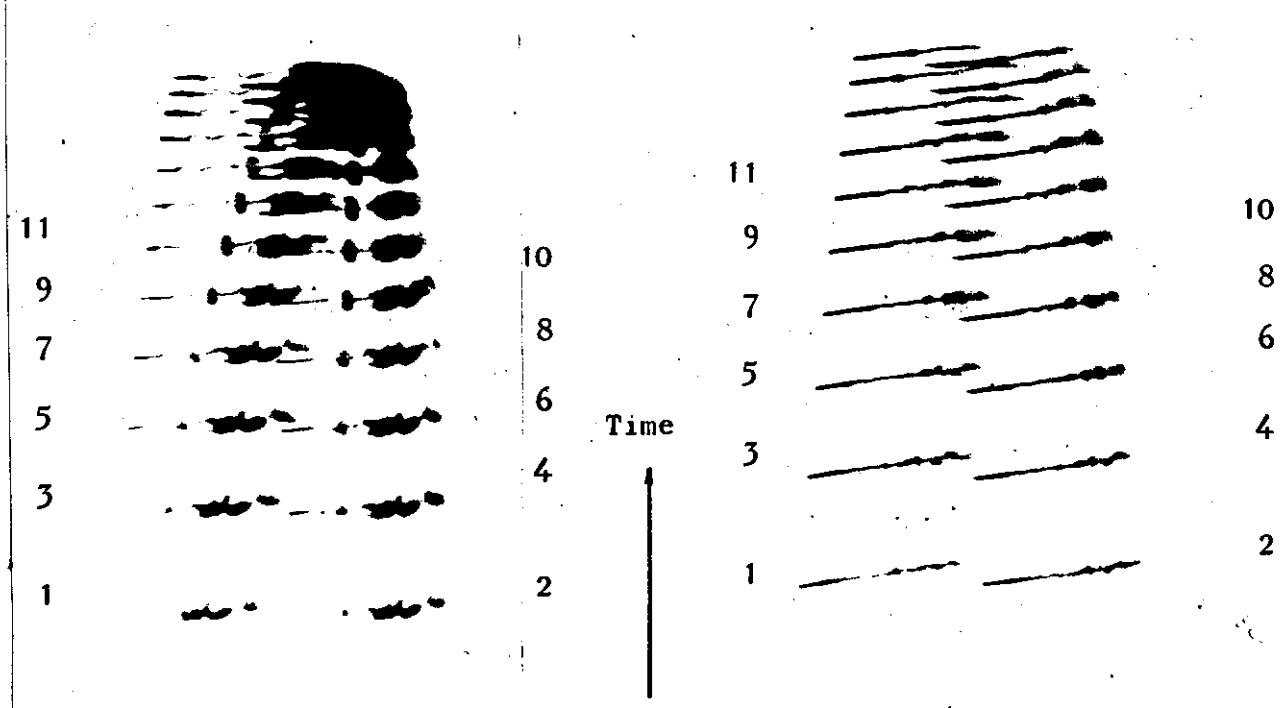

Electrode Reynolds No. 2.5×10^5.

$u_\infty = 9 \times 10^3$ cm/sec. $p_\infty = 2$ Atmos.

10^5 Pictures/sec.

Electrode Reynolds No. 7×10^5.

$u_\infty = 2 \times 10^4$ cm/sec. $p_\infty = 2$ Atmos.

10^5 Pictures/sec.

FIG.34. Arc Behaviour in Turbulent Flow,

Electrode Shape (a).

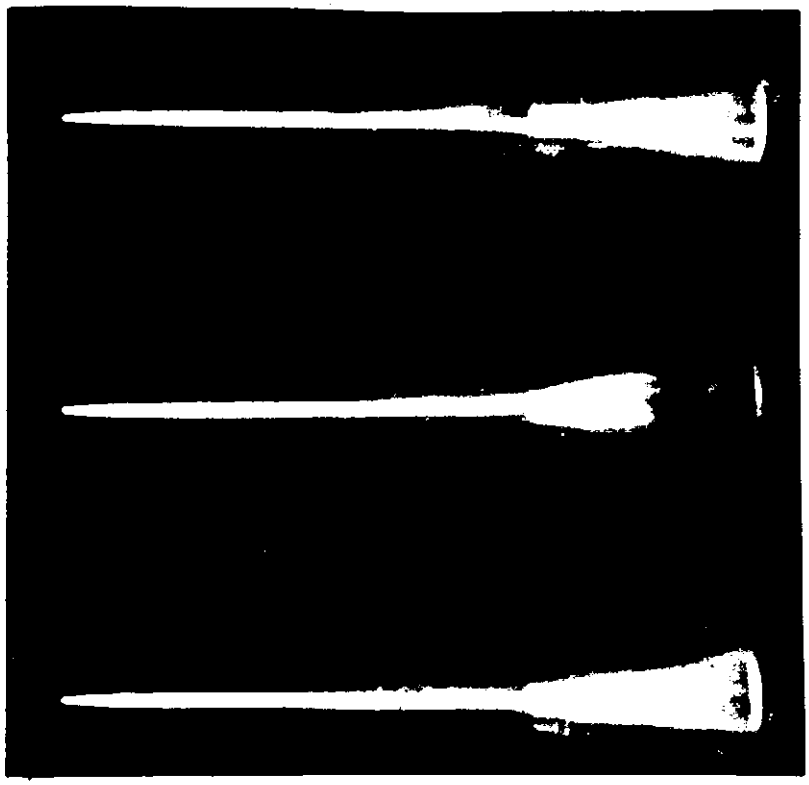

Time

Flow direction

40 Amps.

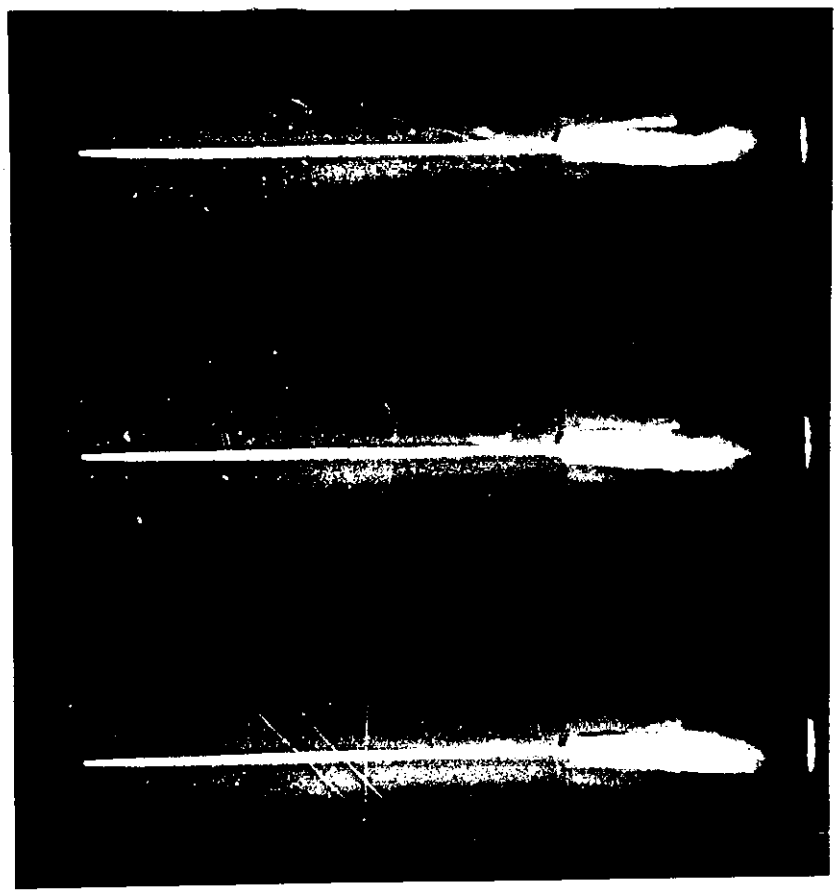

Time.

Flow direction

10 Amps.

FIG. 35. Arc Behaviour in Laminar Flow. x = 3.0cms.

$u_\infty = 2 \times 10^4$, p_∞ = 2 Atmos. 12,000 pictures/sec.

Electrode Shape (b).

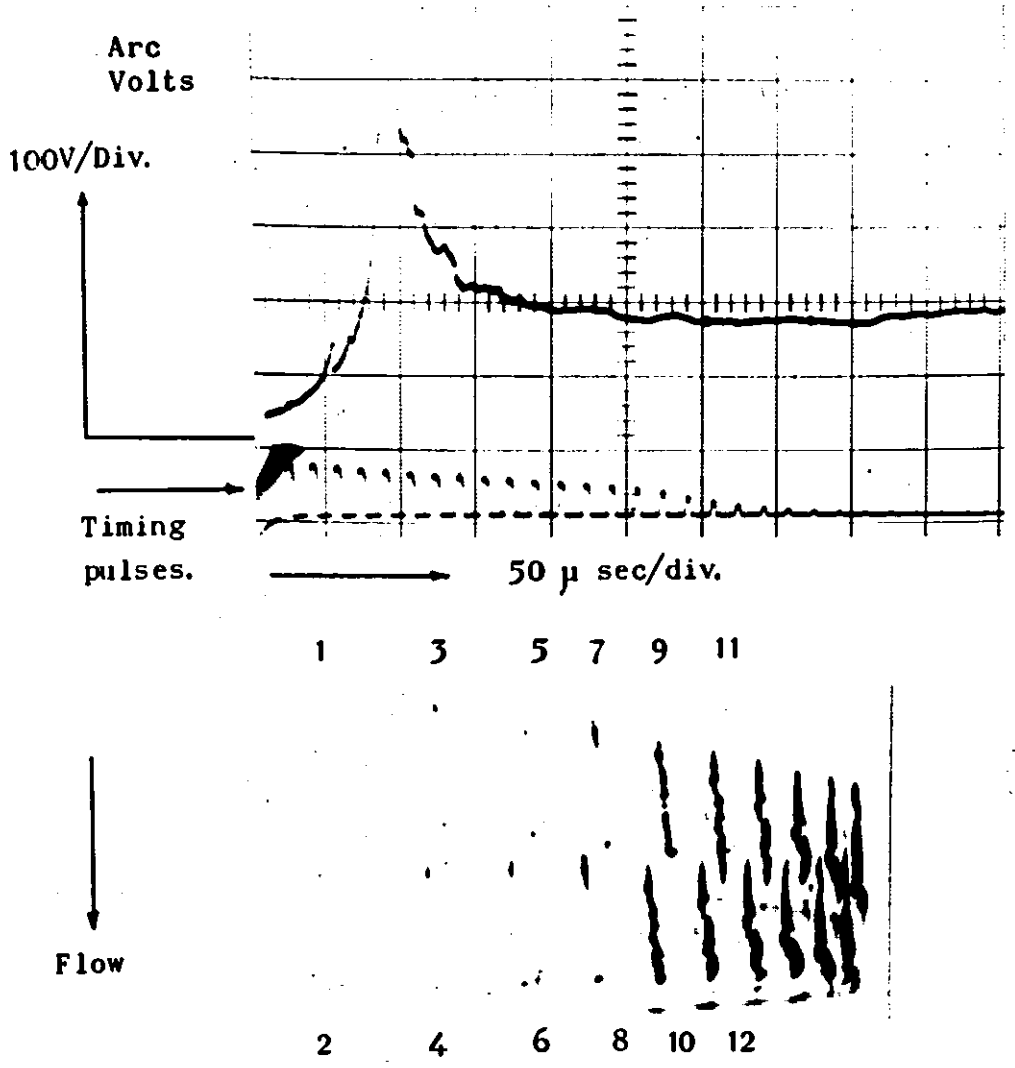

10^5 Pictures/sec. Two Pictures occur between each timing pulse.

FIG.36. Fuse Blowing and Arc Initiation.

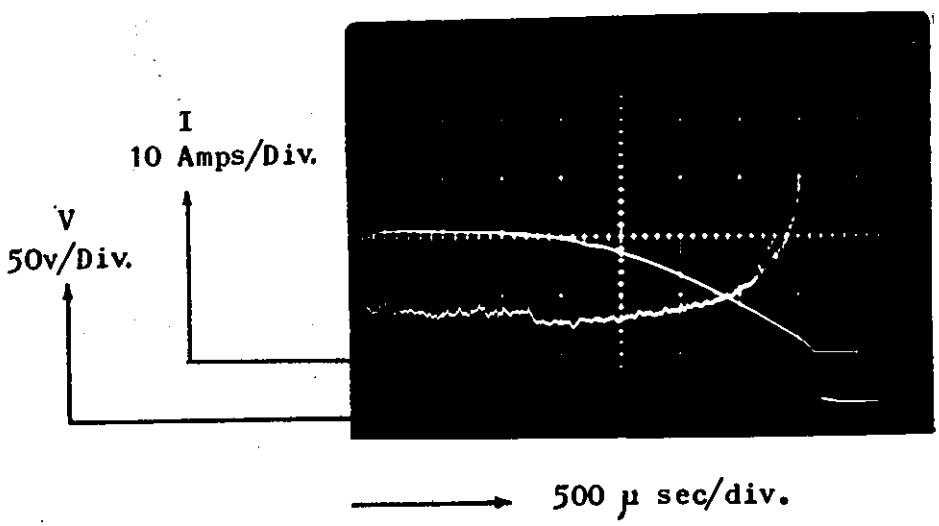

FIG. 37. Arc Voltage showing Change in Cathode Mechanism.

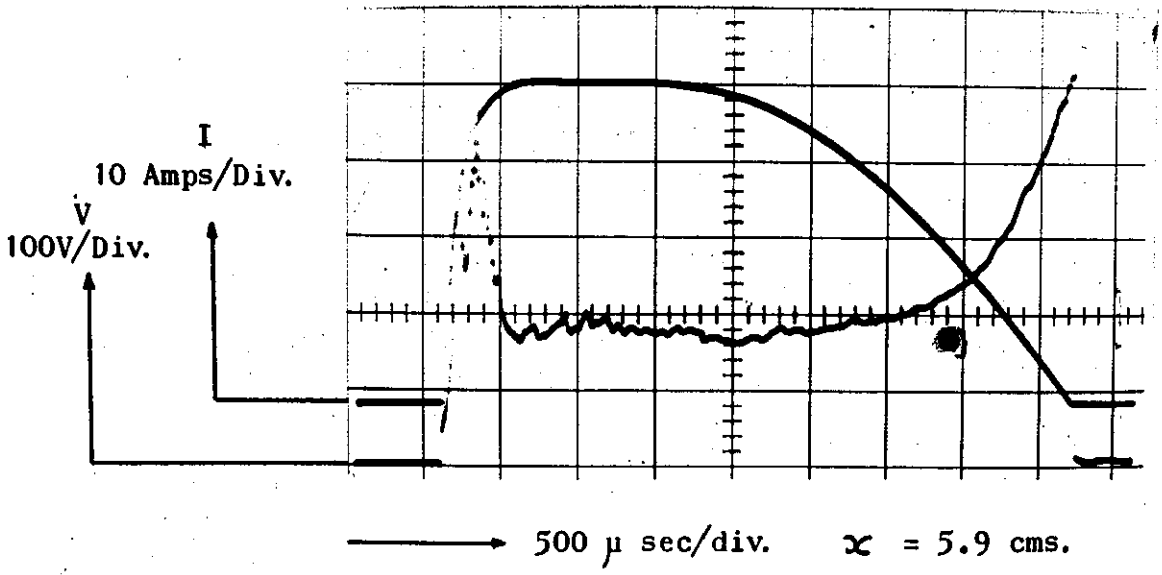

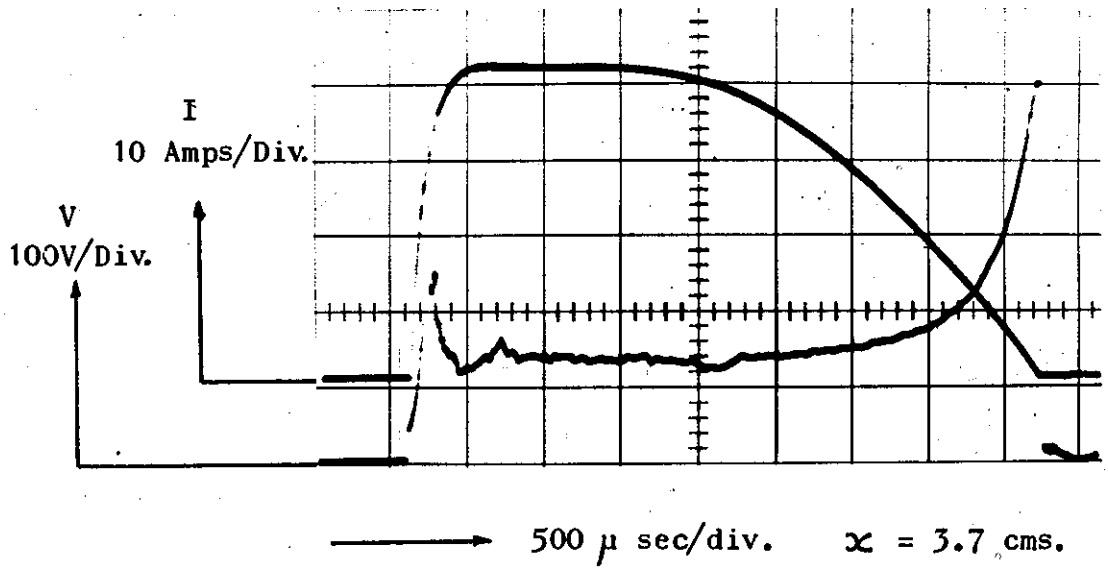

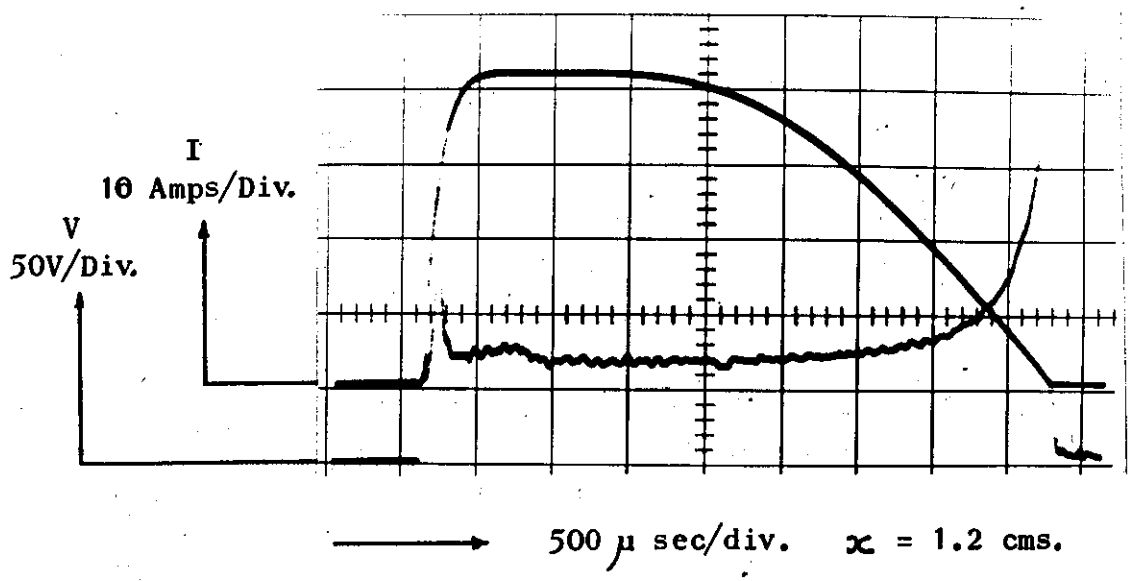

FIG.38. Arc Voltage and Current Records.

$u_\infty = 2 \times 10^4$ cm/sec, p_∞=1 Atmos.

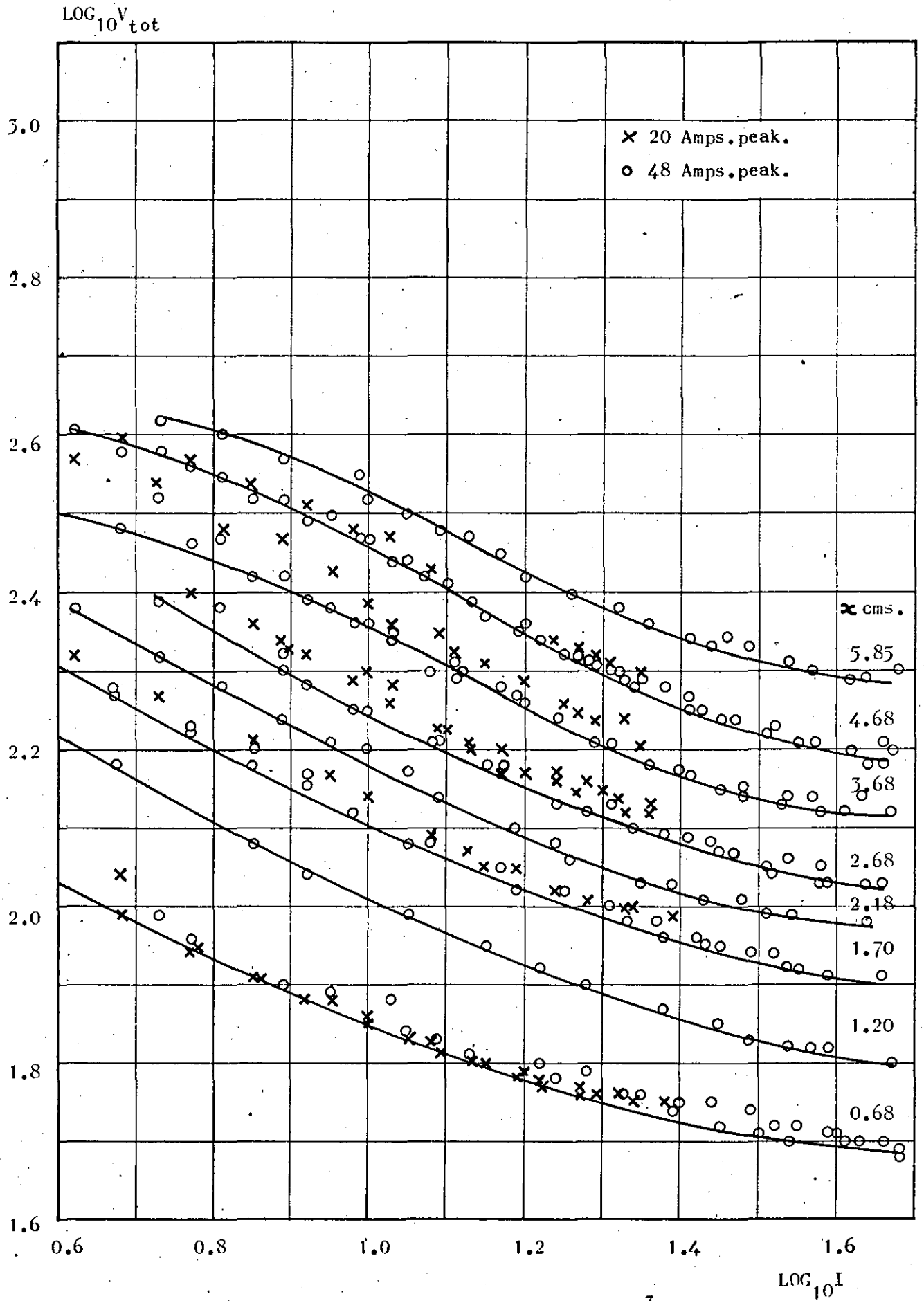

FIG.39. V_{tot} – I Characteristics. $u_{\infty} = 9 \times 10^3$ cms/sec. 2 Atmos.

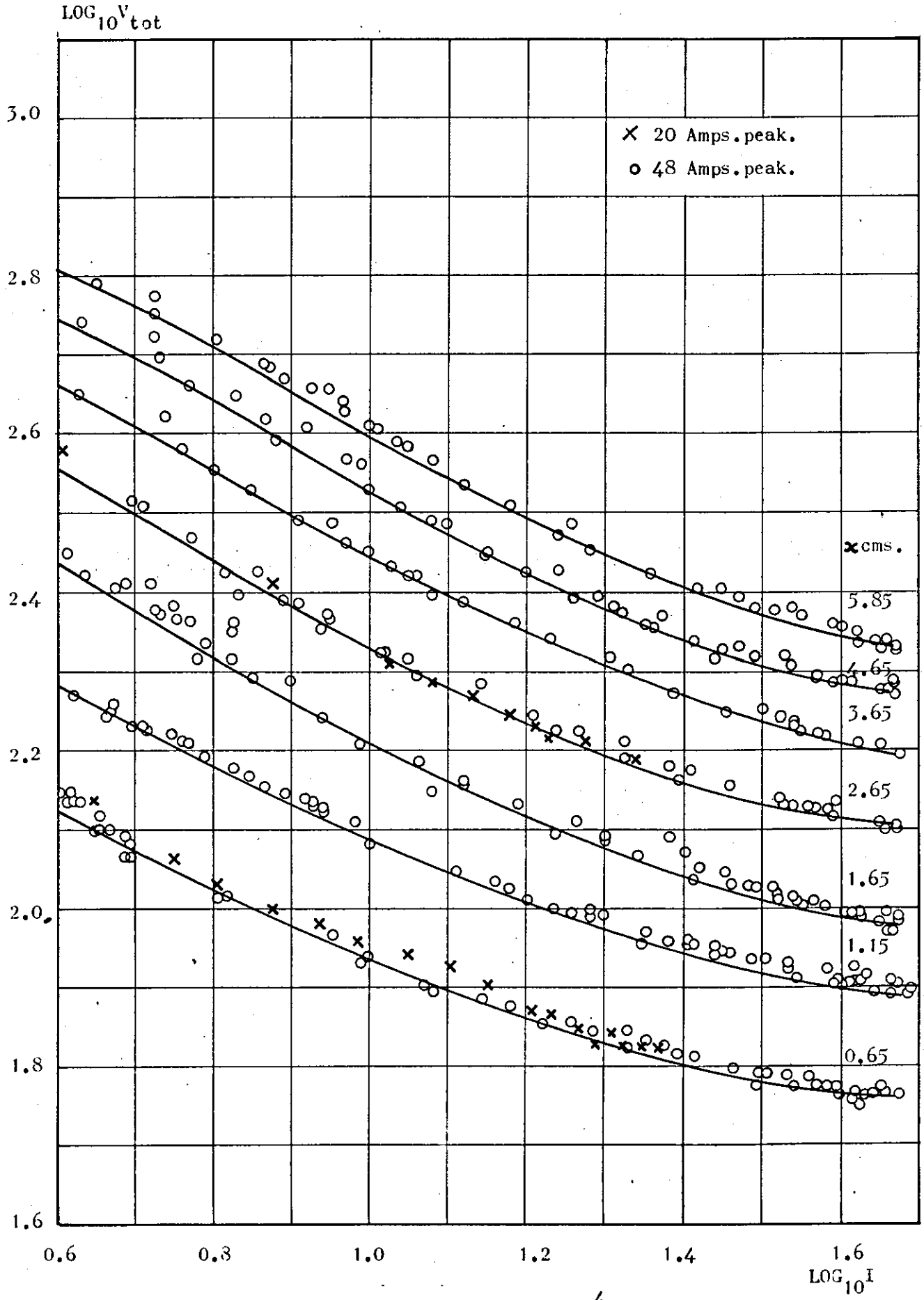

FIG.40. V_{tot} – I Characteristics. $u_\infty = 2 \times 10^4$ cms/sec. 2 Atmos.

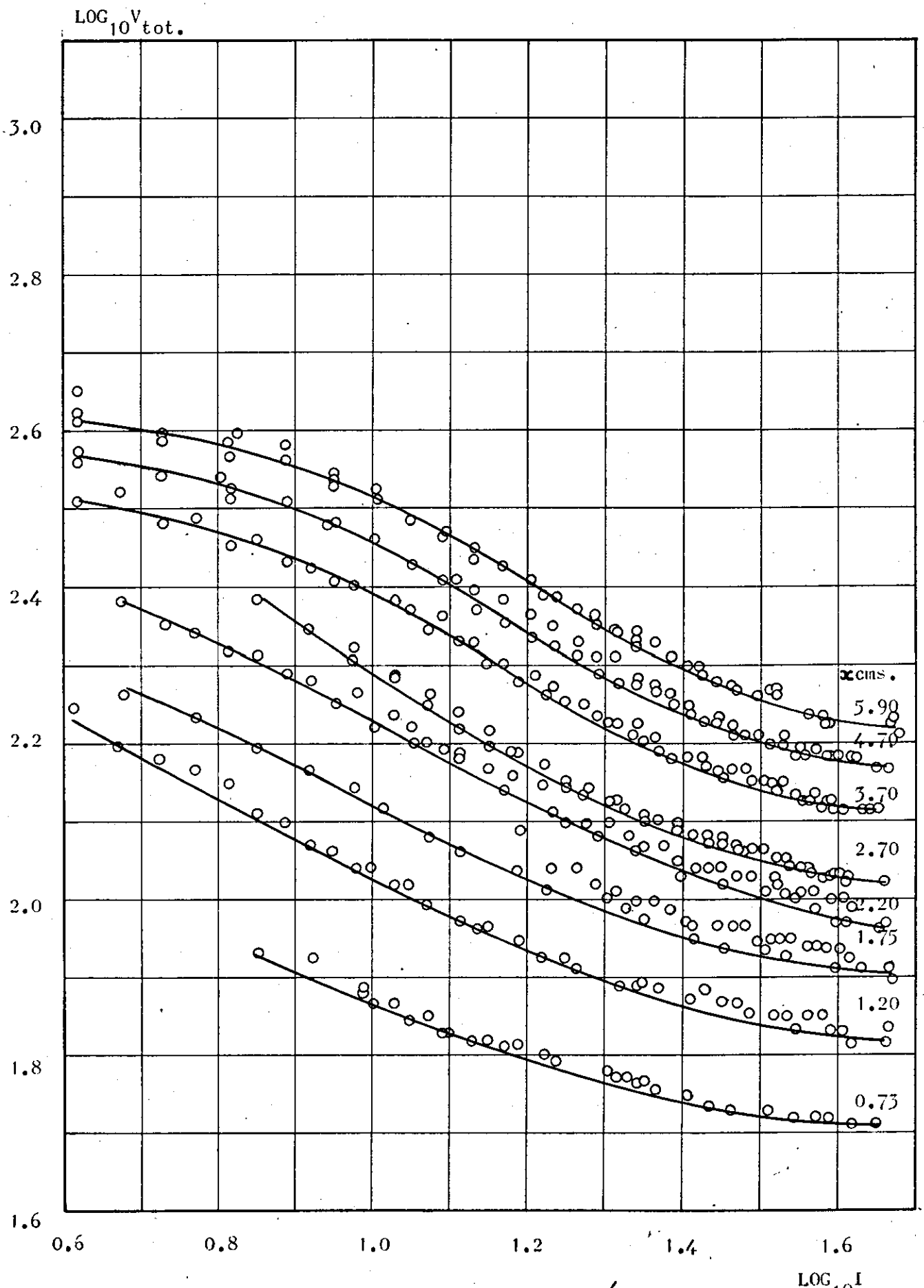

FIG.41. V_{tot} — I Characteristics. $u_\infty = 2 \times 10^4$ cms/sec. 1 Atmos.

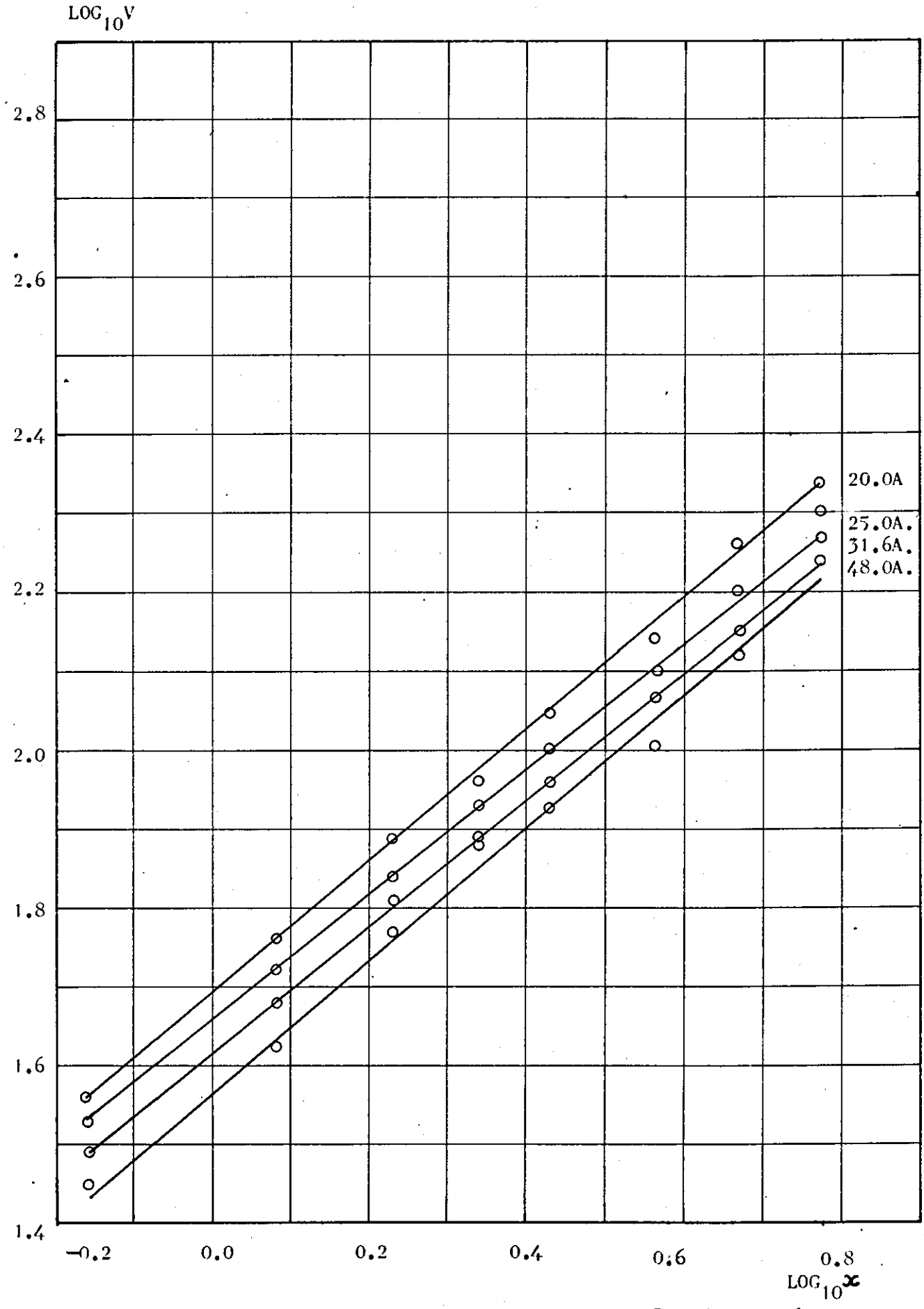

FIG.42. Arc Column Voltage Distribution, $u_\infty = 9 \times 10^3$ cms/sec. 2Atmos.

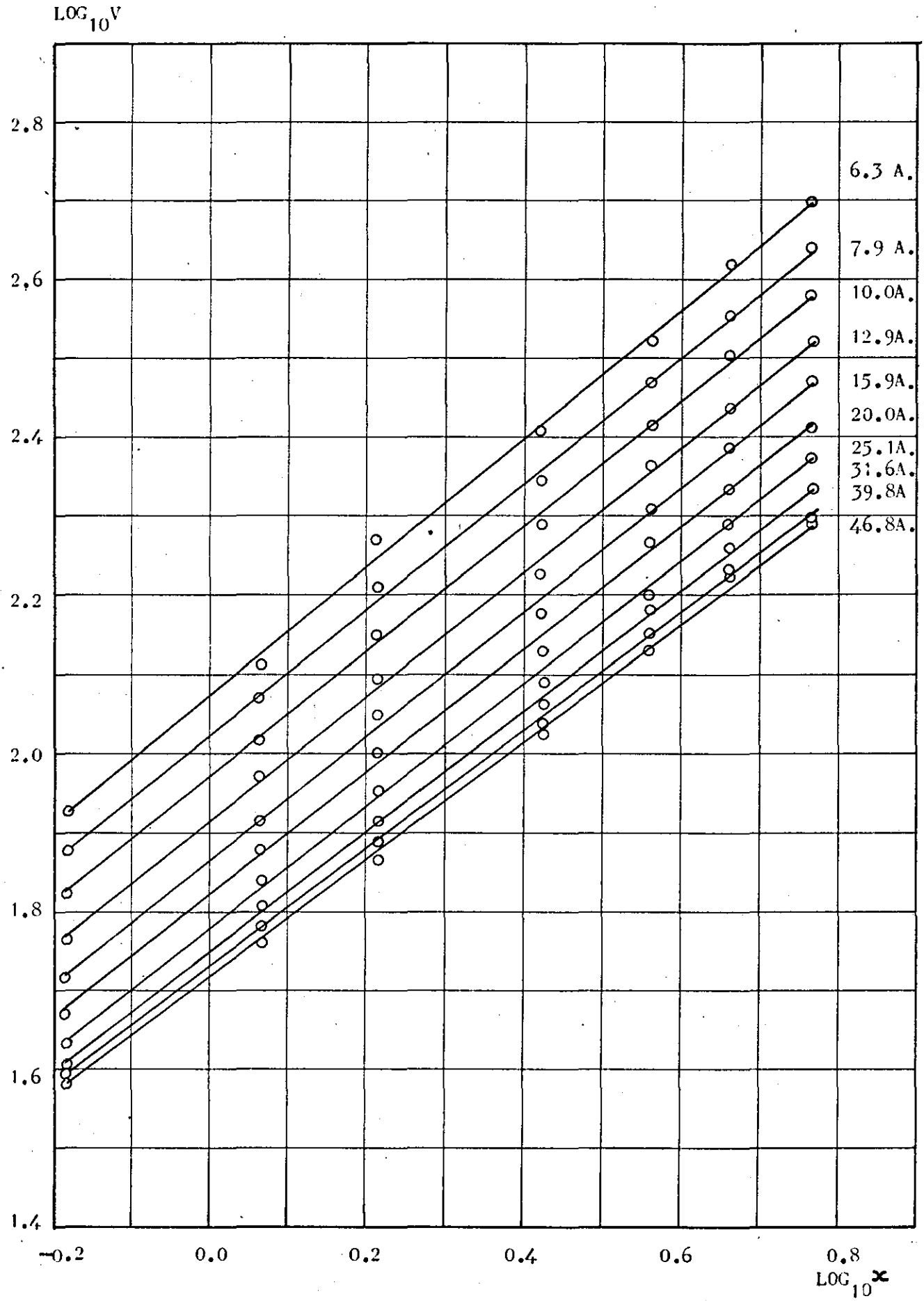

FIG.43. Arc Column Voltage Distribution, $u_\infty = 2 \times 10^4$ cms/sec. 2 Atmos.

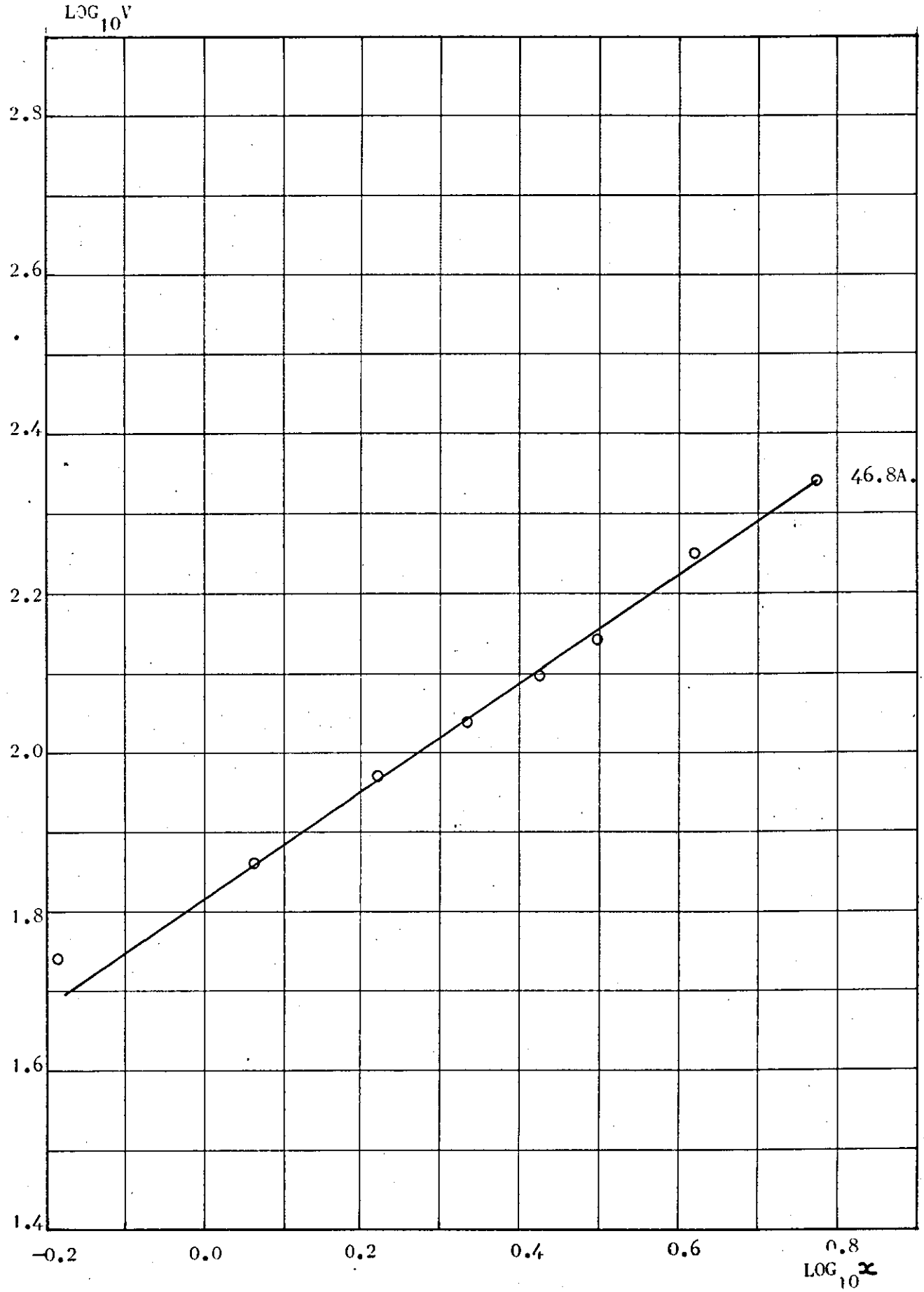

FIG.44. Arc Column Voltage Distribution, $u_o = 3 \times 10^4$ cms/sec. 2 Atmos.

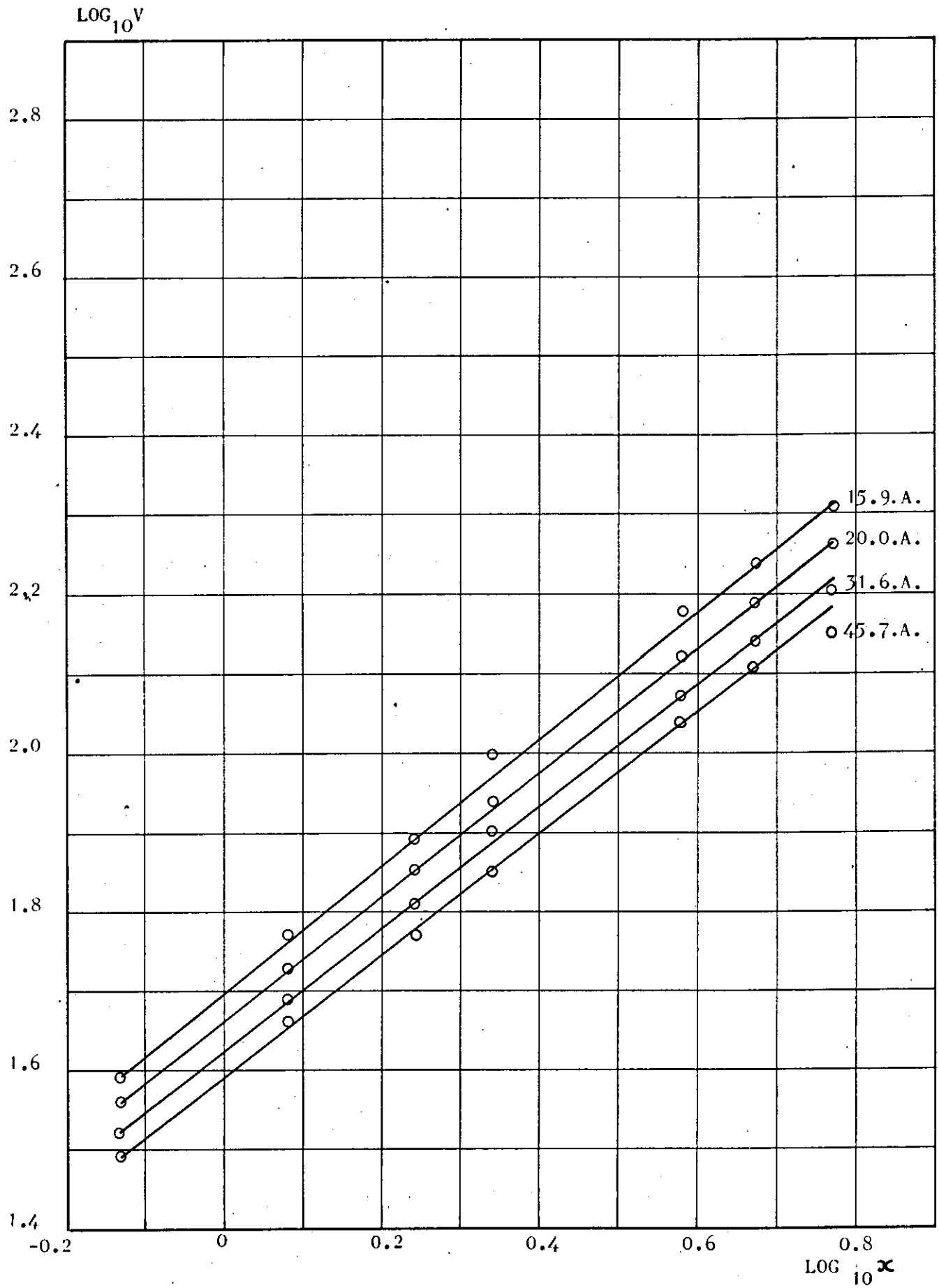

FIG.43. Arc Column Voltage Distribution, $u_\infty = 2 \times 10^4$ cm/sec. 1 Atmos.

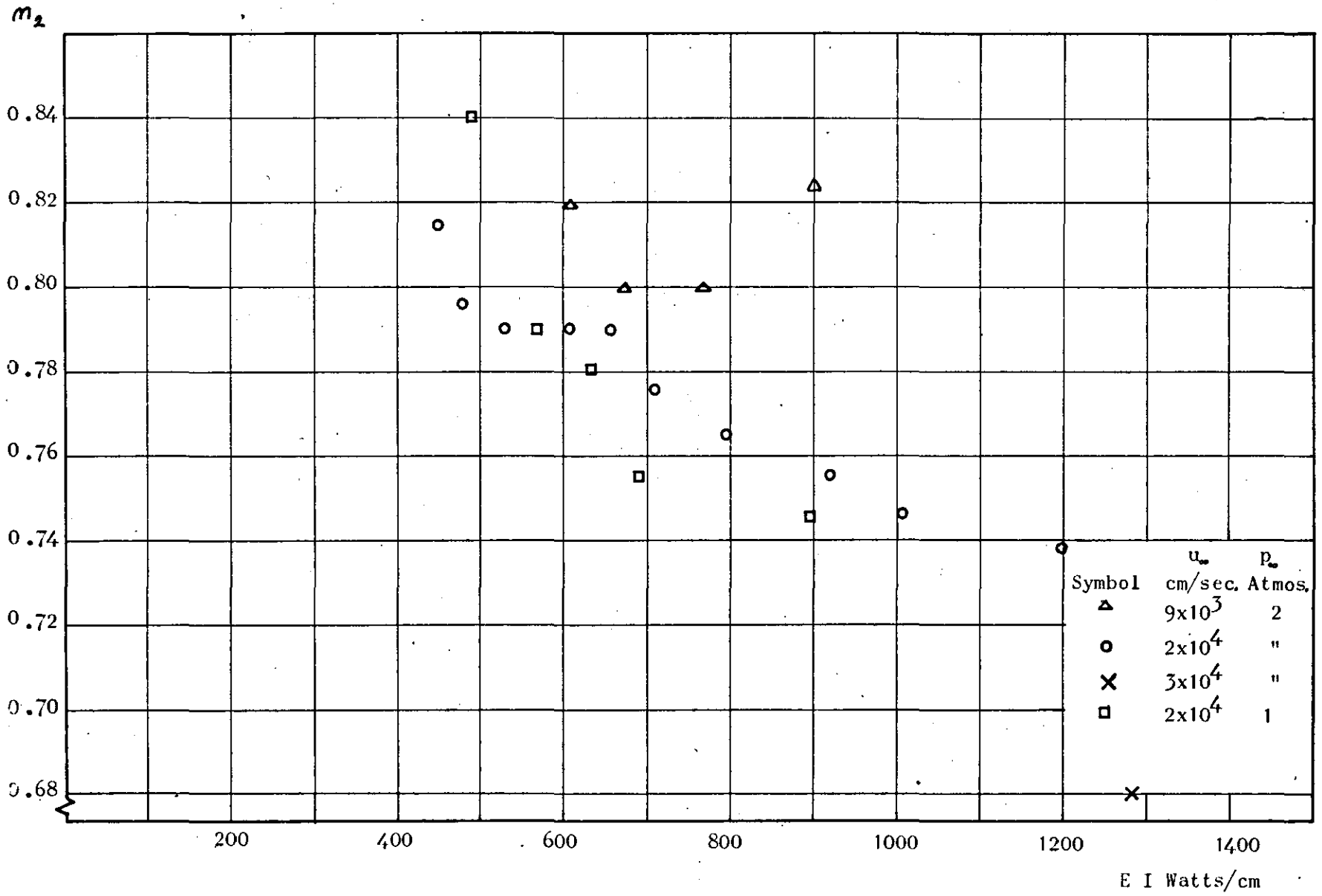

FIG. 46. Variation of Index m_2 with Power Gradient

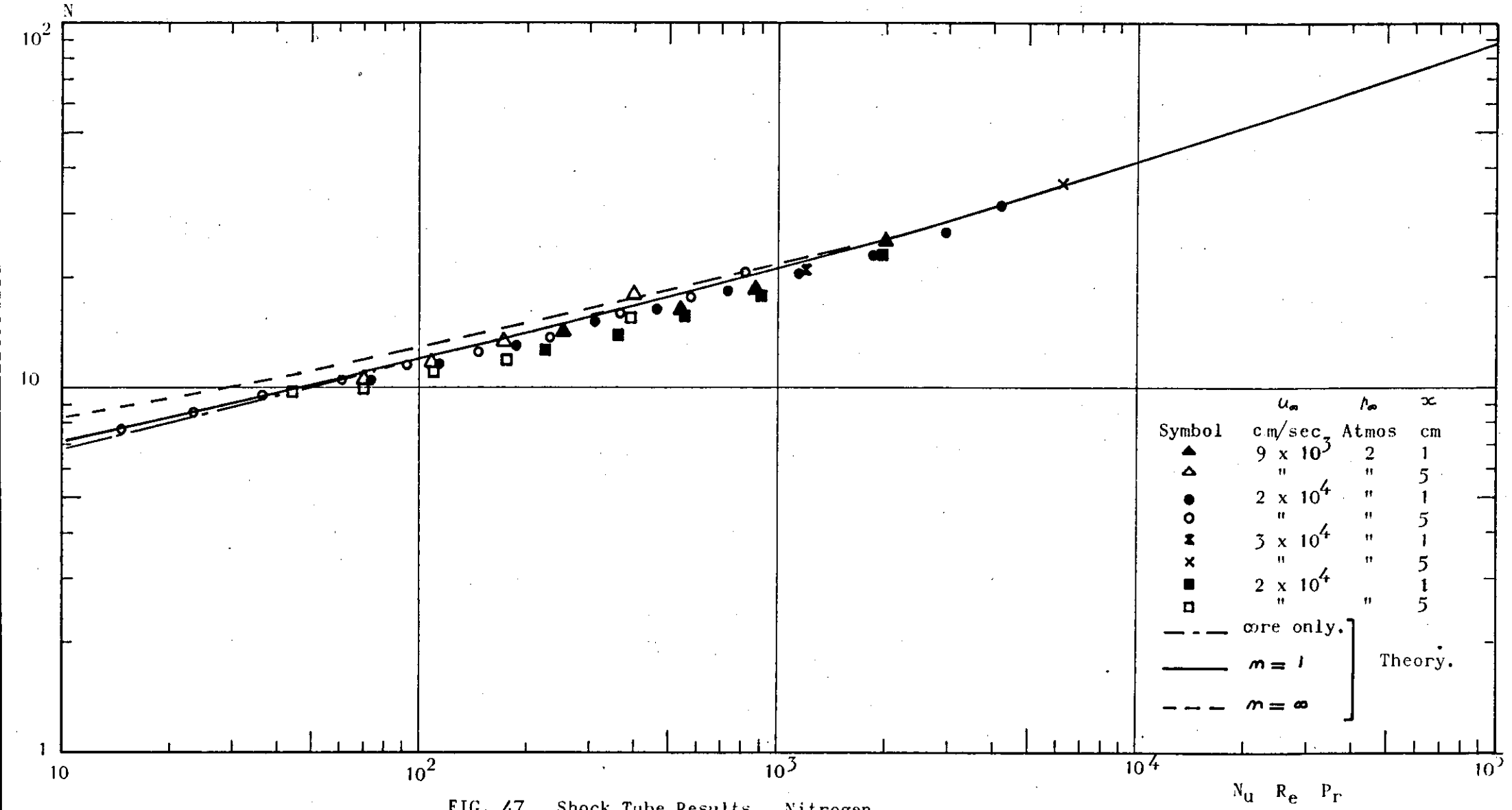

FIG. 47. Shock Tube Results, Nitrogen.

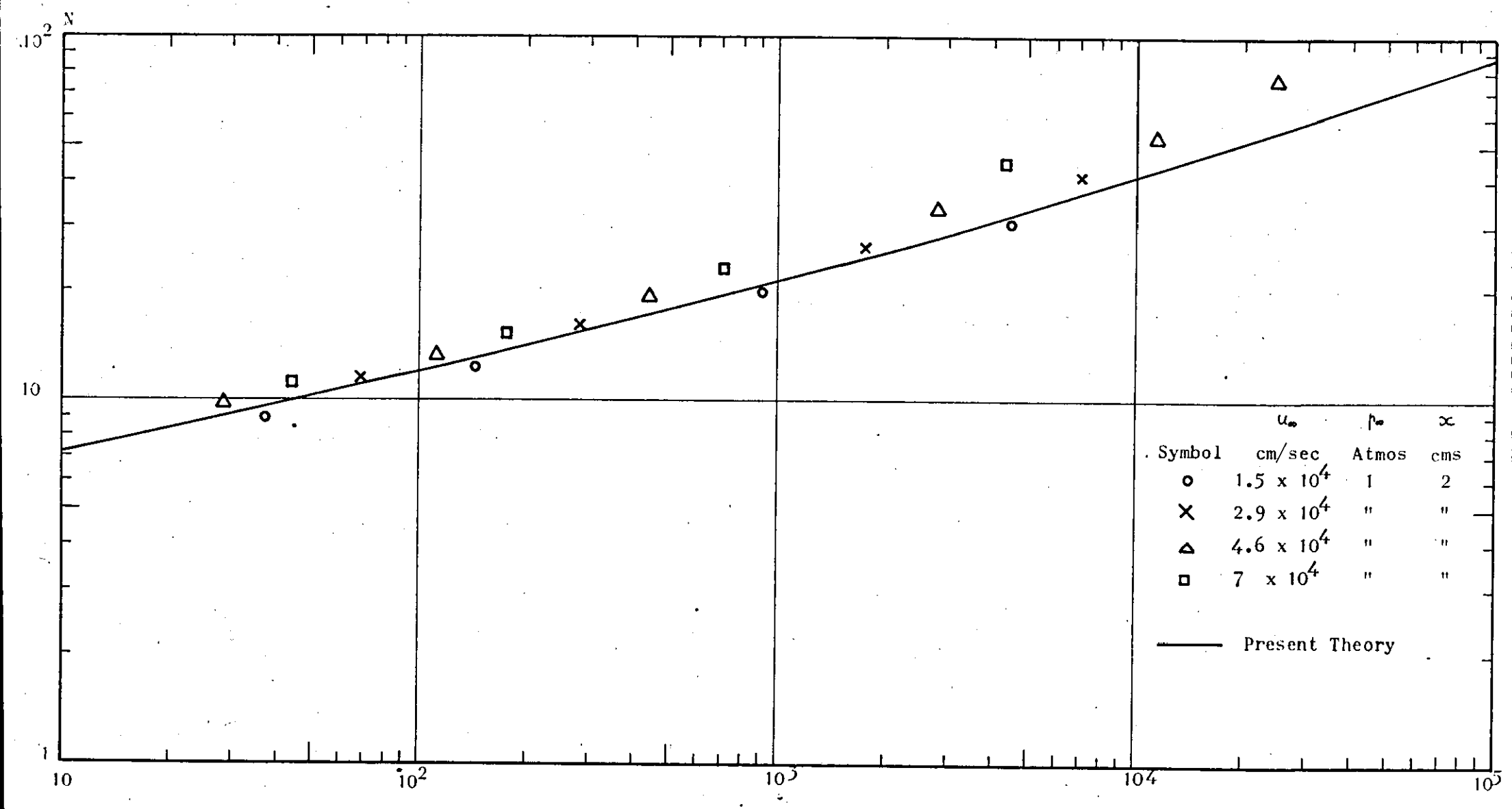

FIG.48. Shock Tube Results, Rowe Ref. 28.

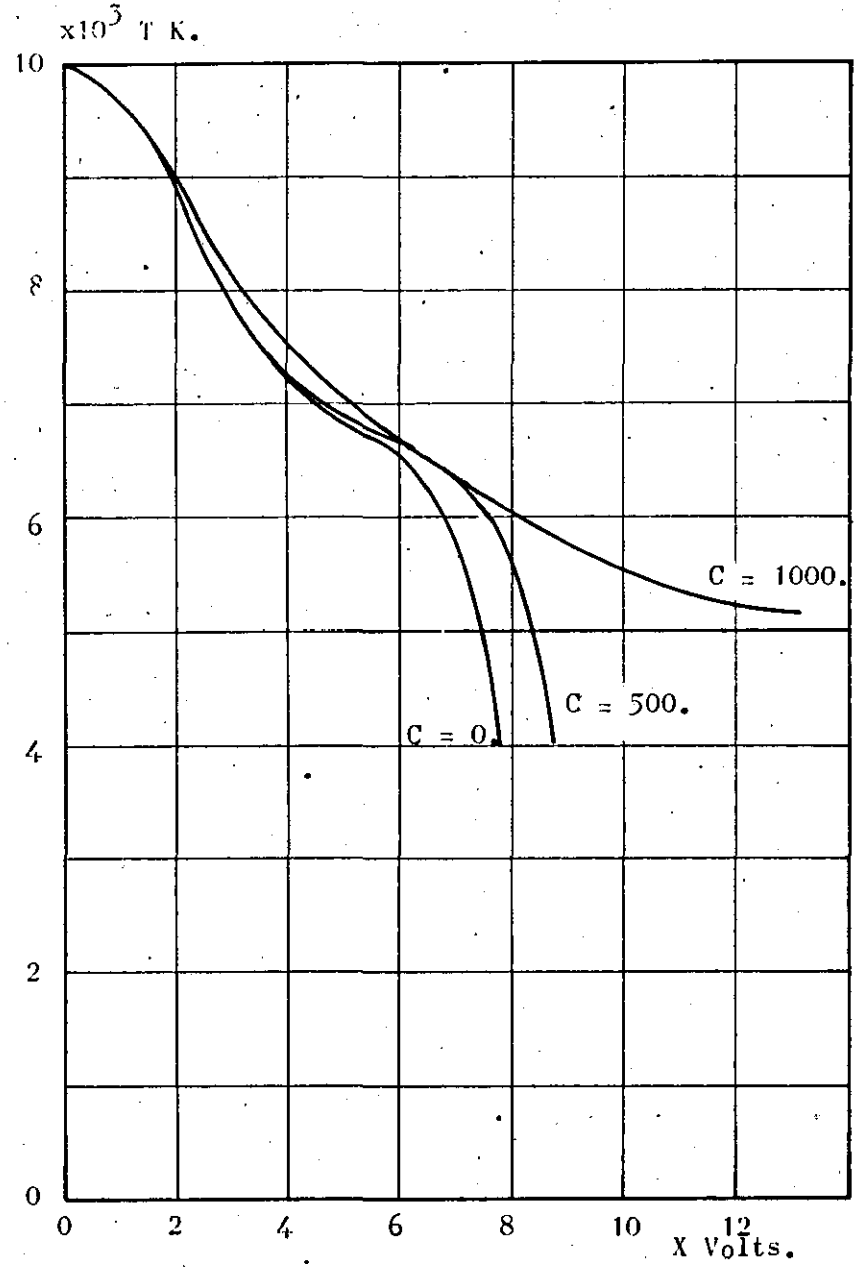

FIG. A_3.1. Effect of Convection on Nitrogen Arc Profiles 10V/cm.

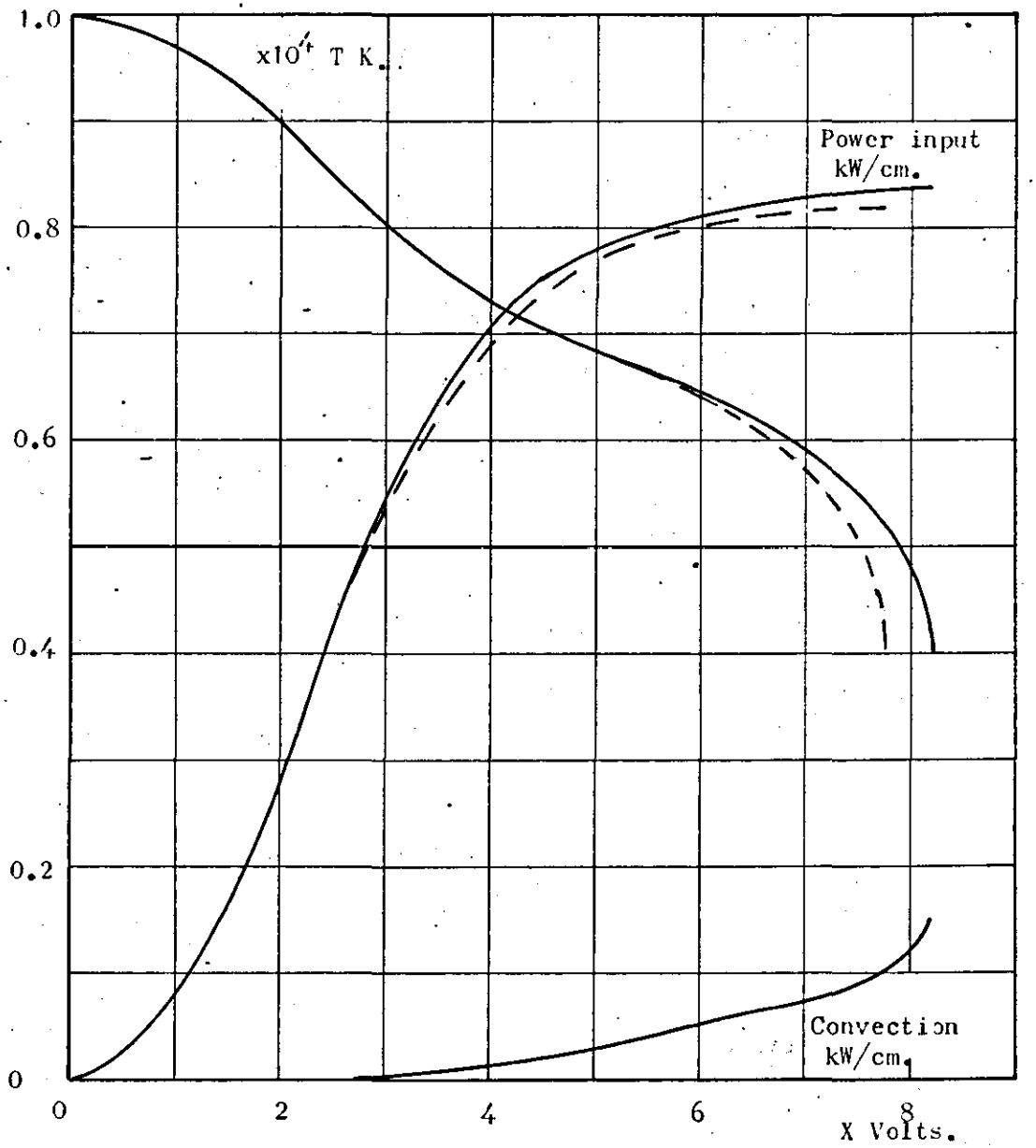

FIG. A_3.2. Convection Across a Constant Pressure Nitrogen Arc. E=25V/cm, 30Amps. ——— C=1000, - - - - C=0.